Vegard Øgård Aksnes

Experimental and Numerical Studies of Moored Ships in Level Ice

Thesis for the degree of Philosophiae Doctor

Trondheim, January 2011

Norwegian University of Science and Technology
Faculty of Engineering Science and Technology
Department of Civil and Transport Engineering

NTNU – Trondheim
Norwegian University of
Science and Technology

NTNU
Norwegian University of Science and Technology

Thesis for the degree of Philosophiae Doctor

Faculty of Engineering Science and Technology
Department of Civil and Transport Engineering

© Vegard Øgård Aksnes

ISBN 978-82-471-2543-4 (printed ver.)
ISBN 978-82-471-2544-1 (electronic ver.)
ISSN 1503-8181

Doctoral theses at NTNU, 2011:14

Printed by NTNU-trykk

Abstract

Moored ships are believed to be feasible for marine operations in ice-covered waters. A variety of ice features, such as broken ice, level ice, ridged ice and icebergs, will pose potential challenges with respect to design and operations. This thesis presents studies on the actions of level ice on moored ships and the resulting vessel response. Focus was put on both analysing physical measurements and deriving suitable numerical models. The thesis is thus articulated around three parts:

- analysis of ice failure modes, vessel response and mooring forces from model tests of a concept called the *Arctic Tandem Offloading Terminal*;
- analysis of ice forces and mooring forces from model tests of a moored simplified hull;
- development of methodology for numerical modelling of moored ships in level ice with constant drift direction.

A concept for offloading of hydrocarbons in ice-infested waters was tested in the Large Ice Model Basin at the Hamburg Ship Model Basin (HSVA). The Arctic Tandem Offloading Terminal consists of two vessels; a turret moored offloading icebreaker, and a shuttle tanker moored in tandem at the stern of the offloading icebreaker. Studies of the coupled response of both vessels to ice actions and the resulting tandem mooring forces show that the concept was stable in yaw when the ice drift direction changed slowly in level ice. The response of the offloading icebreaker moored alone in level ice with variable drift direction and the corresponding ice failure modes were investigated with both slow and sudden changes of ice drift direction. The study underlines how ice actions and the ice failure modes depend on the relative angle between the ice drift direction and the vessel's heading, the hull shape and the vessel's response. The test campaign showed that with the present concept, the magnitude of the mooring forces in severe ice drift events can be comparable to those experienced in ridges. Actions from level ice with variable drift direction should therefore be considered as a possible design criterion for moored ships in certain areas.

Model tests of a moored simplified hull in level ice with constant drift direction have been performed at HSVA. The hull was instrumented to measure the local ice actions on the bow, as well as the mooring forces and the surge response. The test setup enabled studies of the dynamic properties of both ice and mooring forces by independently varying the ice drift speed and the stiffness of the mooring system. Average mooring forces and local ice forces on the bow increased with the ice drift speed, except for the softest mooring system, and were highest for the soft mooring system and lowest for the stiff one at all speeds. A semi-empirical method for modelling local ice forces on the bow was developed based on observations from the model tests. Ice actions are split into actions in the vicinity of the waterline, caused by breaking of intact ice and rotation of broken ice floes, and actions below the waterline, caused by ice-hull friction. The method is probabilistic and includes speed dependence.

Numerical modelling of the surge response of moored ships interacting with intact level ice with constant drift direction was performed with two different approaches for the ice actions:

- the ice was modelled as an elastic beam on an elastic foundation and applied on a simplified 2D hull design;
- the above-mentioned semi-empirical local ice force formulation was implemented and applied on a model of the offloading icebreaker.

Ice forces depended on the penetration of the ship into the ice and enabled feedback effects of the surge response on the ice actions. Such effects were mainly present at low ice drift speeds and often induced large mooring forces. The local ice force formulation induced mooring forces comparable to those measured in model tests of the same hull. The author believes that the method is suited for studies of the dynamic response of moored ships in level ice with constant ice drift direction and can be extended to level ice with variable ice drift direction.

Acknowledgements

Three years as a PhD-student has come to an end and there are several people I would like to thank for making it an enjoyable experience.

First of all I would like to thank my two supervisors Basile Bonnemaire and Sveinung Løset. Basile Bonnemaire worked extensively with experimental and numerical modelling of moored ships in ice in the industry and his combined knowledge about modelling challenges and industry needs has been very beneficial for me. Basile has guided me throughout the PhD in an excellent way. Sveinung Løset organized a scholarship through the PetroArctic project, which is part of the PetroMaks project of the Norwegian Research Council (NFR). Sveinung was always very positive and supported me. I am also thankful for interesting discussions with Knut Vilhelm Høyland, Ove Tobias Gudmestad and Øivind Arntsen. Marion Beentjes administrated the project in an outstanding way.

I spent two months in total at the Hamburg Ship Model Basin (HSVA). Karl-Ulrich Evers, Peter Jochmann, Klaus Niederhausen and Roland Koch ensured that our tests were carried out in the best possible way. I always felt very welcome at HSVA. The model tests at HSVA were supported by European Community's Sixth Framework Programme through the grant to the budget of the Integrated Infrastructure Initiative HYDRALAB III within the Transnational Access Activities, Contract no. 022441. Statoil ASA provided additional funding for the model tests.

Arnor Jensen, Trond Sagerup, Trine Lundamo and Basile Bonnemaire took care of me during my visits at Barlindhaug Consult in Tromsø and made my stays enjoyable.

There is a long list of former and present colleagues with whom I shared numerous coffee breaks, lunches and more or less scientific discussions: Oddgeir Dalane, Kenneth Eik, Christian Lønøy, Yangkyun Kim, Wolfgang Kampel, Ada Repetto, Felix Breitschädel, Nicolas Serré, Haiyan Long, Raed Lubbad, Sergey Sukhorukov, Anton Kulyakhtin, Johan Wåhlin, Marit Reiso, Eric van Buren, Michael Muskulus, Daniel Zwick, Karl Merz, Jenny Trumars, Paul Thomassen, Alex Klein-Paste, Fredrik Sandquist, Lucie Strub-Klein, Aleksey Shestov, Arne Gürtner, Fengwei

Guo, Katherine Dykes and Wenjun Lu. Oddgeir Dalane worked with closely related topics and we have had a very fruitful cooperation since the beginning of our PhD-studies, thanks!

I am thankful for valuable comments and advices from some of the former PhD-students from the basement, Morten Bjerkås and Pavel Liferov.

My family and friends supported me from start to end. The support was highly appreciated.

Last, but definitely not least, thanks to my patient wife, Marte. Without you it would never have been possible.

Contents

Chapter 1

Introduction

1.1 General

Large reserves of hydrocarbons are predicted to be located offshore in the Arctic. The demand for hydrocarbons is high and will probably remain so for a number of years. Thus, arctic areas will most likely be attractive for the hydrocarbon industry in the future.

Arctic areas present additional challenges with respect to both design and operation of offshore structures compared to most existing areas of hydrocarbon exploration. Sea ice, icebergs, spray ice, polar lows, remoteness and darkness need to be dealt with and will heavily affect the structure choice and design, as well as the operational strategies.

Moored structures are believed to be attractive in many arctic waters, mainly due to water depths. Actions from sea ice may have to be taken into account in addition to actions from waves, current and wind, and can have a major influence on the design of both the hull and the mooring system. Nevertheless, the latest design code for arctic offshore structures ISO/FDIS 19906 (2010) gives limited information on how to estimate ice actions on moored structures. The aim of this thesis is to contribute with knowledge about ice actions on moored ships, how they can be estimated, as well as vessel response.

1.2 Scope and thesis outline

This thesis is a continuation of earlier research on moored ships in ice conducted by Hansen (1998), Jensen (2002) and Bonnemaire (2005). Jensen and Bonnemaire focused on aspects related to submerged turret loading in ice, while Hansen worked with numerical modelling of the response of moored ships in broken or managed ice. The intention of this thesis has been to contribute with increased knowledge

about the interaction between moored ships and level ice, by studying model test results and by developing methodology for numerical studies.

The main objectives have been the following:

Model tests of a tandem offloading system in level ice:

- study vessel response of turret moored ships in level ice with varying ice drift direction;
- study coupled vessel response of two ships moored in tandem in ice;
- study the ice-hull interaction processes and their dependence on hull shape and vessel response.

Model tests of a moored simplified hull in level ice:

- study mooring forces at various ice drift speeds and with various mooring systems;
- study ice forces at various ice drift speeds and with various mooring systems;
- develop an ice force model based on measured data.

Numerical modelling of moored ships in level ice:

- establish methodology for modelling of moored ships in level ice with constant drift direction;
- study vessel response and ice forces resulting from simulations with the numerical model.

This thesis consists of an introductory chapter followed by seven papers. Four papers are published in international conference proceedings, while the three others have been published in international journals.

Chapter 2 presents an overview of existing literature on full scale experiences with moored ships in ice, as well as on model tests and numerical modelling.

Chapters 3 and 4 consist of two papers about a particular concept called the Arctic Tandem Offloading Terminal. Chapter 3 discusses the performance of the tested tandem mooring system in ice, while Chapter 4 analyses the response of a moored icebreaking ship in ice with variable drift direction.

Chapters 5 and 6 deal with methodology for modelling of moored ships in level ice, based on physical principles such as elastic beam theory and friction theory.

Chapters 7 and 8 present results from model tests of a simplified moored hull in level ice. A new test setup was used, which enabled simultaneous measurements of mooring forces and local ice forces. The measured ice forces were used to develop a methodology for the estimation of local ice forces on moored ships.

Chapter 9 applies the method developed in Chapter 8 on the hull of the moored icebreaking vessel from the Arctic Tandem Offloading Terminal.

Chapter 10 concludes the work and outlines possibilities for further research.

1.3 Readership

The thesis focuses on the interaction between moored ships and level ice, both experimentally and numerically. The primary readership is students, researchers and engineers interested in or working with:

- design and operation of moored structures for marine operations in ice-infested waters;
- dynamic behaviour of moored ships in level ice;
- numerical modelling of the interaction between level ice and moored ships.

References

Bonnemaire, B., 2005. Arctic Offloading: Submerged Turret Loading and Loading Downtime in Drifting Ice. Norwegian University of Science and Technology, Doctoral Thesis.

Hansen, E., 1998. A discrete element method to study marginal ice zone dynamics and the behaviour of vessels moored in broken ice. Norwegian University of Science and Technology, Doctoral Thesis.

ISO/FDIS 19906, 2010. Petroleum and natural gas industries - Arctic offshore structures, ISO TC 67/SC 7. Final Draft International Standard, International Standardization Organization. Geneva, Switzerland.

Jensen, A., 2002. Evaluation of Concepts for Loading of Hydrocarbons in Ice-infested Waters. Norwegian University of Science and Technology, Doctoral Thesis.

Chapter 2

Background

The Norwegian explorer and scientist Fridtjof Nansen was possibly the first person to explore stationkeeping in ice during his 1893-96 voyage with the vessel *Fram* in the Arctic Ocean (Nansen, 1999). The goal of Nansen's expedition was to prove the existence of an ocean current from Northern Russia, going over the North Pole and to the east coast of Greenland, by getting stuck in the pack ice and drift along with it. Nowadays, stationkeeping in ice might be viewed from a different perspective. For arctic marine operations one would like to keep a geostationary position and *not* drift along with the pack ice. Nansen's journey in the pack ice posed challenges with respect to the design of the hull, perfectly handled by the naval architect Colin Archer. Stationkeeping in ice for marine operations faces different challenges with respect to design and operations.

This chapter gives an overview of the existing research literature regarding full scale experiences with stationkeeping in ice, model basin tests of moored structures, as well as numerical models. Some theory about modelling of icebreaking ships in level ice and level ice actions on sloping structures is given at the end, as this material is needed to fully appreciate the chapters treating modelling of moored ships in the sequel.

2.1 Full scale experiences with stationkeeping in ice

Moored structures were first deployed in the Beaufort Sea off the north coast of Canada in the late 1970s, when Canmar used moored ships for exploration drilling (Wright, 1999). The drillships by Canmar had fairleads above the waterline and thus their mooring lines were exposed to drifting ice. Moreover, their heading was fixed and they had no possibilities to weathervane. These drilling operations were performed in open water or in light ice conditions in summer and early autumn. Gradual improvement of the ice management techniques made it possible to extend the season.

Problems with weathervaning and mooring lines through the water surface were taken care of when the next generation of drilling vessel for the Beaufort Sea was designed, namely the *Kulluk* (Wright, 2000). In contrast to the drillships, Kulluk was designed to be used in relatively heavy pack ice. It operated from spring break-up to early winter and was therefore exposed to a variety of ice conditions. Kulluk had the shape of a downward breaking cone and was radially symmetric. The symmetry implied that it had no preferred ice drift direction. All drift directions were handled equally well and ice vaning was therefore not an issue. Further, the hull was constructed to give a good ice clearance. This was done by adding an outward bending skirt in the lower part of the hull. The purpose of the skirt was to minimize the interaction between ice and mooring lines, ice and risers, and to avoid ice in the moonpool. The mooring system of the Kulluk was substantially improved from the drillships. The mooring lines were stronger and the fairleads were submerged. The mooring system consisted of twelve mooring lines in a radially symmetric configuration. In case of emergency situations, remote anchor releases were installed for rapid disconnection. Kulluk operated from 1983 to 1993 in the same locations as the drillships, but with an extended season. Mooring line tensions and ice conditions were monitored during operations and the experiences with the Kulluk have been utilized in the design of moored vessels in other ice-infested areas, such as the Grand Banks offshore Newfoundland and Labrador on the east coast of Canada.

Terra Nova and White Rose are two hydrocarbon developments on the Grand Banks, both using FPSO (floating, production, storage and offloading) concepts, see Lever et al. (2001), Ewida and Kean (2001) and Norman et al. (2008). Operations with moored structures at the Grand Banks differ from those in the Beaufort Sea, as the former ones are year round operations, whereas the latter were performed in the extended summer season. Further, the sea ice conditions at the Grand Banks are far less severe than in the Beaufort Sea. Nevertheless, actions from sea ice had to be taken into account in the design of the FPSOs for the Grand Banks. These vessels are ship-shaped and moored with disconnectable internal turret systems. Turret mooring systems enable weathervaning to minimize environmental loads and disconnection from the mooring buoy is possible within minutes in case of extreme environmental loads, such as iceberg collisions. Hydrocarbons have been produced at Terra Nova and White Rose since 2002 and 2005, respectively, and the FPSOs are both intended to operate for a minimum of 20-25 years.

A floating production unit is currently being considered for the Shtokman gas condensate field in the Russian part of the Barents Sea (Liferov and Metge, 2009). Sea ice intrusions are more common at Shtokman than at the Grand Banks and actions from sea ice have been taken into account in the design process. The planned vessel is ship-shaped and will be moored with a disconnectable turret system. The production is expected to start in 2016.

Stationkeeping is needed for tankers during loading operations in ice. Offloading of

oil in ice has been performed offshore Varandey in the Pechora Sea, Russia, since 2000 (Barents Observer, 2010). Currently, a fixed ice-resistant offloading tower, installed in 2008, is used for export of crude oil from the onshore field Yuzhno Khylchuyu to the floating, storage and offloading vessel *Belokamenka* in the ice-free zone outside Murmansk. Another field in the Pechora Sea is the Prirazlomnoye field, where a gravity based structure will be installed in 2011 (Prirazlomnoye Oilfield, 2010). Crude oil will be offloaded to icebreaking tankers through two loading arms and transported to Belokamenka.

Stationkeeping in ice has also been provided by dynamic positioning (DP). Two different operations involving DP in ice have been reported in the literature. The first DP operation in ice was performed offshore the Sakhalin Island on the east coast of Russia in May and June 1999 (Keinonen et al., 2000). A diving operation was undertaken to finalize the construction work in order to start hydrocarbon production later in the summer. The ice conditions were relatively severe with level ice thicknesses up to 1.5 m and ridge keels down to 10 m. The DP vessel was supported by two icebreakers which broke incoming ice into smaller floes and thus reduced the ice actions.

The Arctic Coring Expedition (ACEX) took place in August and September 2004 (Moran et al., 2006; Pilkington et al., 2006; Keinonen et al., 2006). The main objective of the Arctic Coring Expedition was to sample sediments from the Lomonosov ridge close to the North Pole. At the drilling location the water depth is 1100 - 1300 m and is among the shallowest areas in the central Arctic Ocean. Nevertheless, this is considered as deep water compared to other drilling sites and before ACEX there was no experience with deep water drilling in ice-covered seas. Thus the planning had to be based on experiences from shallow water drilling in the Canadian Arctic.

A new research vessel funded by the EU, *Aurora Borealis*, is currently being planned (Ericon - Aurora Borealis, 2010). The construction will start in 2012 and the vessel will be put into operation two years later. Aurora Borealis will be an icebreaker with capability for deep-sea drilling with dynamic positioning in ice and open water, in addition to be a multi-purpose research vessel. One of the planned activities for Aurora Borealis will be to continue the work from the ACEX, sampling seabed sediments from the Arctic Basin. This will involve stationkeeping by dynamic positioning in permanently ice covered seas.

A brief overview of full scale experiences with stationkeeping in ice has been given above and is summarized in Table 2.1. Even though the first operations involving stationkeeping in ice started more than thirty years ago, the operations have been limited to a few areas and to a few types of structures. Except for Kulluk, there is not much publicly available data on measured mooring forces, nor on the corresponding ice conditions.

Table 2.1: Summary of full scale stationkeeping operations in ice.

Location	**Stationkeeping method**	**Type of operation**	**Length of operation**
Beaufort Sea *(Canmar drillships)*	Mooring lines through the waterline	Drilling	Long term, 1976 - late 1980's
Beaufort Sea *(Kulluk)*	Submerged mooring system	Drilling	Long term, 1983 - 1993
Grand Banks *(Terra Nova)*	Submerged turret mooring system	Hydrocarbon production	Long term, 2002 -
Grand Banks *(White Rose)*	Submerged turret mooring system	Hydrocarbon production	Long term, 2005 -
Pechora Sea	Loading tower	Offloading	Long term, 2000 -
Offshore Sakhalin	Dynamic Positioning	Diving	Short term, 1999
Arctic Basin	Dynamic Positioning	Core drilling	Short term, 2004

2.2 Model tests of moored vessels in ice

Model testing of moored structures in ice basins is possibly the most reliable tool available for studying vessel response to various drift ice scenarios and has been used as a tool for design (of moored structures) for more than 30 years (Comfort et al., 1999). Experiments with moored structures in model test basins are performed in a controlled environment. This enables simulation of various realistic ice scenarios, such as level ice, broken ice and ridges, with constant or varying drift direction and speed. A good visual impression of the behaviour of the structure is obtained, in addition to measured response and mooring forces. However, there are challenges related to model tests in ice, especially with respect to scaling of ice properties.

The ratio between compressive and flexural strength has been challenging to model correctly. The geometry of the part of the hull interacting with ice will vary greatly for moored ships in drifting ice with variable direction. The midship section is often almost vertical, while the stem angle on an icebreaking vessel may be as low as 20°. The incoming ice will experience different failure modes (crushing, bending) depending on the relative ice drift direction and it is important that all relevant failure modes are scaled consistently.

The full scale geometry of ice ridges is relatively easy to reproduce in basins, but the mechanical properties are more challenging. Mechanical properties are difficult to measure both in the field and in basins, and challenging to scale as they are results of thermodynamic processes which are challenging to scale (Høyland, 2010).

Comfort et al. (1999) made a comprehensive review of the available information about model tests of moored structures in ice. Several concepts have been tested extensively after the review by Comfort et al. in connection with industrial developments. Some of these have been made publicly available, such as tests of struc-

tures similar to the Kulluk (Dalane et al., 2008, 2009), SPAR platforms (Bruun et al., 2009; Murray et al., 2009) and TLP platforms (Bezzubik et al., 2004). Results from model tests of moored ships have also been published recently. A submerged turret loading concept was studied by Jensen et al. (2000), while a tandem mooring concept was discussed by Jensen et al. (2008); Bonnemaire et al. (2008); Aksnes et al. (2008); Aksnes and Bonnemaire (2009a). The two latter papers can be found in Chapters 3 and 4 of this thesis, respectively.

Mooring forces and vessel response are usually reported from model tests of moored structures in ice. However, these are particular to the vessel and its mooring system. There are several strategies for how to apply model test data to other structures:

- extrapolation by using empirical conversion factors
- back-calculation of ice forces
- direct measurements of ice forces.

Extrapolation of mooring forces and vessel response can be based on both model tests results and full scale measurements. A problem with this approach is that large amounts of data are needed in order to estimate reliable conversion factors. Resistance predictions for icebreakers are often based on such an approach, see e.g. Keinonen et al. (1991). Additional challenges for moored structures are the inclusion of a mooring system and the need for dynamic response predictions in addition to predictions of the mean offset.

Back-calculation of ice actions have been performed by considering the ice force as the unknown in the equations of dynamic equilibrium for moored structures (Karulin et al., 2004; Lundamo et al., 2008; Dalane et al., 2008; Murray et al., 2009). The resulting ice force can then be applied in response predictions with numerical tools.

Instrumentation of hulls for direct measurements of ice forces is complicated for moored structures, in particular for ships. In Aksnes (2010a), ice actions on the bow of a moored simplified hull were measured and analysed. Based on the measurements, a method for modelling local ice forces on moored vessels was developed (Aksnes, 2011a) and applied to a moored ship (Aksnes, 2011b). Mooring forces from the numerical simulations in Aksnes (2011b) are in good agreement with the mooring forces obtained from the model tests. These three papers constitute Chapters 7, 8 and 9.

2.3 Numerical modelling of moored vessels in ice

Numerical modelling could be used as a tool for studies of moored structures in ice. The interactions between moored ships in ice are complex and so far there is no general agreement on how to model them. During the last decade or so a few

papers about modelling of moored structures in ice have been published, focusing on either broken ice, level ice, rubble or ridges.

Broken or managed ice is perhaps the most relevant ice condition regarding operations. Incoming ice will often be managed by assisting icebreakers, hence only smaller ice floes will interact with the moored structure. Tseng et al. (1987) briefly described a software which is able to simulate interaction between moored ships and broken ice, as well as level ice. However, few details and no results were given and it is difficult to assess the validity of their model. Murray and Spencer (1997) combined two approaches to estimate actions from broken ice and the resulting response and mooring force for a turret moored tanker. They used model test data to estimate inertial and damping coefficients caused by broken ice and a discrete element model to calculate ice forces without inertial and damping contributions. A discrete element model was also developed by Hansen and Løset (1999a,b). Their model was compared with model tests of a turret moored ship described by Løset et al. (1998) and gave reasonable results. A different approach was chosen by Barker et al. (2000). They described broken ice as a cohesionless Mohr-Coloumb material and compared simulations against full-scale data from Kulluk.

Actions from ice ridges may cause the highest loads on a moored structure operating in ice, and it is crucial to estimate ridge actions with high accuracy. Nevertheless, there is limited research literature on the topic, except the recent paper by Bonnemaire et al. (2009). They applied two different methods to estimate mooring forces for a turret moored ship and a SPAR platform. In the first method, they defined the ridge load a priori as a function of the penetration of the structure into the ice ridge, while in the other method the ridge load was found by simultaneously integrating the equations of motion for the structure and the ice ridge.

Intact level ice in large ice floes may be encountered in the case when no ice management is applied. Further, level ice actions are relevant for scenarios with broken ice when the ice floes are large, or for ridges, as the consolidated layer of a ridge is often treated as level ice. Toyama and Yashima (1985) studied dynamic response of a moored Kulluk-shaped vessel in level ice. The method by Nevel (1961) was used to calculate breaking forces and the corresponding surge response of the vessel was estimated. Their numerical results showed fairly good agreement with with model tests. Shkhinek et al. (2004) simultaneously integrated the equations of motion for two different moored structures (TLP and SPAR platforms) and a semi-infinite ice sheet to find acceptable correspondence with measured mooring forces from both model scale and full scale data. Finally, three papers (Aksnes and Bonnemaire, 2009b; Aksnes, 2011b, 2010b) concerning simulation of dynamic surge response of moored ships in level ice are included in this thesis.

All of the above-mentioned papers about level ice actions on moored structures have to some extent used ideas from level ice actions on fixed sloping structures or from theory of icebreaking ships. These topics will therefore be briefly discussed in the following sections.

2.4 Level ice actions on sloping structures

Forces on sloping and conical structures have been considered by several researchers. According to ISO/FDIS 19906 (2010) there are two basic methods relevant for the design of arctic offshore structures; one based on plasticity theory (Ralston, 1977, 1979) and one based on elastic beam theory (Croasdale, 1980; Croasdale et al., 1994). Nevel has considered elastic wedges instead of elastic beams in a series of papers, see Nevel (1992) and references therein. More recently, Dempsey et al. (1999) included hydrodynamic effects in elastic beam theory and studied velocity effects.

The above-mentioned papers have mainly focused on the force needed to break ice in bending. For simulation of dynamic response of fixed or moored structures caused by bending failure, it is necessary to consider the time evolution of the icebreaking process. That is, forces need to be described from initial contact between the structure and the ice sheet, through the force build up in the breaking phase and until the broken ice piece has been transported away and a new contact with intact ice is obtained. This has been a focus area for fixed structures in China, as jacket structures in the Bohai Sea have experienced vibrations due to level ice actions. On the contrary, Canadian bridge piers and Finnish lighthouses with conical waterline sections have not experienced vibrations caused by ice (Brown and Määttänen, 2008).

Ice force models in both time and frequency domain have been derived from measurements on narrow conical jacket structures in the Bohai Sea (Qu et al., 2006; Yue et al., 2007). The time domain model has been recommended by ISO/FDIS 19906 (2010) and is based on a sawtooth shaped cyclic function, where each cycle is defined as

$$f_i(t) = \begin{cases} \frac{6F_{0i}}{T_i}t, & 0 < t < \frac{T_i}{6} \\ 2F_{0i} - \frac{6F_{0i}}{T_i}t, & \frac{T_i}{6} < t < \frac{T_i}{3} \\ 0, & \frac{T_i}{3} < t < T_i \end{cases} . \tag{2.1}$$

The total force is defined as

$$F(t) = \sum_{i=1}^{N} f_i(t - t_i^0), \tag{2.2}$$

where $t_1^0 = 0$ and $t_i^0 = \sum_{j=1}^{i-1} T_i$. The peak force F_{0i} and the duration T_i of each cycle were assumed to follow independent normal distributions. The model has been slightly generalized in ISO/FDIS 19906 (2010). In Chapter 8 of this thesis, a similar approach is applied in the derivation of a local ice force model based on model test measurements of ice forces on a moored vessel.

2.5 Modelling of icebreaking ships

A lot of research has been performed on the performance of icebreakers since Runeberg (1888/1889) published the first paper more than hundred years ago. Jones (1989) has summarized the historical development of the understanding of ship performance in level ice. Most research literature on icebreaker performance has focused on the average resistance in various ice conditions. This includes some more recent papers as well, such as Lindqvist (1989) and Keinonen et al. (1991). However, for applications to dynamic behaviour of moored ships, it is most relevant to look at studies where the time evolution of the interaction process between ice and ship is considered.

Jebaraj et al. (1992) applied the finite element method to study the dynamic response of an ice sheet to an advancing ship, whose speed was constant. Valanto has also contributed with sophisticated finite element modelling (Valanto, 2001), as well as theoretical and experimental studies of two dimensional icebreaking (Valanto, 1992). Valanto pointed out that even though the icebreaking process is complex, it is possible to split the process into various phases and study the phases separately. This idea has played an important role in the modelling papers included in this thesis (Chapters 5, 6, 8 and 9).

2.6 Summary

Experiences with full scale stationkeeping operations in ice are few, especially in severe ice conditions. Mooring forces and ice conditions were reported from Kulluk. However, the ice was always managed and the reports of ice properties were based on observations, as few measurements of ice properties were performed. Thus, it is difficult to apply Kulluk data in the design of new concepts. This accounts in particular for concepts with a different hull shape, such as ship-shaped vessels.

Relatively large amounts of model test data exist. Some of the data have been published in research papers, but most of the data are only available to the industry. As opposed to full scale measurements of mooring forces, ice properties are easily controllable in model tests and it is easy to study various ice scenarios. Nevertheless, it is challenging to extrapolate results from model tests to other hulls and mooring systems, as response and mooring forces are particular to a vessel and its mooring system.

The research on numerical modelling of moored structures in ice is scattered in time and reflects industry needs. There is a need for more continuity in the research to enable better scientific progress. Full and model scale data are important for numerical models and should be used for calibration and validation. Vessel response and mooring forces can then be extrapolated to other ice conditions and thus numerical models can be useful tools in the design of new moored structures for marine operations in ice-infested waters.

References

Aksnes, V., 2010a. Model tests of the interaction between a moored vessel and level ice. In: Proceedings of the 20th IAHR International Symposium on Ice. Lahti, Finland.

Aksnes, V., 2010b. A simplified interaction model for moored ships in level ice. Cold Regions Science and Technology 63 (1-2), 29–39.

Aksnes, V., 2011a. A panel method for modelling level ice actions on moored ships. Part 1: Local ice force formulation. Cold Regions Science and Technology 65 (2), 128–136.

Aksnes, V., 2011b. A panel method for modelling level ice actions on moored ships. Part 2: Simulations. Cold Regions Science and Technology 65 (2), 137–144.

Aksnes, V., Bonnemaire, B., 2009a. Analysis of the behaviour of a moored ship in variable ice drift. In: Proceedings of the 20th International Conference on Port and Ocean Engineering under Arctic Conditions. Luleå, Sweden, POAC09-25.

Aksnes, V., Bonnemaire, B., 2009b. A simplified approach for modelling stochastic response of moored vessels in level ice. In: Proceedings of the 20th International Conference on Port and Ocean Engineering under Arctic Conditions. Luleå, Sweden, POAC09-134.

Aksnes, V., Bonnemaire, B., Løset, S., Lønøy, C., 2008. Model testing of the Arctic Tandem Offloading Terminal - Tandem mooring forces and relative motions between vessels. In: Proceedings of the 19th IAHR International Symposium on Ice. Vol. 2. Vancouver, British Columbia, Canada, pp. 687–698.

Barents Observer, 2010. Cited: July 20th, 2010.
URL `http://www.barentsobserver.com`

Barker, A., Sayed, M., Timco, G., 2000. Numerical simulation of the "Kulluk" in pack ice conditions. PERD/CHC report HYD-TR-050.

Bezzubik, O. N., Bitsulya, A. V., Karulin, E. B., Karulina, M. M., Klementyeva, N. Y., Sazonov, K. E., Chernetsov, V. A., Kulakov, A. V., Kupreev, V. V., 2004. Experimental investigation of interaction of moored platforms with drifting ice features. In: Proceedings of the 17th IAHR International Symposium on Ice. Vol. 1. St. Petersburg, Russia, pp. 76–83.

Bonnemaire, B., Lundamo, T., Evers, K. U., Løset, S., Jensen, A., 2008. Model testing of the Arctic Tandem Offloading Terminal - Mooring ice ridge loads. In: Proceedings of the 19th IAHR International Symposium on Ice. Vol. 2. Vancouver, British Columbia, Canada, pp. 639–650.

Bonnemaire, B., Shkhinek, K., Lundamo, T., Liferov, P., Le Guennec, S., 2009. Dynamic effects in the response of moored structures to ice ridge interaction. In: Proceedings of the 20th International Conference on Port and Ocean Engineering under Arctic Conditions. Luleå, Sweden, POAC09-135.

Brown, T., Määttänen, M., 2008. Comparison of Kemi-I and Confederation Bridge cone ice load measurement results. Cold Regions Science and Technology 55 (1), 3–13.

Bruun, P. K., Husvik, J., Le Guennec, S., Hellmann, J. H., 2009. Ice model test of an Arctic SPAR. In: Proceedings of the 20th International Conference on Port and Ocean Engineering under Arctic Conditions. Luleå, Sweden.

Comfort, G., Singh, S., Spencer, D., 1999. Evaluation of Ice Model Test Data for Moored Structures. PERD/CHC report 26-195.

Croasdale, K. R., 1980. Ice forces on fixed rigid structures. In: 1st IAHR State of the Art Report on Ice Forces on Structures. pp. 34–106.

Croasdale, K. R., Cammaert, A. B., Metge, M., 1994. A method for the calculation of sheet ice loads on sloping structures. In: Proc. 12th Int. Symposium on Ice. Vol. 2. The Norwegian Institute of Technology, Trondheim, Norway, pp. 874–885.

Dalane, O., Aksnes, V., Løset, S., Aarsnes, J. V., 2009. A moored arctic floater in first-year sea ice ridges. In: Proceedings of the 28th International Conference on Ocean, Offshore and Arctic Engineering. Honolulu, Hawaii, USA, OMAE2009-79945.

Dalane, O., Gudmestad, O. T., Løset, S., Amdahl, J., Fjell, K. H., Hildèn, T. E., 2008. Ice tank testing of a surface buoy for Arctic conditions. In: Proceedings of the 27th International Conference on Offshore Mechanics and Arctic Engineering. Estoril, Portugal, OMAE2008-57331.

Dempsey, J. P., Fox, C., Palmer, A. C., 1999. Ice-slope interaction: transitions in failure mode. In: Proceedings of the 18th International Conference on Offshore Mechanics and Arctic Engineering. St. Johns, Newfoundland, Canada, OMAE99/P&A-1156.

Ericon - Aurora Borealis, 2010. European Research Icebreaker Aurora Borealis. Cited: June 25, 2010, `http://www.eri-aurora-borealis.eu`.

Ewida, A., Kean, J. R., 2001. Terra Nova Design Challenges and Operational Integrity Strategy. In: Proceedings of the Eleventh International Offshore and Polar Engineering Conference. Vol. 1. Ottawa, Ontario, Canada, pp. 4–12.

Hansen, E., Løset, S., 1999a. Modelling floating offshore units moored in broken ice: comparing simulations with ice tank tests. Cold Regions Science and Technology 29 (2), 107–119.

Hansen, E., Løset, S., 1999b. Modelling floating offshore units moored in broken ice: model description. Cold Regions Science and Technology 29 (2), 97–106.

Høyland, K. V., 2010. Thermal aspects of model basin ridges. In: Proceedings of the 20th IAHR International Symposium on Ice. Lahti, Finland.

ISO/FDIS 19906, 2010. Petroleum and natural gas industries - Arctic offshore structures, ISO TC 67/SC 7. Final Draft International Standard, International Standardization Organization. Geneva, Switzerland.

Jebaraj, C., Swamidas, A. S. J., Shih, L. Y., Munaswamy, K., 1992. Finite element analysis of ship/ice interaction. Computers and Structures 43 (2), 205–221.

Jensen, A., Bonnemaire, B., Løset, S., Breivik, K. G., Evers, K. U., Ravndal, O., Aksnes, V., Lundamo, T., Lønøy, C., 2008. First ice model testing of the Arctic Tandem Offloading Terminal. In: Proceedings of the 19th IAHR International Symposium on Ice. Vancouver, British Columbia, Canada.

Jensen, A., Løset, S., Høyland, K. V., Hellmann, J., Vodahl, B. P., 2000. Model tests of an arctic tanker concept for loading oil Part II: Barge in moored position. In: Proceedings of the 15th International Symposium on Ice (IAHR). Vol. 1. Gdansk, Poland.

Jones, S. J., 1989. A review of ship performance in level ice. In: Proceedings of the 8th International Conference on Offshore Mechanics and Arctic Engineering. Vol. 4. The Hague, Netherlands, pp. 325–342.

Karulin, E. B., Karulina, M. M., Sazonov, K. E., Chernetsov, V. A., 2004. Mathematical model for motion of moored platform interacting with ice. In: Proceedings of the 17th IAHR International Symposium on Ice. Vol. 1. St. Petersburg, Russia, pp. 85–92.

Keinonen, A., Browne, R. P., Revill, C. R., Bayly, I. M., 1991. Icebreaker performance prediction. SNAME Transactions 99, 221–248.

Keinonen, A., Liljestrom, G., Pilkington, R., 2006. Transit and Stationary Coring Operations in the Central Polar Pack. ICETECH06-125-RF.

Keinonen, A., Wells, H., Dunderdale, P., Pilkington, R., Miller, G., Brovin, A., 2000. Dynamic positioning operation in ice, Offshore Sakhalin, May-June 1999. In: Proceedings of the tenth ISOPE Conference. Vol. 1. Seattle, Washington, USA, pp. 683–690.

Lever, G. V., Kean, J. R., Muggeridge, K. J., 2001. Terra Nova FPSO on the Grand Banks of Canada. In: Proceedings of the 16th International Conference on Port and Ocean Engineering under Arctic Conditions. No. 3-20. Ottawa, Ontario, Canada.

Liferov, P., Metge, M., 2009. Challenges with ice-related design and operating philosophy of the Shtokman Floating Production Unit. In: Proceedings of the 20th International Conference on Port and Ocean Engineering under Arctic Conditions. Luleå, Sweden, POAC09-139.

Lindqvist, G., 1989. A straightforward method for calculation of ice resistance of ships. In: Proceedings of the 10th International Conference on Port and Ocean Engineering under Arctic Conditions. Vol. 2. Luleå, Sweden, pp. 722–735.

Løset, S., Kanestrøm, Ø., Pytte, T., 1998. Model tests of a submerged turret loading concept in level ice, broken ice and pressure ridges. Cold Regions Science and Technology 27, 57–73.

Lundamo, T., Bonnemaire, B., Jensen, A., Gudmestad, O. T., 2008. Back-calculation of the ice load applying on a moored vessel. In: Proceedings of the 19th IAHR International Symposium on Ice. Vol. 2. Vancouver, British Columbia, Canada, pp. 861–872.

Moran, K., Backman, J., Farrell, J. W., 2006. Deepwater drilling in the Arctic Ocean's permanent sea ice. In: Proceedings of the Integrated Ocean Drilling Program. Vol. 302. Edinburgh.

Murray, J., Le Guennec, S., Spencer, D., Yang, C. K., Yang, W., 2009. Model tests on a SPAR in level ice and ice ridge conditions. In: Proceedings of the 28th International Conference on Ocean, Offshore and Arctic Engineering. Honolulu, Hawaii, USA, OMAE2009-79733.

Murray, J. J., Spencer, D. S., 1997. A simulation model for a turret moored tanker in pack ice cover. In: Proceedings of the 16th International Conference on Offshore Mechanics and Arctic Engineering. Vol. 4. Yokohama, Japan, pp. 135–146.

Nansen, F., 1999. Farthest north. Modern library, New York.

Nevel, D. E., 1961. The narrow free infinite wedge on an elastic foundation. Research report 79, U.S. Army Cold Regions Research and Engineering Laboratory.

Nevel, D. E., 1992. Ice forces on cones from floes. In: Proceedings of the IAHR Symposium on Ice. Banff, Alberta, Canada, pp. 1391–1404.

Norman, P., Lochte, G., Hurley, S., 2008. White Rose: Overview of current development and plans for future growth. In: Proceedings of the Eighteenth International Offshore and Polar Engineering Conference. Vol. 1. Vancouver, BC, Canada, pp. 206–214.

Pilkington, R., Keinonen, A., Sheikin, I., 2006. Ice Observation adn Forecasting During the Arctic Coring Project, August - September 2004. ICETECH06-171-RF.

Prirazlomnoye Oilfield, 2010. Cited: July 20th, 2010.
URL `http://www.offshore-technology.com/projects/Prirazlomnoye/`

Qu, Y., Yue, Q., Bi, X., Kärnä, T., 2006. A random ice force model for narrow conical structures. Cold Regions Science and Technology 45, 148–157.

Ralston, T. D., 1977. Ice force design considerations for conical offshore structures. In: Proceedings of the 4th International Conference on Port and Ocean Engineering under Arctic Conditions. Vol. 2. St. John's, New Foundland, Canada, pp. 741–752.

Ralston, T. D., 1979. Plastic limit analysis of sheet ice loads on conical structures. In: Tryde, P. (Ed.), Physics and Mechanics of Ice. International Union of Theoretical and Applied Mechanics. Symposium Copenhagen. Springer, Berlin.

Runeberg, R., 1888/1889. On Steamers for Winter Navigation and Ice-breaking. Proceedings of Institution of Civil Engineers 97, 277–301.

Shkhinek, K. N., Bolshev, A. S., Frolov, S. A., Malyutin, A. A., Chernetsov, B. A., 2004. Modeling of level ice action on floating anchored structure concepts for the Shtokman field. In: Proceedings of the 17th IAHR International Symposium on Ice. Vol. 2. St. Petersburg, Russia, pp. 84–95.

Toyama, Y., Yashima, N., 1985. Dynamic response of moored conical structures to a moving ice sheet. In: Proceedings of the 8th International Conference on Port and Ocean Engineering under Arctic Conditions. Vol. 2. Narssarssuaq, Greenland, pp. 677–688.

Tseng, J., Allyn, N., Charpentier, K., 1987. Computer software to analyze ice interaction with moored ships. In: Proceedings of the 9th International Conference on Port and Ocean Engineering under Arctic Conditions. Fairbanks, Alaska, USA, pp. 607–617.

Valanto, P., 1992. The icebreaking problem in two dimensions: experiments and theory. Journal of Ship Research 36 (4), 299–316.

Valanto, P., 2001. The resistance of ships in level ice. SNAME Transactions 109, 53–83.

Wright, B., 1999. Evaluation of Full Scale Data for Moored Vessel Stationkeeping in Pack Ice. PERD/CHC report 26-200.

Wright, B., 2000. Full Scale Experience with Stationkeeping Operations in Pack Ice. PERD/CHC report 25-44.

Yue, Q., Qu, Y., Bi, X., Kärnä, T., 2007. Ice force spectrum on narrow conical structures. Cold Regions Science and Technology 49, 161–169.

Chapter 3

Model testing of the Arctic Tandem Offloading Terminal - Tandem mooring forces and relative motions between vessels

By Vegard Aksnes, Basile Bonnemaire, Sveinung Løset and Christian Lønøy

Proceedings of the 19th IAHR International Symposium on Ice, Vancouver, British Columbia, Canada, Vol. 2, pp. 687-698, 2008.

19th IAHR International Symposium on Ice
"Using New Technology to Understand Water-Ice Interaction"
Vancouver, British Columbia, Canada, July 6 to 11, 2008

Model Testing of the Arctic Tandem Offloading Terminal – Tandem Mooring Forces and Relative Motions between Vessels

Vegard Aksnes[1], Basile Bonnemaire[2,1], Sveinung Løset[1] and Christian Lønøy[1]
[1]*Norwegian University of Science and Technology (NTNU), Trondheim, Norway.*
[2]*Barlindhaug Consult AS, Tromsø, Norway.*
vegard.aksnes@ntnu.no, basile.bonnemaire@barlindhaug.no, sveinung.loset@ntnu.no and lonoy@stud.ntnu.no

The Arctic Tandem Offloading Terminal (ATOT) is an innovative concept for offloading of hydrocarbons in ice-infested waters. The concept includes an offloading icebreaker (OIB) with a submerged turret loading system and a shuttle tanker. The OIB is moored to a turret buoy, and shuttle tankers moor at the stern of the OIB for offloading. The ATOT concept has been tested in model scale in the Large Ice Model Basin at HSVA in Hamburg, Germany. This paper discusses results from two tests in level ice and ridges; that is, the measured forces in the tandem mooring system between the vessels as well as the relative motions between the tanker and the OIB. The interaction between the ATOT and ridges is studied and it is seen that the largest tandem mooring forces are occurring during ridge penetration. The qualitative behaviour of the ATOT during slow changes of ice drift direction is analysed.

1. Introduction

The Arctic Tandem Offloading Terminal (ATOT) is a concept for offloading of hydrocarbons in ice-infested waters. The concept includes an offloading icebreaker (OIB) which is moored to a submerged turret and a shuttle tanker which is moored at the stern of the OIB, see Figure 1. The ATOT concept was tested in June 2007 in the Large Ice Model Basin at HSVA in Hamburg, Germany and the general results from these tests are described by Jensen et al. (2008). The tests were performed in level ice, ice ridges and broken ice. Two other companion papers describe different aspects of the model tests of ATOT; the turret mooring forces caused by ridges are discussed in Bonnemaire et al. (2008a) and the subsurface ice interaction under the OIB is analysed in Bonnemaire et al. (2008b). This paper focuses on the measured forces in the tandem mooring system between the vessels and the relative motions between the OIB and the tanker in level ice and ridges.

The tandem mooring system is explained in full scale and in model scale. Further, the ice conditions and the test runs are described. Instrumentation and processing procedures are then followed by results and a discussion about the forces in the tandem mooring system and their connections to ice conditions and relative vessel motions.

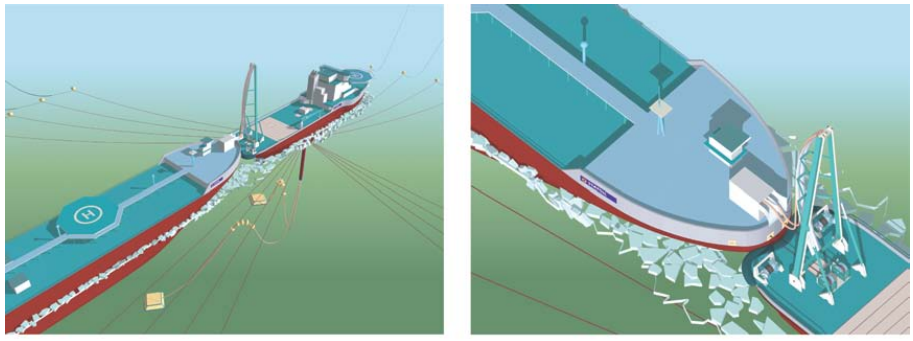

Figure 1. a) The ATOT concept in full scale. **b)** Close-up view of the tandem mooring system in full scale.

2. Model setup

The Large Ice Model Basin at HSVA is 78 m long, 10 m wide and 2.5 m deep. Froude scaling was used because of the importance of gravitational and inertial forces, see Ashton (1986), and the scaling ratio was $\lambda = 24$. In this text, all presented values are scaled to represent full scale data. The length between perpendiculars of the OIB was 109 m, there were two different draughts, 12 and 14 m, for open water and ice respectively and thus the beam varied between 26 and 30 m. It had a displacement of 21000 t and was equipped with reamers to increase manoeuvrability and to reduce the ice forces on the tanker. The length of the tanker was 288 m, the beam and draught was 35.5 and 15 m respectively, and it had a displacement of 108000 t. The OIB was equipped with four azimuth propellers with a power of 7.1 MW each, two at the bow and two at the stern, while the tanker was passive, with no propulsion. Further details regarding the vessels can be found in Jensen et al. (2008).

For practical reasons, the turret mooring system of the OIB was modelled with a dry mooring system. The stiffness of the mooring system was different in the two test runs. In test run 3100 it was 2.2 MN/m and in test run 4100 it was 4.4 MN/m, adapted to 150 m and 40 m water depth respectively. In the model tests the ice sheet was frozen to the tank walls and the OIB was pulled by the mooring system through the ice to simulate ice drift. More details about the dry mooring system and the related mooring forces can be found in Bonnemaire et al. (2008a).

The tandem mooring system has two basic operational modes, distant loading and close loading. Distant loading is intended for loading in open water and light ice conditions, that is, ice coverage of less than 20 %, while close loading is the preferred operational mode in medium and severe ice conditions.

The tandem mooring system consists in full scale of two mooring lines which are fixed to the bow of the tanker and are reeled on to two hawser winches located at the stern of the OIB as shown in Figure 1. The preliminary design of each of the winches is a pull in capacity of 2 MN, a braking capacity of 3 MN and a payout rate of 1 m/s. It is possible to disconnect the mooring lines and the risers within seconds. The loading system consists of two 20 inch risers with a transfer rate of 9000 m^3/h, which makes a loading time of 6 hours achievable for the present tanker. The ice drift is often tidal driven and changes of ice drift direction are believed to cause the highest mooring forces, as reported by Danielewicz et al. (1995) and Comfort et al. (1999). By loading within half a tidal cycle it is therefore assumed that the worst scenarios are avoided. The influence of changes of ice drift direction on different loading concepts is discussed in Bonnemaire (2006). During changes of ice drift direction, the tandem mooring system will be active and provide a constant pretension in the mooring lines as long as there is no opening between the vessels.

In the model tests, the tanker was moored in close tow at the notch of the OIB. The notch was equipped with a fender system which consisted of a row of thick cylindrical fenders and a row of thinner block fenders as shown in Figure 2. The stiffness of the fender system in surge was tested in cold conditions and estimated to be 16.1 MN/m at 0 - 0.4 m penetration and 164 MN/m at 0.4 - 0.5 m penetration. The model scale mooring system consisted of two steel wires which were connected to load cells mounted on hinges at the stern of the OIB. The wires ran through steel guiders at the tanker bow and to a weight system in the tanker, as shown in Figure 3. One meter of each of the wires was replaced with synthetic rope to model the elasticity of the mooring lines.

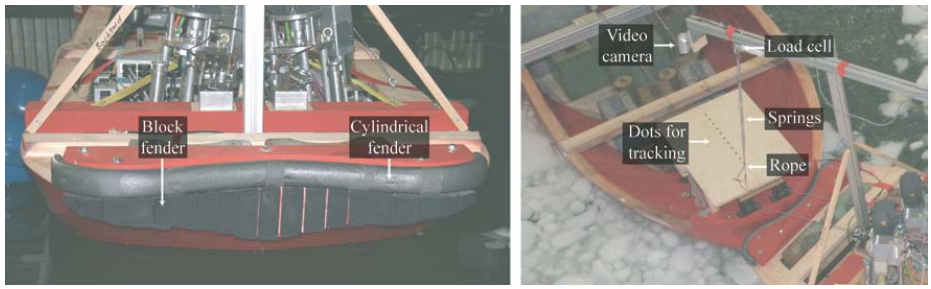

Figure 2. The fender system and the setup for measuring the relative motions.

The model of the tandem mooring system worked as follows:

- The weight system consisted of two times two weights. The upper weights were 2 x 1.2 MN and modelled the pretension in the lines, while the lower weights were 2 x 1.8 MN, so that the total weight represented the breaking capacity of the winches.
- When there was a distance between the tanker bow and the fender system both weights were lifted with a distance between them. The mooring line forces were then constant and did not depend on the distance from the tanker bow to the fender, as long as there was no contact. This simulated the payout of the winches at constant breaking force.
- At the moment when there was contact between the tanker bow and the fender, there was also contact between the lower weight and the floor of the tanker.
- As the tanker bow compressed the fender, the distance between the weights decreased and finally the upper weight was in contact with the lower one. At this point, the mooring lines would be slack, the mooring forces would be zero and the tanker bow would have penetrated into the stiffer part of the fender.
- The weight system did not model the pretension correctly during changes of drift direction. When the vessels were in contact with each other and there was a large yaw angle, one mooring line became slack, while the other was subjected to higher tension than the pretension.

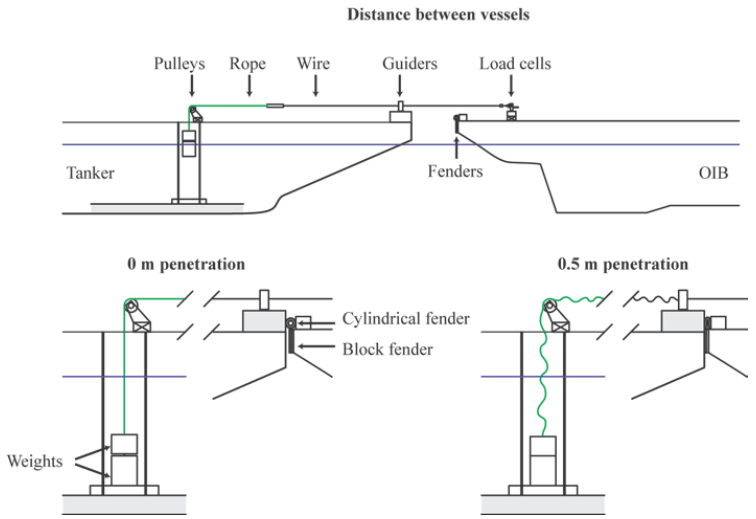

Figure 3. The tandem mooring system as modelled in the ice tank.

3. Test runs

The ATOT concept was tested in unbroken level ice and ridges, in level ice and ridges with a broken channel nearby and in broken ice with a drift speed of 0.5 m/s. The ice drift was straight or slowly varying in level ice and broken ice, but always straight in ridges. In this text, only intact level ice and ridges are considered. Figure 4 shows sketches of the vessel traces in each of the test runs.

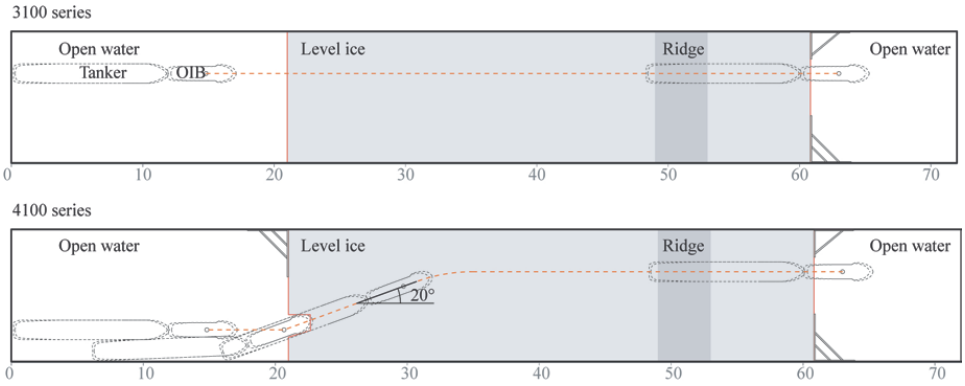

Figure 4. The figure shows the traces of the vessels from the test runs.

The model ice was prepared as described by Evers and Jochmann (1993) and the ice ridges by pushing level ice against a beam as outlined by Høyland et al. (2001). The main characteristics of the level ice and the ridges are summarized in Table 1. Both ridges had a consolidated layer of approximately two level ice thicknesses, in order to model first-year ridges.

Table 1. The main characteristics of the level ice and the ridges are listed in the table below. The notation is as follows: h_i is level ice thickness, σ_f is flexural strength, h_k is ridge keel depth, h_s is ridge sail height and w_k is ridge width.

Test run	h_i [m]	σ_f [kPa]	h_k [m]	h_s [m]	w_k [m]
3100	1.03	720	13.0	2.2	96
4100	1.15	480	14.9	1.9	96

4. Measurements

More than 60 different channels were recorded during each test run. The most relevant measurements regarding the tandem mooring system will be described here, meaning the measurements of the relative horizontal and vertical motion of the vessels as well as the forces in the tandem mooring system.

- The forces in each of the mooring lines in the tandem system were measured with uniaxial load cells of type HBM U9B and sampled at a frequency of 100 Hz. In the time series plots later in the text, “port” and “starboard” will refer to the mooring lines on port and starboard side, respectively.
- The motion of the OIB was measured in all 6 degrees of freedom, see Figure 5 for definition of the modes of rigid body motion, but the absolute tanker motions were not measured directly. However, the relative horizontal and vertical motions between the vessels were measured as described below:
- The relative horizontal motions between the vessels were recorded with a video camera fixed at the stern of the OIB and looking downwards on a dotted plate fixed in the bow of the tanker, see Figure 2. The motion of the dots was then tracked with the free software

Video Spot Tracker developed by the Department of Computer Science, University of North Carolina at Chapel Hill. By fitting a straight line to the dots, the relative surge, sway and yaw motions of the tanker relative to the OIB were found. The motions were found in a coordinate system fixed to the uncompressed fender, as shown in Figure 5. It can be seen that relative surge is negative when there is space between the tanker bow and the midpoint of the fender system, while relative surge is positive when the fender system is compressed.

- The relative vertical motion was measured with a mechanical spring system. Three springs were connected in series, with one end fixed to a load cell which was mounted on a beam, fixed to the OIB. The vessels were aligned and the other end of the system of springs was connected to a point in the bow of the tanker directly under the load cell. The stiffness of the springs was estimated and by recording the force in the springs, we found the relative vertical motion between the vessels by applying Hooke's law. From this, the pitch and heave motion of the tanker could be found. In our coordinate system, the pitch angle is increasing when the bow is moving downwards.

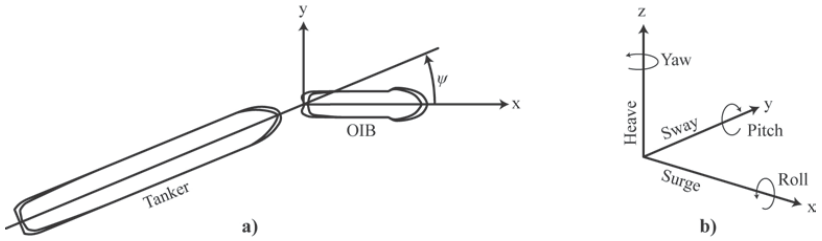

Figure 5. The sketches show **a)** the coordinate system fixed to the centre of the uncompressed fender at the stern of the OIB, which the tanker bow moves relative to and **b)** the six modes of rigid body motion.

5. Results

This section contains plotted time series of the total tandem mooring forces as well as the mooring forces in each individual mooring line. In Figures 6 and 7, the number ❶ indicates when the bow of the tanker entered level ice and the moment when the bow of the tanker started to penetrate the ridge is marked with the number ❷. Note that both vessels are embedded in ice at the end of the time series. In addition to mooring forces, the relative yaw angle and the relative surge between the OIB and the tanker in test run 4100 are plotted. The pitch motion of the tanker and the OIB is given for test run 3100. Key numbers from each of the test runs are highlighted in the text, and the maximal tandem mooring forces are summarized in Table 2.

Table 2. Maximal tandem mooring forces in individual mooring lines and in total from both test runs.

Test run	Max mooring forces in level/broken ice			Max mooring forces in ridges		
	Port [MN]	Starboard [MN]	Total [MN]	Port [MN]	Starboard [MN]	Total [MN]
3100	2.4	2.0	3.7	2.6	3.3	5.9
4100	3.9	3.9	7.8	3.2	3.0	6.2

Test run 3100

The tandem mooring forces from test run 3100 are shown in Figure 6. The maximal total mooring force was 3.7 MN and 5.9 MN in level ice and the ridge, respectively. The mean total mooring force was calculated from $t = 800$ s to $t = 1800$ s, that is, the time period when the tanker was totally embedded in level ice, giving a mean of 3.0 MN with standard deviation 0.4 MN. The relative yaw angle is not plotted since the ice drift was straight throughout the entire test run. The lower plot of Figure 6 shows the pitch motion of both vessels.

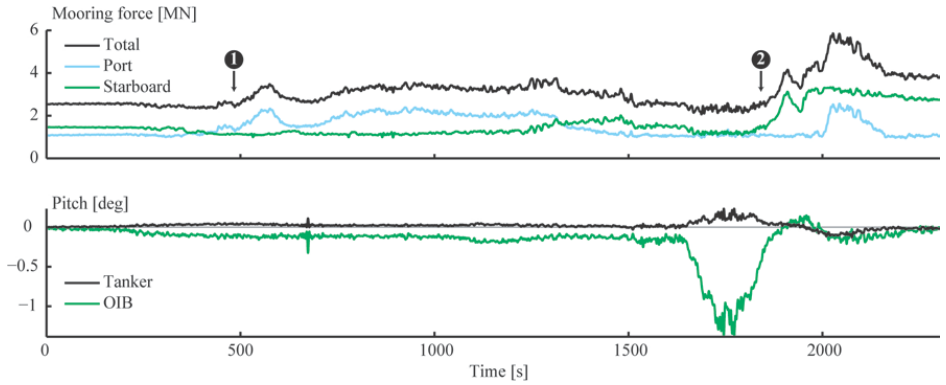

Figure 6. Tandem mooring forces between the vessels and pitch angle of both vessels during test run 3100.

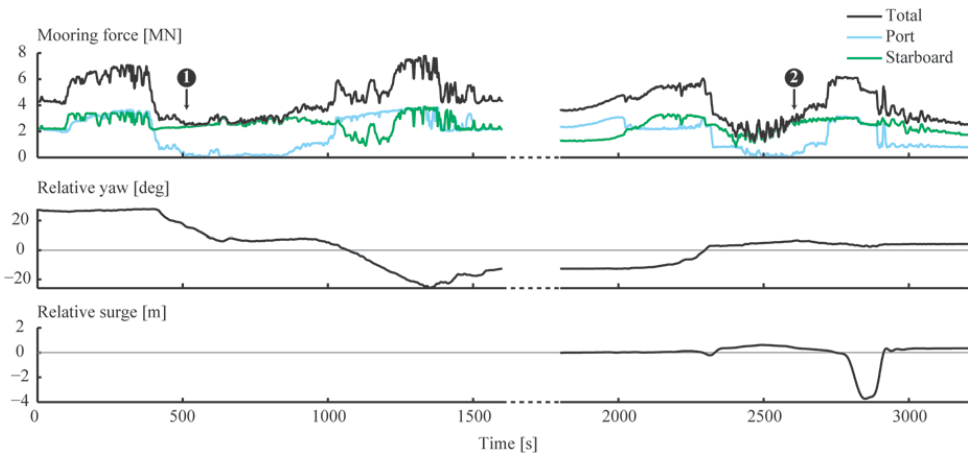

Figure 7. Tandem mooring forces, relative yaw and relative surge between the vessels during test run 4100.

Test run 4100

In Figure 7, the recorded time series of the tandem mooring forces and the video tracked relative yaw angle from test run 4100 are plotted. The test run was temporarily stopped before the OIB

entered the ridge, thus there is a gap in the time series indicated by a dashed interval on the time axis. The maximal total mooring force was 7.9 MN in level ice and 6.2 MN in the ridge. The extreme relative yaw angles were 28º and -26º. The figure also shows the relative surge between the tanker and the OIB during the last part of test run 4100. The largest displacement was 3.7 m. Figure 8 shows a drawing sequence of how the heading of the vessels changed during a change of ice drift direction of 20º.

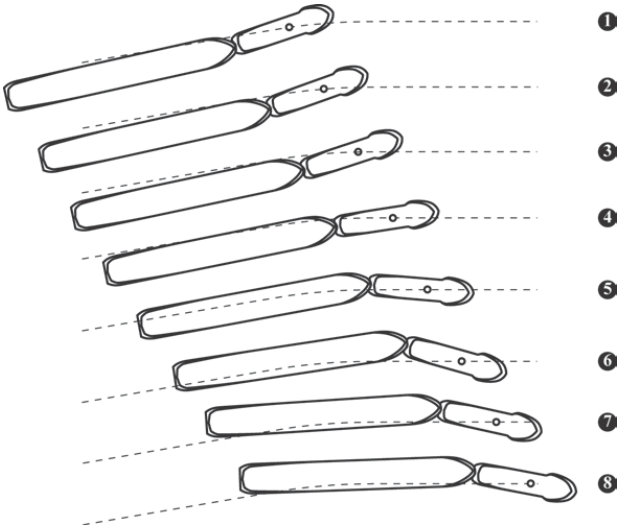

Figure 8. Drawing sequence of the vessel heading and alignment during a change of ice drift direction. The ice drift direction is indicated by a dotted line and the time step between each drawing is 122 seconds.

6. Discussion

The discussion will be divided into three parts; ridge interaction in test runs 3100 and 4100, large yaw motions during test run 4100 and mean tandem mooring forces in the part of test run 3100 where both vessels were embedded in level ice.

Interaction with ridges

During both test runs, the total tandem mooring force increased significantly when the tanker started to penetrate the ridge. In test run 3100, the largest total tandem mooring force was 5.9 MN, which is just below the total capacity of the hawser winches. Consequently, there was no significant relative surge motion between the tanker and the OIB.

The situation was different in test run 4100. The maximal total tandem mooring force was then 6.5 MN and this is above the capacity of 6 MN. At this event, both weights were lifted off the tanker floor and the distance between the vessels increased, as can be seen in Figure 7. In full scale, the winches would have started to pay out. The largest relative distance between the vessels was 3.7 m. However, the tanker came back to the OIB before the OIB stopped at the end

of the basin. This means that in this case it would not have been necessary to start the disconnection procedure in a corresponding full scale situation.

The large tandem mooring forces were induced by large ridge forces on the tanker. They were larger in test run 4100 than in 3100 and this indicates that the forces exerted by the ridge were more severe in the former. When the OIB penetrated the ridges, it was exposed to large vertical ice forces because larger vertical forces are needed to fail the consolidated layer of a ridge in bending than to fail level ice. This resulted in pitch motions of the vessel. In test runs 3100 and 4100 the maximal pitch angle of the OIB was -1.4º and -1.9º, respectively. The volume of the ridge keel in test run 4100 was larger than it was in 3100, which may have caused larger vertical ice forces and hence larger pitch motions. The tanker pitched considerably less than the OIB and this was mainly because the ridge already had failed, but also because it has a larger restoring capacity due to larger water plane area.

The pitch motion of the OIB in ridges reduced the effect of the reamers. In fact, the effective beam of the OIB was estimated to be 28.5 and 28 m in the ridges in test runs 3100 and 4100, respectively, compared to 30 m in level ice. This caused a smaller channel for the tanker. The contact area between intact ice and the tanker hull increased and thus larger forces were induced in the tandem mooring system.

Spencer et al. (1997) studied model tests of a tanker moored behind a terminal and the effect of the terminal size on the mooring forces. They presented a relationship between peak mooring force reduction and the ratio between terminal diameter and the beam of the tanker. However, it is difficult to use the results by Spencer et al. (1997) to compare the difference in mooring forces between 3100 and 4100, since the difference in effective beam of the OIB is less than 2 %. The difference in the tandem mooring forces could be caused by the fact the ridge in 4100 was bigger and by inhomogeneities in the ridge, in addition to the difference in width of the wake after the OIB.

Slow change of ice drift direction

During the first part of test run 4100 there was a slow change of ice drift direction of 20º. A drawing sequence of the heading of both the OIB and the tanker during this drift change is shown in Figure 8. A qualitative description of this event follows:

- The OIB met the new drift direction first. It experienced local ice forces caused by bending failure in the bow area and by crushing failure further aft. Crushing forces are in general larger than forces caused by bending failure and in combination with use of azimuth propellers, this made it possible for the OIB to turn, see steps 3 to 5 in Figure 8.
- The yaw motion of the OIB pulled the tanker by the tandem mooring system and the tanker slowly started to change heading. However, the inertia of the tanker and the fact that the tanker had a long vertical sided parallel body, forced the tanker to continue in its old path and thus pushed the stern of the OIB as can be seen in step 6 in Figure 8.
- At this time the tanker bow reached the port side of the wake after the OIB. In the starboard bow area of the tanker, the ice was mainly broken by the OIB, giving a low lateral pressure. In front of amidships on the starboard side of the tanker, intact ice was met and combined crushing and buckling failure against the tanker hull resulted in large ice forces, see Figure 9. On the port side of the tanker, the ice was partly broken. The

milder ice conditions in the bow area and on the port side in combination with crushing on the starboard side of the hull, made the tanker vane efficiently, see steps 6 to 8 in Figure 8. At step 8, the tanker was almost aligned with the new drift direction.

- It should be noted that there was no propulsion on the tanker, and with for instance azimuth propellers, it might have turned more efficiently.

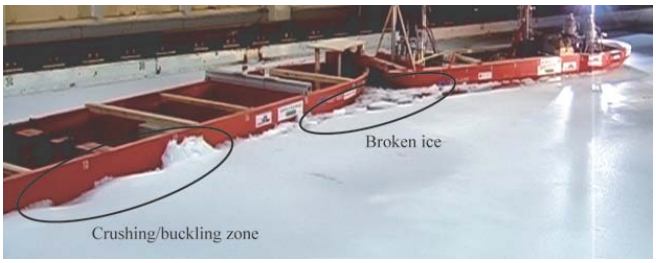

Figure 9. The picture shows the crushing/buckling zone on the hull of the tanker during the slow change of ice drift direction during test run 4100. An area with broken ice is indicated to illustrate the milder ice conditions in the bow of the tanker.

The plot in Figure 7 shows large mooring forces. However, the model of the tandem mooring system did not represent the full scale system well with respect to mooring forces when there was significant yaw between the vessels. It can be seen that during moderate yaw motions, one line was slack, while the other line was exposed to high tension. In full scale, the hawser winches would have been active and provided constant tension, evenly distributed in the mooring lines. At about 1300 s, there was a large relative yaw (up to 26º) between the vessels and the distribution of mooring forces between the mooring lines was even. Both weights were lifted off the tanker floor because of the large yaw angle, but the vessels stayed close to each other and the disconnection procedure would not have been initiated in full scale.

The mooring forces at this incident were larger than what one would expect from the weight system. This can be explained by the friction between the mooring lines and the guiders, both made of steel. Using the standard formula for the friction force between a rope and a cylindrical pole, see for instance Irgens (2005), the friction force F_{fric} between one mooring line and a guider can be expressed as

$$F_{fric} = F_{lc}(1 - e^{-\mu\psi}) \qquad \textbf{[1]}$$

In Equation [1], F_{lc} is the force measured in the load cell. A typical static friction coefficient between steel and steel is μ = 0.6. The measured force in the load cell was 3.9 MN and the relative yaw angle was approximately ψ = 25º (0.44 rad). An approximate value for the friction force is then F_{fric} = 0.9 MN. This example illustrates why the measured forces were higher than what they should be according to the weight system. The friction between the mooring lines and the guiders could have been reduced in model scale by using pulleys.

Mean tandem mooring forces

The mean total mooring force and standard deviation was estimated for the part of test run 3100 where the whole tanker is embedded in level ice and the drift direction was straight. This gave a mean total mooring force of 3.0 MN, which is half of the capacity. The standard deviation was 0.4 MN. The period over which the mean and standard deviation was estimated corresponds to approximately two times the length of the tanker.

7. Conclusions

Results from model tests of a tandem mooring system in level ice and ridges have been reported. The main findings were the following:

- The tandem mooring loads were higher in ridges than in level ice when the ice drift was straight.
- The capacity of the winches was overloaded once, due to large tandem mooring forces induced by interaction between the tanker and a ridge.
- The maximal relative distance between the vessels during this incident was 3.7 m. The tanker bow came back to the stern of the OIB while the tanker still was in the ridge, i.e. the disconnection procedure would not have been initiated in full scale.
- The OIB pitched significantly in the ridges and the effects of the reamers were reduced. This caused high tandem mooring forces during ridge interaction.
- The model of the full scale tandem mooring system did not work well with respect to mooring loads when there was relative yaw between the vessels.
- The tanker vaned efficiently when there was a slow change of ice drift direction, but over steered the OIB before they aligned.

Acknowledgements

The work described in this publication was supported by the European Community's Sixth Framework Program through the grant to the budget of the Integrated Infrastructure Initiative HYDRALAB III, Contract no. 022441(RII3). The authors would like to thank the Hamburg Ship Model Basin (HSVA), especially the ice tank crew, for the hospitality, technical and scientific support and the professional execution of the test program in the Research Infrastructure ARCTECLAB. We would also like to thank StatoilHydro for funding of the physical models. The video tracking was done with *Video Spot Tracker*, developed by the University of North Carolina at Chapel Hill and is available at URL: http://www.cs.unc.edu/Research/nano/cismm /download/spottracker/video_spot_tracker.html. The opportunity to use this software is highly appreciated.

References

Ashton, G. D., ed., 1986. *River and Lake Ice Engineering*. Water Resources Publications, Book Crafters Inc., Chelsea, Michigan.

Bonnemaire, B., 2006. Arctic Offshore Loading Downtime Due to Variability in Ice Drift Direction. *The Journal of Navigation*, vol. 59, pp. 9-26.

Bonnemaire, B., Lundamo, T., Evers, K. U., Løset, S. and Jensen, A., 2008a. Model Testing of the Arctic Tandem Offloading Terminal – Mooring Ice Ridge Loads. *Proceedings of the 19th International Symposium on Ice*. Vancouver, British Columbia, Canada.

Bonnemaire, B., Lundamo, T., Jensen, A. and Rupp, K. H., 2008b. Subsurface Ice Interactions under a Moored Offloading Icebreaker. *Proceedings of the 19th International Symposium on Ice.* Vancouver, British Columbia, Canada.

Comfort, G., Singh, S. and Spencer, D., 1999. *Evaluation of Ice Model Test Data for Moored Structures*. Report submitted to the National Research Council of Canada, PERD/CHC Report 26–195, 77 p.

Danielewicz, B. W., Jolles, W. H., Dunderdale, P., Keinonen, A., Browne, R. P., Spencer, D. and Jones, S. J, 1995. *Loading of Tankers from Arctic Platforms.* Prepared for Transport Development Centre, Policy and Coordination, Transport Canada, Report no. TP 12531E, Montreal Canada.

Evers, K. U. and Jochmann, P., 1993. An Advanced Technique to Improve the Mechanical Properties of Model Ice Developed at the HSVA Ice Tank. *Proceedings of the 12th International Conference on Port and Ocean Engineering under Arctic Conditions.* Hamburg, Germany, pp. 877-888.

Høyland, K. V., Jensen, A., Liferov, P., Heinonen, J., Evers, K. U., Løset, S. and Määttänen, M., 2001. Physical Modelling of First-Year Ridges – Part I: Production, Consolidation and Physical Properties. *Proceedings of the 16th International Conference on Port and Ocean Engineering under Arctic Conditions, Vol. 3*. Ottawa, Canada, pp. 1483-1492.

Irgens, F., 2005. *Statikk.* Tapir akademiske forlag, Trondheim, Norway.

Jensen, A., Bonnemaire, B., Rupp, K. H., Løset, S., Breivik, K. G., Evers, K. U., Ravndal, O., Aksnes, V., Lundamo, T. and Lønøy, C., 2008. First Ice Tank Model Testing of the Arctic Tandem Offloading Terminal. *Proceedings of the 19th International Symposium on Ice*. Vancouver, British Columbia, Canada.

Spencer, D., Jones, S. J. and Jolles, W., 1997. Effect of ice drift angle on a mooring hawser. *Proceedings of the International Conference on Offshore Mechanics and Arctic Engineering (OMAE)*, Yokohama, Japan, pp. 127–133.

Chapter 4

Analysis of the behaviour of a moored ship in variable ice drift

By Vegard Aksnes and Basile Bonnemaire

Proceedings of the 20th International Conference on Port and Ocean Engineering under Arctic Conditions, Luleå, Sweden, POAC09-25, 2009.

POAC 09
Luleå, Sweden

Proceedings of the 20th International Conference on
Port and Ocean Engineering under Arctic Conditions
June 9-12, 2009
Luleå, Sweden

POAC09-25

ANALYSIS OF THE BEHAVIOUR OF A MOORED SHIP IN VARIABLE ICE DRIFT

Vegard Aksnes[1] and Basile Bonnemaire[2,1]
[1] Norwegian University of Science and Technology, Trondheim, Norway
[2] Barlindhaug Consult, Tromsø, Norway

ABSTRACT

A challenge with moored ships in ice is their response and the mooring forces caused by changes in ice drift direction. Variability in ice drift direction is mostly driven by variations in speed and direction of current and wind. In this paper, the behaviour of a moored ship in level ice is studied in several ice drift scenarios, based on model tests performed at the Hamburg Ship Model Basin (HSVA). Three types of ice drift scenarios are studied; straight drift, drift along circular arcs and sudden changes in drift direction. Ice behaviour, vessel response and mooring forces are reported and discussed for the different ice drift scenarios. It was found that ice failed along large parts of the ship's waterline, due to changes in ice drift direction. The waterline geometry of the ship varied a lot around its perimeter and thus ice failed in various failure modes at different parts of the hull. The failure modes changed with the relative angle between the vessel heading and the ice drift direction, and influenced the response of the ship and the mooring forces. The magnitude of the peak mooring force caused by drifting level ice was comparable to the peak mooring force caused by a relatively large first-year ice ridge. Actions by drifting level ice should be considered as a possible design mooring load for moored ships in certain areas.

INTRODUCTION

As hydrocarbon exploration is moving northwards there is an increased interest in concepts involving moored ships, applicable in areas with sea ice. Sea ice will often drift along paths with varying direction, due to changes in current and wind direction. When a ship is moored in such ice conditions, ice can possibly approach from any direction and interact with the vessel. Since the angle of a hull in the waterline can change from nearly 90° amidships to a low angle such as 20° in the bow, the interaction geometry will vary with the relative ice drift direction.

This variation will induce different ice failure modes along the hull and therefore also different ice forces.

In this paper we analyse failure modes of level ice drifting against a moored icebreaker from various directions and the corresponding vessel response and mooring forces. The analysis is based on observations and measurements from model tests of the Arctic Tandem Offloading Terminal (ATOT) at Hamburg Ship Model Basin (HSVA) in Germany in 2007. Details about the concept and the tests are given by Jensen et al. (2008), Bonnemaire et al. (2008a,b) and Aksnes et al. (2008).

We first explain the model test setup and the ice drift scenarios. Observed failure modes, measured vessel response and mooring forces are reported next. Then follows a discussion on these three issues and how they are related. Some conclusions are drawn in the end.

MODEL TEST SETUP

General

The model tests were performed in the Large Ice Model Basin at HSVA. This basin is 78 m long, 10 m wide and 2.5 m deep. The model was towed through the tank, simulating drifting ice driven by current. Froude scaling was used because of the importance of gravitational and inertial forces (Ashton, 1986), with scaling ratio $\lambda = 24$. All values presented in this paper are scaled to represent full scale data.

Two sheets of model ice were grown according to a preparation technique developed at HSVA, described by Evers and Jochmann (1993). Mean values over the ice sheet for flexural strength σ_f and ice thickness h_i are given in Table 1. The compressive strength σ_c was not measured in the tests, but according to Evers and Jochmann (1993), the ratio σ_c/σ_f is usually in the range 2-2.8 at HSVA. Tests were performed in intact level ice and in level ice with a channel of broken ice nearby.

Table 1. The main parameters of the ice drift scenarios in full-scale values. Mean ice thickness is h_i, σ_f is mean flexural strength, k is mooring stiffness, R_{ice} is ice drift curvature radius, v_{ice} is ice drift speed and a_{ice} is ice drift acceleration. Slow changes of ice drift direction along circular arcs are denoted ARC, while sudden changes of ice drift direction are denoted COD.

Ice sheet	**Drift scenario**	h_i [m]	σ_f [kPa]	k [MN/m]	R_{ice} [m]	v_{ice} [m/s]	a_{ice} [mm/s^2]
1000	Straight (1110)	1.06	580	4.4	-	0.5	-
	30° ARC (1220-2)	1.06	580	4.4	100	0.5	-
	30° ARC (1220-4)	1.06	580	4.4	100	0.5	-
	60° ARC (1220-3)	1.06	580	4.4	100	0.5	-
	90° COD (1210)	1.06	580	4.4	-	$0-0.5$	0.22
	90° COD (1220-1)	1.06	580	4.4	-	$0-0.5$	0.22
2000	Straight (2110-2)	0.94	360	2.2	-	0.5	-
	30° ARC (2110-1)	0.94	360	2.2	100	0.5	-
	30° ARC (2200-3)	0.94	360	2.2	100	0.5	-
	60° ARC (2200-1)	0.94	360	2.2	100	0.5	-
	60° ARC (2200-2)	0.94	360	2.2	100	0.5	-

Vessel properties

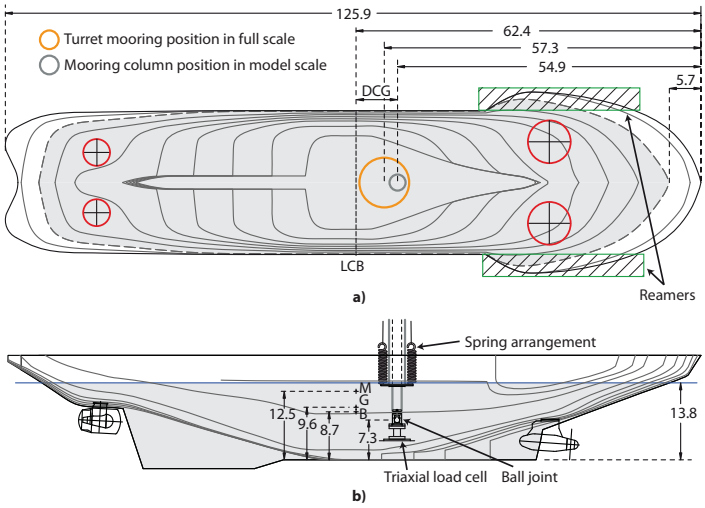

Figure 1. Line drawings of the vessel, with full-scale dimensions in metres. The grey area is the submerged part of the hull. The design is preliminary and done by the Finnish naval architect company ILS.

The tested vessel was a moored icebreaker with a spoon-shaped bow and reamers. Reamers are beam extensions in the bow area intended for channel widening and increased manoeuvrability in ice (Fig. 1a. Line drawings are shown in Fig. 1a and b and the main dimensions of the ship are summarized in Table 2. Four azimuth thrusters were installed on the vessel, two fore and two aft. The thrusters were used actively in most of the tests, with some exceptions.

In full scale, the vessel will be moored on a disconnectable submerged turret buoy with a spread mooring system. Such a mooring system can be used in model tests, but is difficult to use when modelling changes of ice drift direction. A dry mooring system, described in detail by Bonnemaire et al. (2008a), was therefore used. A vertical column was attached to the vessel with a ball joint, see Fig. 1b, such that the vessel was free to rotate around all its three axis and to heave. The column was mounted to a set of linear springs, giving restoring forces in the horizontal plane. Vertical mooring forces were not modelled. Further, the dry mooring system was fixed to a carriage which could move both longitudinally and transversally, thus being able to simulate changes in ice drift direction. Two different spring stiffness's k were used, 2.2 and 4.4 MN/m, applied for water depths of 150 and 40 m, respectively.

Mooring forces were measured by a triaxial load cell which was mounted between the ball joint connection to the mooring column and the bottom of the vessel as shown in Fig. 1b). To obtain mooring reaction forces induced by water and ice, thrust was subtracted from the measured forces in the following way

$$\mathbf{F}^{corr} = \mathbf{F}^{meas} - \tau, \tag{1}$$

where $\mathbf{F}^{meas}$, $\mathbf{F}^{corr}$, and τ are measured and corrected mooring force and thrust, respectively. The longitudinal and transverse components of $\mathbf{F}^{corr}$ in the ship's referential frame are denoted F_{long} and F_{trans} and the total horizontal mooring force is $F_{tot} = (F_{long}^2 + F_{trans}^2)^{1/2}$.

Table 2. Main dimensions of the vessel. *DCG* is the horizontal distance between the attachment point of the mooring system and the vessel's centre of gravity.

Parameter	**Value**
Length overall [m]	133
Length between perpendiculars (L_{pp}) [m]	109
Beam [m]	30
Draught [m]	14
Volume displacement [m^3]	21000
Stem angle [°]	20
Average flare angle [°]	25
Average buttock angle [°]	18
Turret position full scale (DCG/L_{pp})	5%
Turret position model test (DCG/L_{pp})	7%

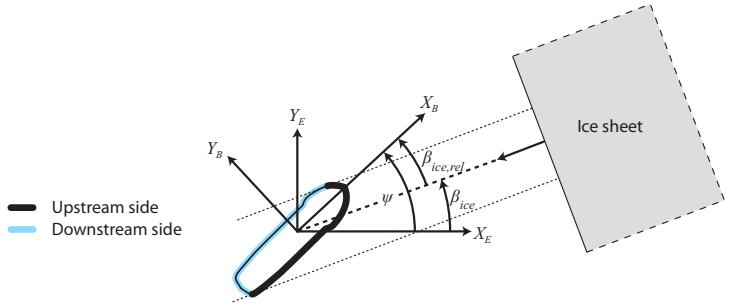

Figure 2. Definitions of earth-fixed reference frame $X_E Y_E Z_E$, body-fixed reference frame $X_B Y_B Z_B$, vessel heading ψ, ice drift direction β_{ice} and relative ice drift direction $\beta_{ice,rel}$.

Ice drift scenarios

Consider an earth-fixed right-handed reference frame $X_E Y_E Z_E$ and a vessel-fixed right-handed reference frame $X_B Y_B Z_B$. Let the heading (yaw) ψ of the vessel be the angle between the X_B-axis and the X_E-axis, as illustrated in Fig. 2. The absolute ice drift direction β_{ice} is defined in the $X_E Y_E Z_E$ system and the relative ice drift direction is defined as $\beta_{ice,rel} = \psi - \beta_{ice}$.

Four different ice drift scenarios were simulated in the model tests; straight ice drift, 30° and 60° slow change of direction and 90° sudden change of direction. The main parameters for each of the scenarios are summarized in Table 1 and the scenarios are illustrated in Fig. 3.

- Straight ice drift means that $\beta_{ice,rel} = 0°$ and the drift speed is constant.
- A 30° or 60° slow change of direction implies that $\Delta\beta_{ice} = |\beta_{ice}(t_1) - \beta_{ice}(t_0)| = 30°$ or $\Delta\beta_{ice} = 60°$ within some time period $\Delta t = t_1 - t_0$ and that the drift speed is constant. In these tests, the ice drift followed circular arcs of curvature radii R_{ice}. The severity of a slow change of direction with respect to ice actions on a moored long body increases when the curvature of the ice drift decreases. An ice curvature radius of 100 m with drift speed 0.5 m/s was used in the tests. This is below the ice curvature radii estimated by Bonnemaire (2006) based on measurements from an ARGOS/GPS buoy in the western part of the Pechora Sea. The changes in ice drift direction in these tests can therefore be considered as severe events.

- In 90° sudden changes of direction the ice was stationary, that is, the ice drift velocity was equal to zero, and the ice cover started to accelerate with 0.22 mm/s^2 and $\beta_{ice,rel} = 90°$. The acceleration used in the tests was calculated with typical coefficients for wind and water drag on level ice from Wadhams (2000).

In the terminology from Spencer et al. (1997), slow changes of drift direction correspond to ARC tests and sudden changes of drift direction to COD tests. These abbreviations will be used in the following.

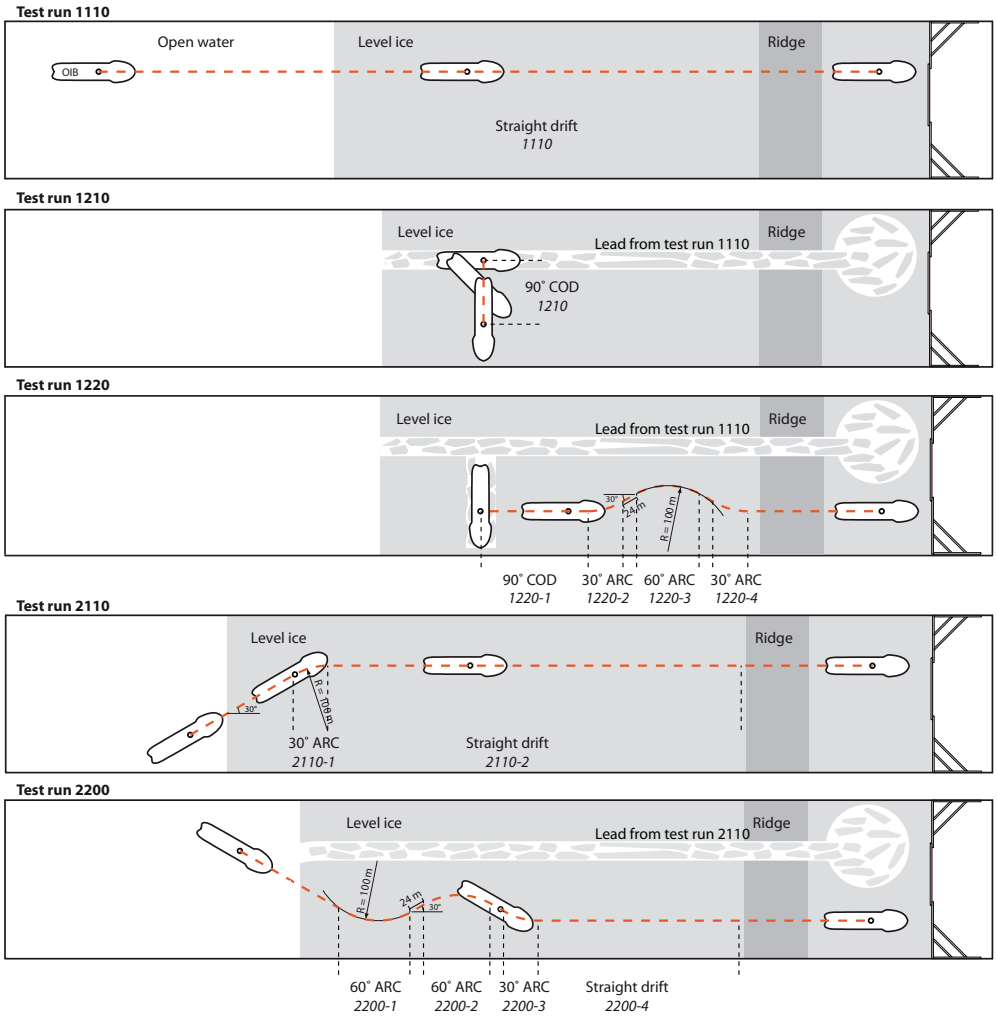

Figure 3. Sketches of all test runs. The ice drift scenarios are indicated and numbered.

RESULTS FROM MODEL TESTS

Observed failure modes of model ice

Kotras et al. (1983) studied ice resistance on icebreakers and suggested that ice-hull interaction can be divided into different phases parametrized by time, that is, a breaking phase, a rotary phase, a sliding phase and a final phase. We assume that the breaking phase dominates the dynamic vessel response and that the other phases mainly determine quasi-static effects, although rubble accumulation may influence the breaking phase. Ice-hull interaction in the breaking phase usually happens at the waterline, and this type of interaction is the main focus in the following. We will refer to the "upstream" and the "downstream" side of the vessel, meaning the part of the hull facing or not facing the drifting ice, respectively, as illustrated in Fig. 2.

30° **ARC:** Ice failed in bending in the bow area and on the reamers as shown in Fig 4a. Some minor crushing was observed behind the reamers. In one of the events, a large crack was initiated on the upstream side of the bow. The crack propagated to a channel with managed ice. There was no failure of intact level ice on the downstream side of the ship, only interaction with broken ice.

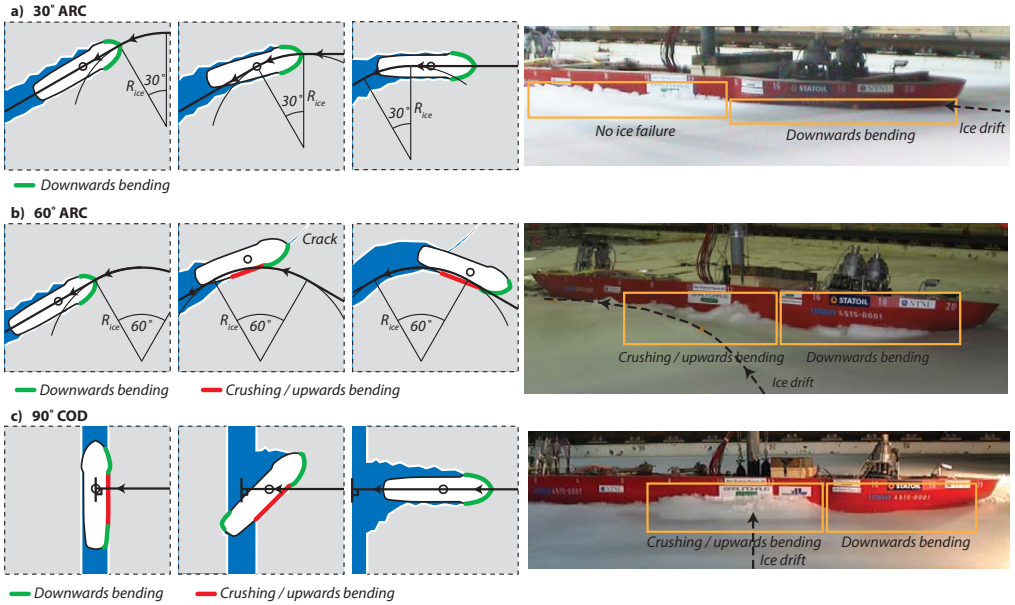

Figure 4. Illustrations of a moored ship in tests in 30° and 60° ARC and 90° COD. Corresponding photos show the ice-hull interaction. Note that in 60° ARC, the vessel had a lateral displacement, which generated large lateral mooring forces.

60° **ARC:** Bending failure was continuously observed in the bow area and on the reamers in all situations with a 60° slow change of ice drift direction. Crushing occurred on the nearly vertical part of the hull behind the reamers and was usually followed by upwards or downwards

bending. Some large cracks propagated from the upstream side of the mid body of the vessel to the channel with managed ice. Crack initiation was also observed in the bow area. These cracks propagated in different directions and not always to an old lead or an old crack. As in tests with 30° slow change of ice drift direction, there was no failure of intact level ice on the downstream side of the vessel. An illustration of a 60° ARC is shown in Fig. 4b.

90° **COD:** The hull was in contact with the intact ice edge when the ice cover started to accelerate in scenario 1210. As seen in Fig. 3, a 7 m wide band of managed ice of high concentration separated the vessel and the intact ice edge in scenario 1220-1. The acceleration was the same in both test runs, thus the vessel met the intact ice edge at a higher speed in the second test run than in the first test run. The first part of the interaction in both test runs was characterized by crushing amidships. During the crushing phase, the contact area increased and after some time the ice failed more or less simultaneously along the hull in upwards and downwards bending, amidships and in the bow area, respectively. In scenario 1220-1 the first simultaneous ice failure was followed by a similar event, but resulted this time in downwards bending amidships. A 90° COD is illustrated in Fig. 4c.

After the vessel started to change heading in scenario 1210, the downstream side of the stern broke intact level ice in downwards bending as illustrated in Fig 4c. In test run 1220-1 there was no ice failure on the downstream side.

Vessel response

Response analysis of moored vessels in changing ice drift is different from wave response analysis. An ice drift change is usually an isolated event, meaning that it is not repeated several times in a row. Statistical response characteristics such as root mean square values or significant single amplitudes do not apply, unless the same test has been repeated many times. Maximum values for yaw rate, roll angle and total mooring offset are reported in Table 3. Pitch and heave motions were small and will neither be reported nor discussed in the following. Time series for heading, absolute and relative ice drift direction, yaw rate and roll motion from test runs 1220 and 2200 are shown in Fig. 5 and 6, respectively.

The four thrusters were used for manoeuvring and clearing of ice in ARC tests, but not in COD tests. The vessel response was heavily influenced by the helmsman in situations with active use of the thrusters. The helmsman reported that his position on the bridge of the driving carriage was unfavourable because it was difficult to see the vessel from there. Due to problems with the sight, it was sometimes difficult for the helmsman to anticipate ice drift direction changes, especially in 60° ARC, simply because of the duration of the event. This lead to under or over steering of the vessel, which again caused large offsets and mooring forces. Such an event is illustrated in Fig. 4b and can also be seen in the time series in Fig. 6.

Mooring forces

For the same reason as maximal values were used for the vessel response, maximum values will be used for mooring forces. The maximal mooring forces in each ice drift scenario are reported in Table 4, together with the total mooring force, the ratio between longitudinal and transverse

Table 3. Maximal roll angle ϕ, yaw rate $\dot{\psi}$ and offsets from mooring equilibrium (full-scale values).

Ice sheet	Drift scenario	Roll ϕ [deg]	Yaw rate $\dot{\psi}$ [deg/s]	Total offset [m]
1000	Straight (1110)	1.0	0.1	0.4
	30° ARC (1220-2)	1.4	0.4	0.4
	30° ARC (1220-4)	2.1	0.3	0.3
	60° ARC (1220-3)	5.5	0.5	0.7
	90° COD (1210)	6.6	0.6	0.8
	90° COD (1220-1)	9.4	0.9	2.1
2000	Straight (2110-2)	1.8	0.1	0.3
	30° ARC (2110-1)	2.1	0.4	0.3
	30° ARC (2200-3)	5.4	0.9	1.8
	60° ARC (2200-1)	3.0	0.3	0.5
	60° ARC (2200-2)	9.8	1.0	3.6

Table 4. Maximal longitudinal mooring force F_{long}, transverse mooring force F_{trans} and total mooring force F_{tot} in different ice drift scenarios (full-scale values).

Ice sheet	Drift scenario	F_{long} [MN]	F_{trans} [MN]	F_{tot} [MN]	F_{trans}/F_{long}	$F_{tot}/F_{tot}^{straight}$
1000	Straight (1110)	2.6	1.0	2.6	0.4	1.0
	30° ARC (1220-2)	0.6	3.1	3.1	5.2	1.2
	30° ARC (1220-4)	0.7	3.2	3.2	4.6	1.2
	60° ARC (1220-3)	1.1	8.0	8.0	7.3	3.1
	90° COD (1210)	2.1	6.7	6.7	3.2	2.6
	90° COD (1220-1)	1.0	11.6	11.6	11.6	4.5
2000	Straight (2110-2)	1.9	1.3	1.9	0.7	1.0
	30° ARC (2110-1)	0.7	2.7	2.7	3.9	1.4
	30° ARC (2200-3)	1.9	8.3	8.4	4.4	4.4
	60° ARC (2200-1)	0.8	3.7	3.7	4.6	1.9
	60° ARC (2200-2)	3.5	12.0	12.2	3.5	6.4

forces and the ratio between maximal total mooring force in each scenario and maximal total mooring force in straight ice drift. Time series of the mooring forces in test runs 1210 and 2200 are shown in Fig. 5 and 6, respectively.

DISCUSSION

Failure modes

The main failure modes were upwards and downwards bending, crushing and splitting, as well as mixtures of these. Downwards bending was the only failure mode in the bow and reamer area. Crushing occurred at the vertical part of the hull amidships and more frequently when the relative ice drift direction was large, sometimes caused by wrong actions by the helmsman. Events with crushing were usually followed by upwards or downwards bending failure. Time series from test run 1220 with a 90° sudden change of direction are shown in Fig. 5. The label ❶ denotes situations with crushing amidships, while the transitions to ❷ and ❸ indicate occurrence of upwards and mixed upwards and downwards bending failure amidships, respectively. The

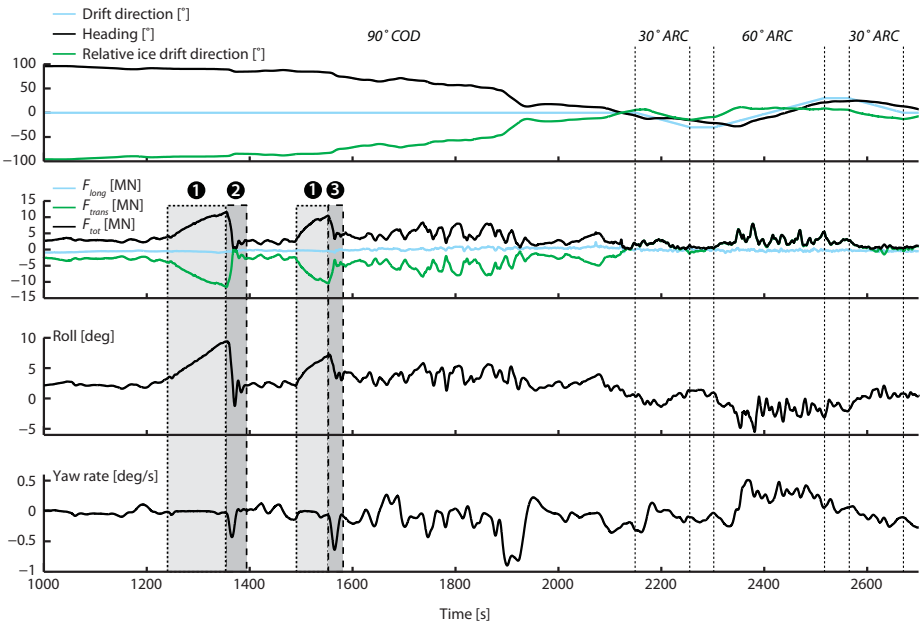

Figure 5. Time series for drift direction, heading, mooring forces, roll motion and yaw rate from test run 1220. The label ❶ indicates occurrence of crushing amidships leading to simultaneous bending failure in the transition to labels ❷ and ❸. These labels indicate the mooring forces and vessel response resulting from the bending failures.

zones marked by ❷ and ❸ show the effect of the ice failure on vessel motions and mooring forces. Bending failure occurred almost simultaneously along the hull and consequently the mooring forces dropped, resulting in rapid change of vessel heading. It is also observed that the maximal roll angle was smaller in the case of mixed upwards and downwards bending failure, indicating a dependency between roll angle and failure mode. For a ship with another angle between hull and waterline the failure mode dependence on roll angle will be different. The occurrences of upwards bending failure could partly be caused by buoyancy of rubble underneath the ice sheet.

Splitting occurred both in the bow area and amidships. Cracks initiated amidships usually propagated to a nearby channel with managed ice. Splitting did not induce drops in the load levels and the reason is probably the confinement in the ice cover given by the tank walls. In test runs with virgin level ice, splitting was not observed.

There was only interaction between intact ice and the downstream side of the vessel when the vessel was in a narrow channel with a 90° sudden change of ice drift direction. A vessel without reamers or with larger distance between the stern and the turret would probably experience more actions from intact ice on the downstream side.

Although the failure modes seem reasonable, one should keep in mind that the tests were performed in model ice.

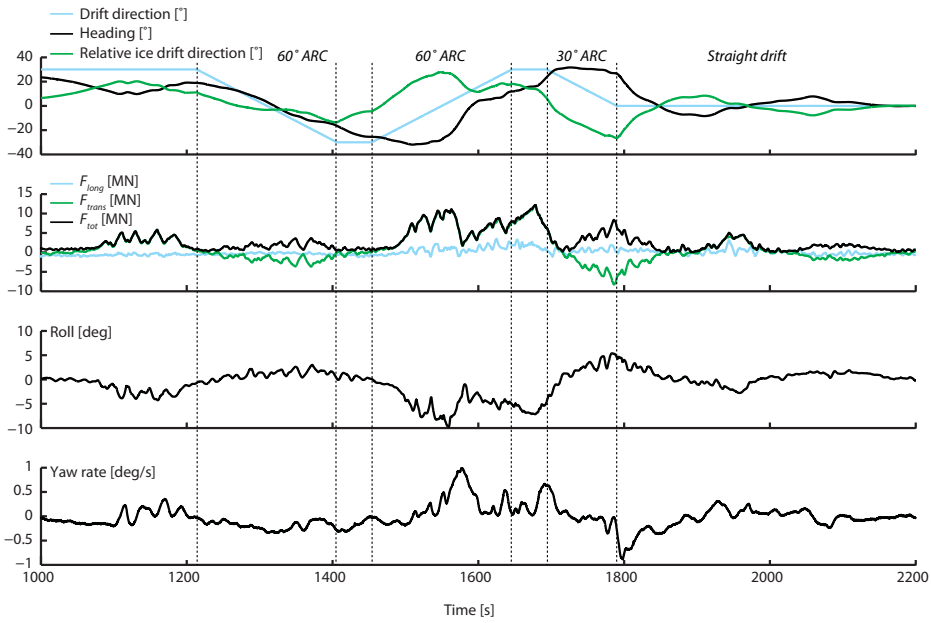

Figure 6. Time series for drift direction, heading, mooring forces, roll motion and yaw rate from test run 2200.

Horizontal motions

As discussed above, the midship was exposed to higher ice forces than the bow area, caused by crushing failure on the vertical sides. The difference in ice forces on the bow and midship together with the relative turret position is decisive for the yaw stability of a moored ship. If the ice force (assuming that this is the only external force acting on the vessel) aft the turret is larger than the ice force fore the turret, the ship will vane with the bow upstream. The ship will be unstable if the ice force is larger in front of the turret than behind. This is illustrated in Fig. 7. The present mooring/hull configuration had a low horizontal stability, as the ship did not vane efficiently without thrusters.

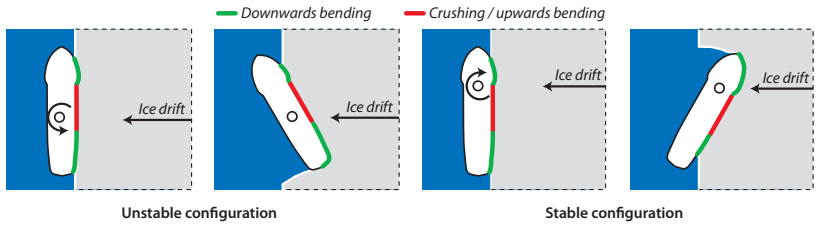

Figure 7. Illustrations showing two turret positions. The ice induced yaw moment about the turret is indicated by an arrow.

The helmsman used the thrusters to follow the ice drift path in ARC scenarios. This was often successful during 30° ARC scenarios, but less successful in 60° ARC scenarios. The latter tests were of longer duration than the former and together with the low yaw stability of the vessel,

this made it difficult for the helmsman to follow the drift path. Another factor which affected the helmsman actions was that time was scaled, which forced him to react five times faster than in real life. Further, the helmsman knew the exact ice drift path in the tests. In full scale, it will be necessary with accurate ice drift estimates for the helmsman to make rational decisions regarding manoeuvring.

The vessel usually changed heading stepwise, regardless of whether the thrusters were used or not. This can be seen for instance in Fig. 5 where the yaw rate is plotted. Heading changes were usually caused by simultaneous ice failure along a large portion of the hull. Stepwise heading changes are probably unique for moored ships in ice, as it is unlikely to experience such response in waves.

Roll motion

Roll is an important mode of motion, especially with respect to human safety, accelerations and the risk of capsizing. For straight ice drift and 30° ARC, the maximal roll angles were 5° or less, which was the case for two of the three 60° ARC scenarios as well. The third scenario with 60° ARC gave a maximal roll angle of approximately 10°. This scenario was a continuation of a preceding ice drift change. The relative heading was not zero when the ice drift change started, thus a high roll angle was obtained. Roll motions were in general large when the relative drift direction was large, as seen in Fig. 5 and 6, because the roll angle was proportional to F_{trans}, which increased with relative ice drift direction (see next section). As long as the helmsman was able to follow the ice drift path, roll motions were therefore limited.

During 90° COD scenarios, the maximal values were between 6° and 10°. With a nearly vertical midship, the ice failure mode will change from crushing to upwards bending for large roll angles, since the nearly vertical part of the hull will turn into an upward sloping plane. For this particular concept it means that maximum roll angle will be restricted by the ice failure mode transition.

The vertical coordinate of the attachment point of the mooring system to the vessel is an important parameter related to roll response, especially in ice. This point was too high in the tests compared to full scale because of the dry mooring system configuration. The mooring torque arm was therefore too short and the mooring induced roll moment was not modelled correctly. Another parameter affecting roll motions is the transverse metacentric height $\overline{GM}_T$, which was rather low in the tests. A larger $\overline{GM}_T$ would have increased the hydrostatic restoring moment in roll, but on the other hand lowered the natural period in roll, which in turn would affect the behaviour of the vessel negatively in waves.

Mooring forces

The ratio between the maximal total mooring force in each ice drift scenario and in straight ice drift is shown in Fig. 8a. The scenarios 2200-2 and 2200-3, indicated by the shaded area in Fig. 8a, were influenced by an earlier scenario, as mentioned above, thus the initial conditions for these drift scenarios were different from the others. By neglecting these events in Fig. 8a, we observe that the maximal mooring force increased with the severity of the ice drift scenarios.

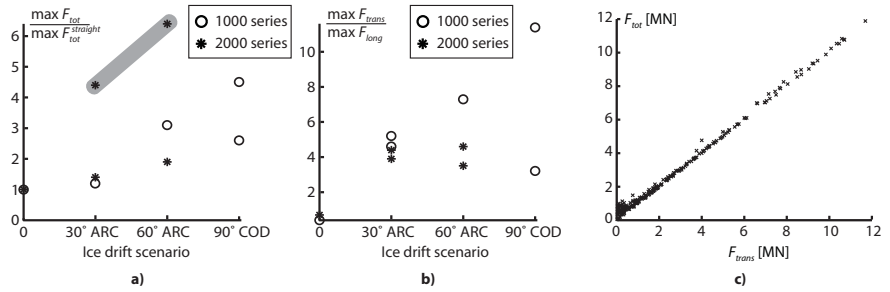

Figure 8. a) Ratio between the maximal total mooring force in each ice drift scenario and in straight ice drift. b) Ratio between the maximal transverse and maximal longitudinal mooring force in each ice drift scenario. c) Total mooring force against transverse mooring force in test run 2200.

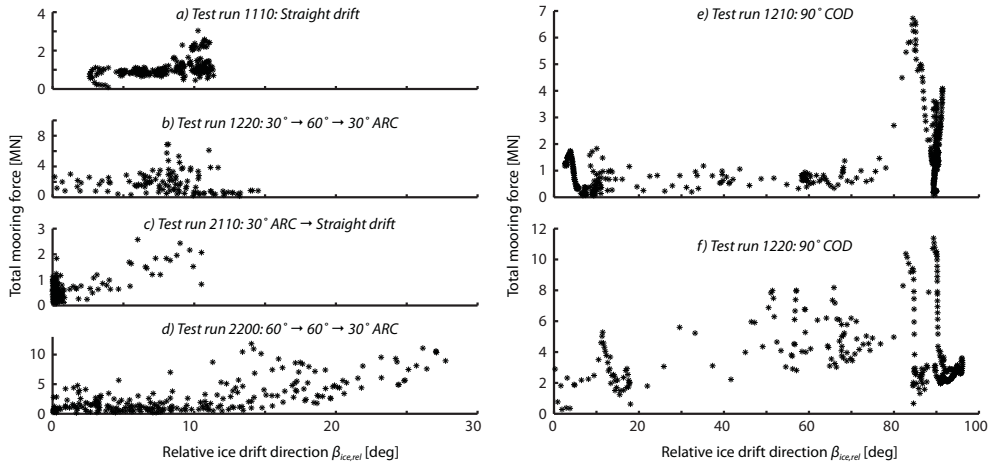

Figure 9. Total mooring force against relative ice drift direction $\beta_{ice,rel}$ (see Fig. 2) for all test runs.

The mooring forces would have been reduced in events with 90° COD if the thrusters had been used to vane against the drift, as the vessel was able to turn on the spot in level ice.

By analysing the time series from all ice drift scenarios we found that

$$\text{mean } F_{long}^{ARC,COD} \ll \text{mean } F_{trans}^{ARC,COD} \tag{2}$$

for all ice drift scenarios, meaning that the total mooring force during changes in ice drift direction was mainly determined by the transverse force. This can also be observed in the time series in Fig. 5 and 6, in Fig. 8c, as well as in the plot of the ratio between transverse and longitudinal maximal forces against ice drift scenario in Fig. 8b. In this figure one can see that transverse maximal mooring forces were 3 to 11 times larger than longitudinal maximal mooring forces for the various drift scenarios.

The total mooring force was in general large when the relative ice drift direction $\beta_{ice,rel}$ was large, as seen in Fig. 9. Since the transverse force determined the total force, this is expected.

The contact area between ice and hull increased when $\beta_{ice,rel}$ increased. Since ice forces increase with contact area and crushing occurred more often when $\beta_{ice,rel}$ was large, the ice force also increased. The magnitude of the ice force component normal to the vessel's long axis also increased when $\beta_{ice,rel}$ increased. However, no clear relation between F_{moor} and $\beta_{ice,rel}$ could be derived. One cause for the variability between the curves is differences in initial conditions.

With increased yaw stability, the time periods with large relative drift direction would have been shorter and this would probably have a positive effect on the mooring forces. As mentioned above, the main factors influencing the yaw stability were turret position, waterline geometry and helmsman actions.

A peak total mooring force of 15.5 MN was measured in a first-year ridge with a keel depth of 15.5 meters in the same test series, see Jensen et al. (2008). This is only 30% higher than the peak total mooring force in ice drift changes. In areas without ridges or with small ridges, actions by level ice with varying drift direction should be considered as a potential design mooring load for the present concept. However, events with changes in ice drift direction and level ice, may be easier to manage with assisting icebreakers than ridges, given that reliable ice drift forecasts are available. Variable ice drift combined with ridges is another challenge for moored ships, which has not been considered herein.

CONCLUSIONS

The main findings of this study are summarized below.

- Model tests of a turret moored ship in ice were studied and it was seen that the response of the vessel and the mooring forces depended significantly on changes in ice drift direction.
- Mooring forces depended on vessel motions, which further depended on the distribution of failure modes of ice along the hull.
- The failure modes were triggered by the hull geometry and partly by vessel response.
- Turret position, waterline geometry of the hull and helmsman actions were decisive parameters for the horizontal stability and the mooring forces.
- The transverse mooring force determined the total mooring force during changes in ice drift direction.
- The magnitude of the peak mooring force caused by level ice with varying drift direction was comparable to the peak mooring force caused by a large first-year ice ridge. Actions by drifting level ice should therefore be considered as a possible design mooring load for moored ships in certain areas.

ACKNOWLEDGEMENT

The work described in this publication was supported by the European Community's Sixth Framework Program through the grant to the budget of the Integrated Infrastructure Initiative HYDRALAB III, Contract no. 022441(RII3). The authors would like to thank the Hamburg

Ship Model Basin (HSVA), especially the ice tank crew, for the hospitality, technical and scientific support and the professional execution of the test programme in the Research Infrastructure ARCTECLAB. We would like to thank StatoilHydro for funding of the physical models. This study was also supported by the PETROMAKS programme of the Research Council of Norway through NTNU's PetroArctic project.

REFERENCES

Aksnes, V., Bonnemaire, B., Løset, S., Lønøy, C., 2008. Model testing of the Arctic Tandem Offloading Terminal - tandem mooring forces and relative motions between vessels. In: Proceedings of the 19th IAHR International Symposium on Ice. Vol. 2. Vancouver, British Columbia, Canada, pp. 687–698.

Ashton, G. D. (Ed.), 1986. River and Lake Ice Engineering. Water Resources Publications. Book Crafters Inc., Chelsea, Michigan.

Bonnemaire, B., 2006. Arctic offshore loading downtime due to variability in ice drift direction. Journal of Navigation 59 (01), 9–26.

Bonnemaire, B., Lundamo, T., Evers, K. U., Løset, S., Jensen, A., 2008a. Model testing of the Arctic Tandem Offloading Terminal - Mooring ice ridge loads. In: Proceedings of the 19th IAHR International Symposium on Ice. Vol. 2. Vancouver, British Columbia, Canada, pp. 639–650.

Bonnemaire, B., Lundamo, T., Jensen, A., Rupp, K. H., 2008b. Subsurface ice interactions under a moored offloading icebreaker. In: Proceedings of the 19th IAHR International Symposium on Ice. Vol. 2. Vancouver, British Columbia, Canada, pp. 663–674.

Evers, K. U., Jochmann, P., 1993. An advanced technique to improve the mechanical properties of model ice developed at the HSVA ice tank. In: Proceedings of the 12th International Conference on Port and Ocean Engineering under Arctic Conditions. Hamburg, Germany, pp. 877–888.

Jensen, A., Bonnemaire, B., Løset, S., Breivik, K. G., Evers, K. U., Ravndal, O., Aksnes, V., Lundamo, T., Lønøy, C., 2008. First ice model testing of the Arctic Tandem Offloading Terminal. In: Proceedings of the 19th IAHR International Symposium on Ice. Vancouver, British Columbia, Canada.

Kotras, T. V., Baird, A. V., Naegle, J. N., 1983. Predicting ship performance in level ice. SNAME Transactions 91, 329–349.

Spencer, D., Jones, S. J., Jolles, W. H., 1997. Effect of ice drift angle on a mooring hawser. In: Proceedings of the International Conference on Port and Ocean Engineering under Arctic Conditions. Yokohama, Japan, pp. 127–133.

Wadhams, P., 2000. Ice in the Ocean. Gordon and Breach Science Publishers, London.

Chapter 5

A simplified approach for modelling stochastic response of moored vessels in level ice

By Vegard Aksnes and Basile Bonnemaire

Proceedings of the 20th International Conference on Port and Ocean Engineering under Arctic Conditions, Luleå, Sweden, POAC09-134, 2009.

POAC 09
Luleå, Sweden

Proceedings of the 20th International Conference on
Port and Ocean Engineering under Arctic Conditions
June 9-12, 2009
Luleå, Sweden

POAC09-134

A SIMPLIFIED APPROACH FOR MODELLING STOCHASTIC RESPONSE OF MOORED VESSELS IN LEVEL ICE

Vegard Aksnes[1] and Basile Bonnemaire[2,1]
[1] Norwegian University of Science and Technology, Trondheim, Norway
[2] Barlindhaug Consult, Tromsø, Norway

ABSTRACT

The topic of this paper is numerical modelling of moored ships in level ice. Dynamic interaction between ice and vessel is modelled with a simplified model, taking the relative motion between vessel and ice into account. The ice force model is applied in a single-degree-of-freedom model of a moored vessel in surge. Randomness is included by sampling ice temperature and salinity and then using well-known empirical formulas to calculate modulus of elasticity and flexural strength. Ice thickness and breaking length are random variables as well.

Monte Carlo simulations are performed with various mooring stiffness's, damping ratios and ice drift speeds, and resulting mooring and ice forces are studied. It is seen that both mooring and ice forces have largest fluctuations at low ice drift speeds. Some nonlinear coupling effects between vessel response and ice force occurring at low speeds, are identified.

INTRODUCTION

Moored vessels have been proposed for use in oil and gas operations in ice-infested waters. Their response caused by dynamic ice actions from drifting level ice should therefore be studied. Understanding of dynamic ice actions on moored vessels is important for identification of possible resonance and frequency lock-in, as well as for prediction of fatigue of risers and mooring lines, and of mooring load levels. Numerical simulations of dynamic ice actions from level ice on moored vessels have been performed by some authors (Toyama and Yashima, 1985; Shkhinek et al., 2004), but there is no standardized method for how it should be done. Further, there seems to be few investigations on how changes in mooring characteristics affect the response of moored vessels exposed to level ice actions.

The new ISO standard on Arctic offshore structures (ISO/DIS 19906, 2009) contains a section on dynamic ice actions, but it only considers fixed structures. ISO outlines the method by Qu

et al. (2006), based on experiences from Bohai Bay, to estimate dynamic ice actions on fixed conical structures. However, this method is purely time dependent and is probably not directly applicable for moored vessels. Moored vessels can oscillate in all modes of motion, depending on the external excitation. In model tests, it has been observed that vessel response can influence the ice-hull interaction process (Aksnes and Bonnemaire, 2009). It is therefore believed that a model for dynamic ice actions on a moored structure should depend on the vessel's motion relative to the ice sheet. This has been done for fixed vertical structures, to be able to study ice-induced vibrations, (Kärnä and Turunen, 1989), but seldom for sloping structures. With such models, the resulting ice actions time series will depend on vessel parameters, such as stiffness of the mooring system and vessel damping, in addition to ice parameters, such as ice breaking length and drift speed.

In this paper a simplified ice force model, depending on the vessel's penetration in the ice sheet, is derived. The model is based on elastic beam theory with stochastic breaking length and ice parameters, such as temperature, salinity and flexural strength. The ice force model is used in a single-degree-of-freedom (SDOF) model for the surge motion of a moored vessel. Time domain simulations with various ice drift speeds, and various vessel and mooring parameters are performed. Simulated mooring and ice force time series are then studied with respect to nonlinear effects and statistical properties.

TWO-DIMENSIONAL ICEBREAKING CYCLE

The main idea is to study a two-dimensional icebreaking cycle (in longitudinal and vertical directions) and apply it to a moored vessel with a single degree of freedom in surge. Kotras et al. (1983) studied ice resistance on icebreakers and suggested that ice-hull interaction can be divided into different phases, that is, breaking, rotation, sliding and final phases. In the breaking phase, the intact ice sheet is deflected at its free end until failure. The broken floe is rotated until it is parallel to the hull, then slides along the hull and finally loses contact with the hull, either by escaping to one of the sides, to the wake or it is milled by the propellers. This approach has also been applied by Valanto (1992, 2001).

VESSEL SETUP

The vessel used in this study is represented by a simplified geometry, as illustrated in Fig. 1. It is assumed to have the same longitudinal cross-section over the whole beam, thus being a purely two-dimensional vessel. Further, we assume that the icebreaking cycle is two-dimensional as described above, and that the ice sheet fails parallel to the bow, simultaneously over the whole beam of the vessel. For simplicity, the vessel will only be able to move in surge, as this is often the dominant mode of motion for a moored ship-shaped vessel.

MATHEMATICAL MODEL

Let m be the mass of the vessel and X its displacement from zero offset. The equation of motion is

$$m\ddot{X} = F_{hd} + F_{moor} + F_{ice}, \tag{1}$$

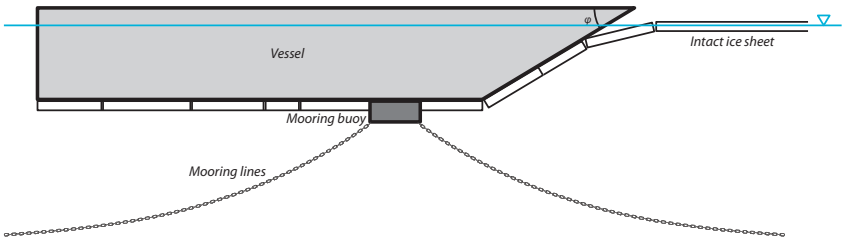

Figure 1: Sketch of the simplified hull-ice interaction process and the vessel's hull geometry.

where F_{hd}, F_{moor} and F_{ice} are hydrodynamic, mooring and ice forces, respectively. The dot denotes differentiation with respect to time and the initial conditions in this text will be $X(0) = \dot{X}(0) = 0$. The hydrodynamic force may be expressed

$$F_{hd} = -A_{11}\ddot{X} - B_{11}\dot{X}, \tag{2}$$

if we assume linear viscous damping. For simplicity, we assume that added mass A_{11} and the damping coefficient B_{11} are frequency independent and constant. The mooring force is assumed to be a linear function of position

$$F_{moor} = -kX, \tag{3}$$

where the constant k will be referred to as the mooring stiffness. The linearity assumption is valid if the vessel experiences small oscillations around a mean position (Faltinsen, 1990). The damping coefficient will include both damping from water and ice. It is convenient to express B_{11} with the damping ratio ζ, such that

$$\zeta = \frac{B_{11}}{2\left(m + A_{11}\right)\omega_0}, \tag{4}$$

where $\omega_0 = \sqrt{k/\left(m + A_{11}\right)}$ is the undamped frequency of oscillation. The equation of motion can then be written

$$\ddot{X} + 2\zeta\omega_0\dot{X} + \omega_0^2 X = \frac{1}{m + A_{11}}F_{ice}. \tag{5}$$

If F_{ice} is a function of time only, the solution to this problem is given by Duhamel's integral (see e.g. Chopra (2006))

$$X(t) = \frac{1}{\left(m + A_{11}\right)\omega_D}\int_0^t F_{ice}(\tau)e^{-\zeta\omega_0(t-\tau)}\sin\left[\omega_D\left(t-\tau\right)\right]d\tau, \tag{6}$$

where $\omega_D = \sqrt{1-\zeta^2}\omega_0$ is the damped natural frequency. For low damping ratios $\omega_D \approx \omega_0$. However, if the ice force depends on the vessel's position in the ice sheet, the solution can not be expressed by Duhamel's integral. This is also the case if the mooring stiffness is nonlinear or if frequency dependency of added mass and/or damping is accounted for.

MODELLING OF ICE FORCES

The ice force is modelled as a cyclic function of penetration of the vessel in the ice sheet. In each cycle, the ice sheet is bent until flexural failure, the broken ice piece is then rotated and

is finally parallel to the hull. After some time, the vessel meets the intact ice edge and a new breaking cycle starts. In this section, a simplified model for the ice force is derived. The ice force is split into three components such that $F_{ice} = F_{ice,break} + F_{ice,rot} + F_{ice,fric}$, as illustrated in Fig. 2. First, the breaking force $F_{ice,break}$ is derived, then the rotation force $F_{ice,rot}$ and finally the friction force $F_{ice,fric}$ caused by submerged ice floes. The approach used herein is not new. Modelling the ice force caused by bending by means of an elastic material model is a common procedure (Croasdale, 1980; Nevel, 1992). The forces caused by rotation and friction is modelled similarly to what was done by Lindqvist (1989), while a similar decomposition of ice forces was used by Valanto (1992, 2001).

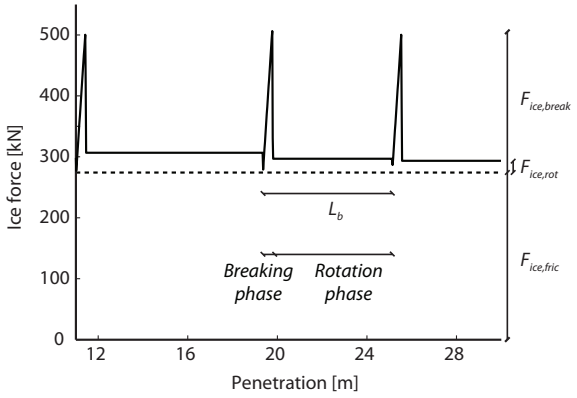

Figure 2: Idealized ice force function. Contributions from breaking force, rotation force and friction force are indicated.

Breaking phase

We assume that the ice sheet in the breaking phase can be described as a semi-infinite elastic beam on elastic foundation. Further, dynamic effects for the beam and the foundation are neglected, due to low indentation speed. The differential equation describing the deflection u of a semi-infinite elastic beam on elastic foundation subjected to a concentrated vertical load P on the free edge with axial compression N is (see e.g. Hetenyi (1946))

$$EI\frac{d^4u}{dx^4} + N\frac{d^2u}{dx^2} + \rho gBu = 0, \quad x > 0, \tag{7}$$

with boundary conditions

$$\lim_{x\to\infty} u(x) = 0, \quad \lim_{x\to\infty} \frac{du}{dx} = 0, \quad \frac{d^2u(0)}{dx^2} = 0, \quad -EI\frac{d^3u(0)}{dx^3} = -P. \tag{8}$$

In Eq. (7), E is modulus of elasticity, I is the second moment of area of the beam, ρ is water density, g is gravitational acceleration and B is width of the beam and the vessel. The solution to this boundary value problem is

$$u(x) = e^{-\beta x}(A\cos\alpha x + B\sin\alpha x), \tag{9}$$

where

$$A = \frac{2P}{EI}\frac{\alpha\beta}{2\alpha^3\beta^2+\alpha\beta^4+\alpha^5}, \tag{10}$$

$$B = \frac{P}{EI}\frac{\beta^2-\alpha^2}{2\alpha^3\beta^2+\alpha\beta^4+\alpha^5} \tag{11}$$

and

$$\alpha = \sqrt{\lambda^2+\frac{N}{4EI}}, \quad \beta = \sqrt{\lambda^2-\frac{N}{4EI}} \quad \text{and} \quad \lambda = \sqrt[4]{\frac{\rho g B}{4EI}}. \tag{12}$$

We can now relate the deflection of the beam edge

$$u(0) = \frac{2P}{EI}\frac{\alpha\beta}{2\alpha^3\beta^2+\alpha\beta^4+\alpha^5} \tag{13}$$

to the distance penetrated by the vessel in the ice sheet $\kappa(t)$. If v_i is assumed to be a constant ice drift speed and $X(0)=0$, then the penetration can be written

$$\kappa(t) = \int_0^t \left[v_i(\tau)-\dot{X}(\tau)\right] d\tau = v_i t - X(t). \tag{14}$$

By denoting the stem angle of the vessel by φ, the edge deflection can be expressed as $u(0) = (v_i t - X(t))\tan\varphi$. Let $N = P(\sin\varphi+\mu\cos\varphi)/(\cos\varphi-\mu\sin\varphi)$, where μ is the friction coefficient between ice and hull. Given a penetration κ, we can solve Eq. (13) for the axial force N. The contact force up to failure has been derived, and we must now determine a failure criterion. The bending moment at point x is

$$M(x) = -EI\frac{d^2u}{dx^2}. \tag{15}$$

The flexural strength σ_f is for a beam of width B and thickness h_i, related to the ultimate bending moment M_0 by

$$\sigma_f = \frac{6M_0}{Bh_i^2}, \tag{16}$$

where h_i is ice thickness. The ice beam fails when the maximal bending moment equals the ultimate bending moment.

The j-th period of the force function associated with breaking can be expressed as

$$F^{(j)}_{ice,break}(t,X(t)) = \begin{cases} N(t,X(t)), & \kappa \in \left[\sum_{i=0}^{j-1} L_b^{(i)}, \sum_{i=0}^{j-1} L_b^{(i)} + a^{(j)}\right) \\ 0, & \text{otherwise} \end{cases} \tag{17}$$

where $\{L_b^{(i)}\}$ is a sequence of breaking lengths, sampled from a probability distribution, and $a^{(j)}$ is the penetration in the ice sheet at failure. For notational convenience, L_b^0 is set to 0. This has no physical consequences. The total ice force associated with bending the ice sheet up to flexural failure is $F_{ice,break}(t,X(t)) = \sum_{j=1}^{n} F^{(j)}_{ice,break}(t,X(t))$, and the ice sheet length is $L_{ice} = \sum_{i=0}^{n} L_b^{(i)}$.

Rotation phase

An energy approach is used for calculation of the rotation force. The difference in potential energy for a floating floe and a floe parallel to the bow, with its upper end in the water plane, is

$$E_p^{(j)} = \frac{1}{2}(\rho_w - \rho_i)g\left(L_b^{(j)}\right)^2 Bh_i \sin(\varphi). \tag{18}$$

We assume that the rotation phase lasts from $\kappa = \sum_{i=0}^{j-1} L_b^{(i)} + a^{(j)}$ to $\kappa = \sum_{i=0}^{j} L_b^{(i)}$, such that the average vertical force needed to submerge floe j is

$$V_{rot}^{(j)} = \frac{E_p^{(j)}}{L_b^{(j)} - a^{(j)}}. \tag{19}$$

The horizontal force on the vessel associated with rotation of floe j is

$$F_{ice,rot}^{(j)}(t, X(t)) = \begin{cases} V_{rot}^{(j)} \frac{\sin\phi + \mu\cos\phi}{\cos\phi - \mu\sin\phi}, & \kappa \in \left[\sum_{i=0}^{j-1} L_b^i + a^{(j)}, \sum_{i=0}^{j} L_b^i\right) \\ 0, & \text{otherwise} \end{cases}, \tag{20}$$

such that the total rotation force is $F_{ice,rot}(t, X(t)) = \sum_{j=1}^{n} F_{ice,rot}^{(j)}(t, X(t))$.

Sliding phase

Due to our simple geometry (Fig. 1), we assume that the bottom of the vessel is covered with broken ice floes, while the sides are not. From hydrostatics we get

$$F_{ice,fric} = \mu\,(\rho_w - \rho_i)\,g\left(L - \frac{T}{\tan\phi}\right)Bh_i, \tag{21}$$

where L and T are length and draught of the vessel, respectively.

Randomization

According to Timco and O'Brien (1994), the flexural strength can be empirically related to the relative brine volume η_b by the relation

$$\sigma_f = 1.76e^{-5.88\sqrt{\eta_b}}. \tag{22}$$

An empirical relation between modulus of elasticity and relative brine volume is (Weeks and Assur, 1967)

$$E = E_0\,(1 - \eta_b)^4, \tag{23}$$

where E_0 is the elastic modulus of freshwater ice. For temperatures between -22.9°C and -0.5°C, the brine volume can be approximated (Frankenstein and Garner, 1967) as

$$\eta_b = S_i\left(\frac{49.185}{|T_i|} + 0.532\right). \tag{24}$$

Randomness is introduced in the ice force model by varying the ice temperature T_i [°C], the salinity S_i [ppt] and the ice thickness h_i [m] for each breaking length L_b [m]. In addition,

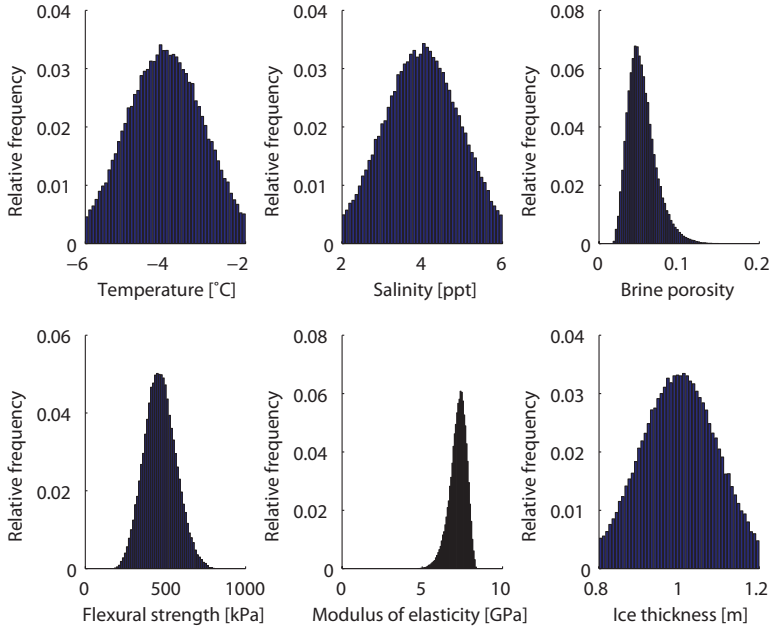

Figure 3: Histograms of simulated temperature, salinity, breaking length, flexural strength, modulus of elasticity and ice thickness.

the breaking length itself is assumed to be a random variable. The probability distributions are as follows; temperature $T_i \sim N(-4,1)$ and zero outside $[-6,-2]$, salinity $S_i \sim N(4,1)$ and zero outside $[2,6]$, ice thickness $h_i \sim N(1,0.01)$ and zero outside $[0.8,1.2]$, breaking length $L_b/h_i \sim N(5,1)$ and zero outside $[3,7]$. Here $N(\cdot,\cdot)$ denotes normal distribution, where the first argument is the mean and the second is the variance. No correlation between the random variables is assumed. Examples of simulated ice properties are shown in Fig. 3.

TIME DOMAIN SIMULATIONS

Monte Carlo simulations were performed to be able to study mooring forces with different structural characteristics. The parameters, which are fixed in the simulations, are given in Table 1. Three different mooring stiffness's were used 100, 400 and 1000 kN/m, corresponding to natural periods of 100, 50 and 32 s, respectively. Damping ratios were 0.05 and 0.15 and ice drift speeds ranged from 0.05 to 0.4 m/s.

Excerpts from time series of mooring and ice forces are shown in Fig. 4. For all stiffness's the mooring force oscillates more for low ice drift speeds and for low damping ratios. The medium stiffness ($k = 400$ kN/m) has a natural period of 50 s. Ice drift speed $v_i = 0.1$ m/s and mean breaking length $L_b = 5$ m, correspond to an ice breaking period of 50 s, meaning that the time series in Fig. 4i and 4j, show near resonant behaviour. Nevertheless, the mooring force has larger amplitudes when $v_i = 0.05$ m/s (Fig. 4c and d). With this ice drift speed, the behaviour is more transient than in the resonant case. The reason is probably that for lower drift speed, the breaking phase lasts longer and the vessel is exposed to a large ice force for a longer time

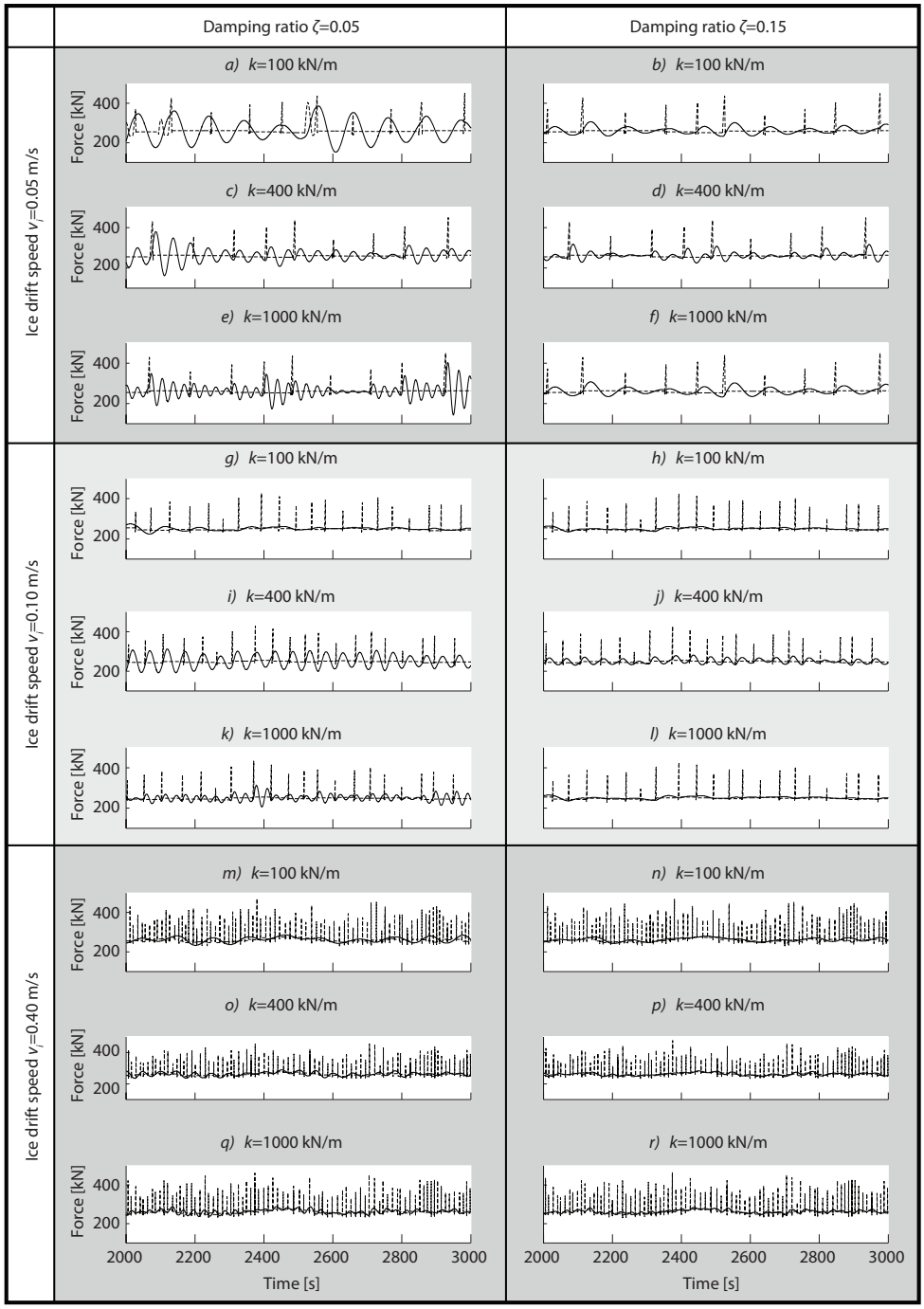

Figure 4: Mooring (solid line) and ice force (dashed line) for different mooring stiffness's k, damping ratios ζ and ice drift speeds v_i.

Table 1: Simulation parameters.

Parameter	**Value**
Stem angle φ [°]	25
Length between perpendiculars L [m]	109
Beam B [m]	25
Draught T [m]	10
Hull-ice friction μ	0.1
Mass m [kg]	$25 \cdot 10^6$
Added mass A_{11} [kg]	$0.02 \cdot m$
Water density ρ_w [kg/m^3]	1025
Ice density ρ_i [kg/m^3]	917

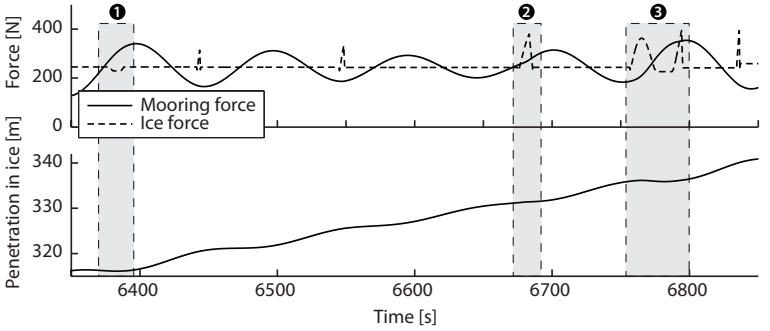

Figure 5: a) Mooring and ice force against time. b) Vessel penetration in ice against time. Mooring stiffness is 100 kN/m, ice drift speed is 0.05 m/s and damping ratio is 0.05. ❶, ❷ and ❸ mark situations with feedback from vessel response in the ice force.

period. With higher drift speeds, the breaking phase appears to be more like an impulse, which is not transmitted to the mooring system unless the impulses occur with a period equal to the vessel's natural period.

Three nonlinear effects in the ice force are depicted in Fig. 5. ❶ shows a situation where the bow loses contact with a floe in the rotation phase. Consequently the ice force drops to only the friction component. Another nonlinear effect which is observed is "stretching" of the breaking phase (❷ in Fig. 5). Due to the vessel's possibility to surge, the breaking phase lasts for a longer time period than it would have if the surge motion had not been taken into account. Label ❸ shows a scenario where the vessel is in the breaking phase. The ice sheet is loaded, but the vessel moves away from the ice and the ice force decreases again. After a while, the contact with the unbroken ice sheet is lost and the friction force is the only ice force. The vessel meets the intact ice edge again, and this time the breaking phase is completed. These three situations (❶, ❷ and ❸) represent feedback effects on the ice force from the vessel response. They were only seen for very low speeds and for soft mooring systems.

In the following, (sample) standard deviation and average are denoted s and $< \cdot >$, respectively. Standard deviations, averages and 99 percentiles are mean values from ten three hour simulations for each set of parameters $\{k, \zeta, v_i\}$.

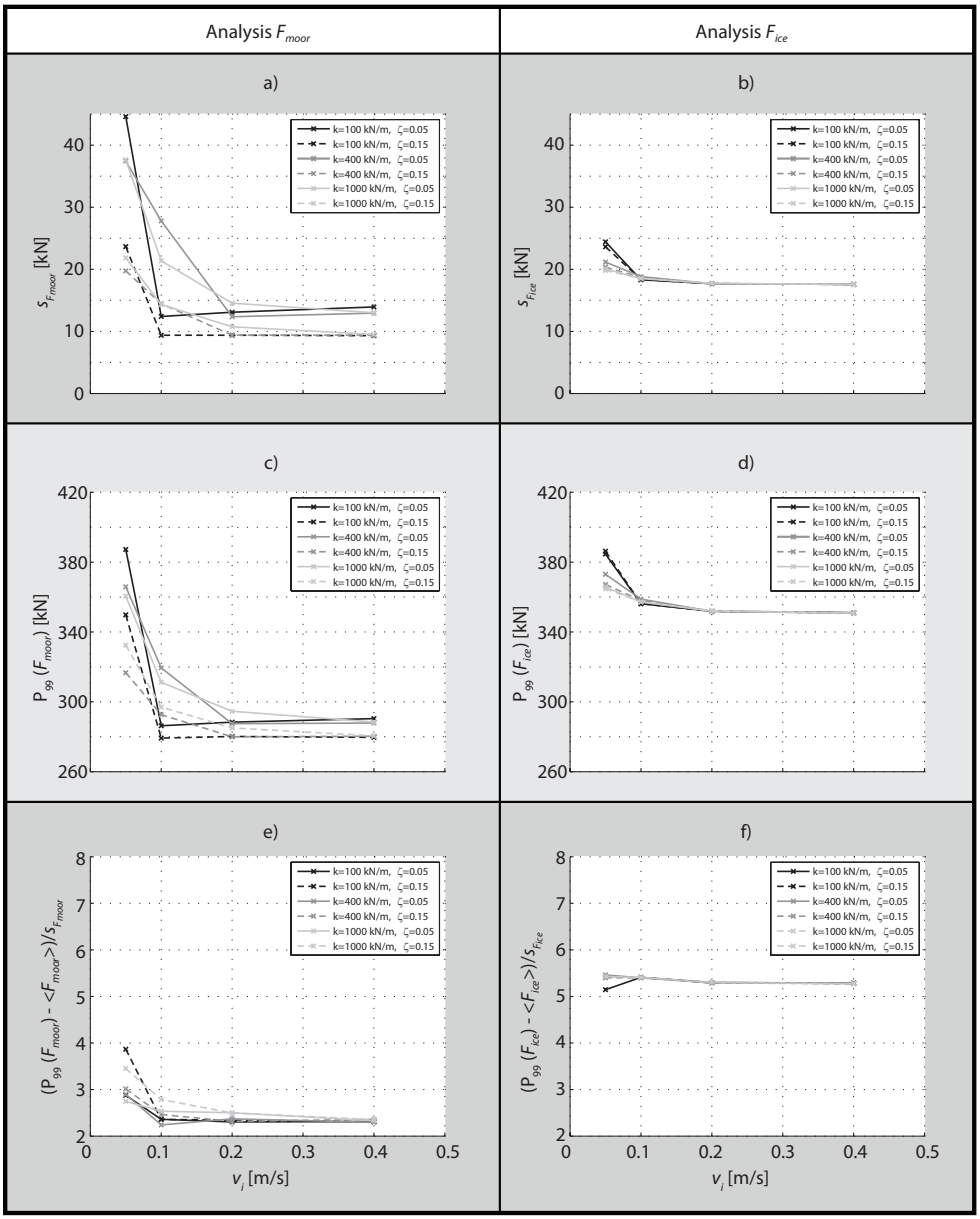

Figure 6: Standard deviation of a) mooring force and b) ice force. 99 percentile of c) mooring force and d) ice force. 99 percentile minus the mean divided by the standard deviation for e) mooring force and f) ice force.

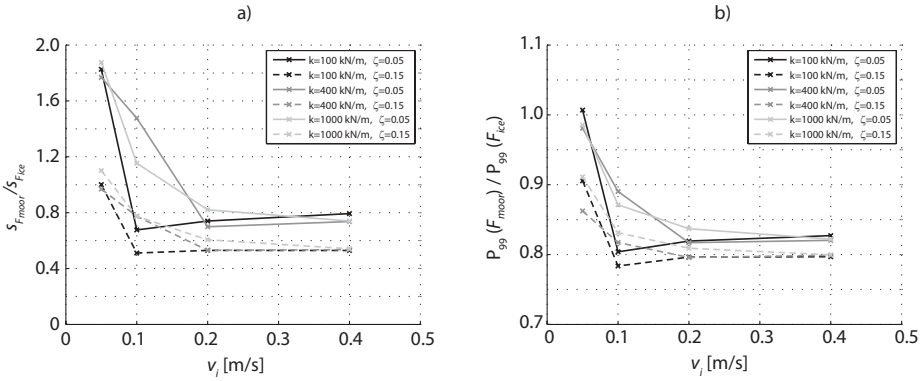

Figure 7: Ratio between a) standard deviations and b) 99 percentiles, for mooring and ice force.

Figure 6a shows the standard deviation of the mooring force. It can be seen that the standard deviation was highest for low speeds, which was also observed by direct inspection of the time series in Fig. 4. The mooring force 99 percentiles (Fig. 6c) decrease with the ice drift speed. The ratio between the difference of 99 percentile and mean, and standard deviation is shown in Fig. 6e. Also this ratio is highest for low speeds.

More time was spend in the breaking phase when the drift speed was low, due to the nonlinearities discussed above. This gave larger standard deviations for the ice force with low speeds, than with higher speeds (Fig. 6b). The same reasoning explains the decrease of 99 percentile with ice drift speed in Fig. 6d. Further, the ratio between the difference of the 99 percentile and mean, and standard deviation is almost constant (Fig. 6f).

It is of interest to compare mooring and ice forces, since ice forces are not as easily measured in model tests or full scale, as mooring forces. The ratio between standard deviations are shown in Fig. 7a. The mooring force standard deviation is larger than the ice force standard deviation for the most dynamic cases ($v_i = 0.05$ m/s with all values of k and $v_i = 0.1$ m/s with $k = 400$ kN/m). Figure 7b gives the ratio between mooring and ice force 99 percentiles. There is only one situation where a mooring force 99 percentile is larger than an ice force percentile, namely for $k = 100$ kN/m with $v_i = 0.05$ m/s and $\zeta = 0.05$.

Lundamo et al. (2008) back-calculated level ice loads on a moored tanker from model tests. The drift speed was 0.5 m/s and the tanker's natural surge periods were approximately 38 s (ballasted) and 46 s (loaded), see Jensen et al. (2000a,b). They found similar values for the ratio $(P_{99}(F_{moor}) - < F_{moor} >)/s_{F_{moor}}$, but lower values ($\sim 4$) for $(P_{99}(F_{ice}) - < F_{ice} >)/s_{F_{ice}}$. Thus, their ratio between force maxima was higher (1.3-1.5). Some reasons for this discrepancy may be the simplifications in our model and that back-calculated ice loads are based on measured mooring forces. As a moored vessel acts as a low-pass filter on the ice forces, back-calculated ice forces will miss some high frequency information which is present in the our theoretical model. This means that back-calculated ice forces will in general have lower peak values than those predicted by the theoretical model.

CONCLUSIONS AND FURTHER WORK

A single-degree-of-freedom model of a moored vessel in level ice has been studied. The ice excitation force depended on the relative motion between drifting ice and the vessel. Randomness was included by sampling ice temperature and salinity and then using well-known empirical formulas to calculate modulus of elasticity and flexural strength. Ice thickness and breaking length were random variables as well.

Time domain simulations were performed for a number of different mooring stiffness's, damping ratios and ice drift speeds. Statistical properties of simulated mooring and ice forces were studied and compared.

- In general, both mooring and ice forces had largest fluctuations (in terms of standard deviation) for very low drift speeds, regardless of the mooring stiffness.
- Mooring forces were largest at the lowest ice drift speed for all mooring stiffness's.
- Three nonlinear phenomena were identified for very slow ice drift speeds, all of them resulting from a feedback effect caused by the relative motion between vessel and ice on the ice force.

The simplification of the problem, especially the hull shape of the vessel and the icebreaking process, may have given more pronounced dynamic effects than what one would expect to encounter in the field. Further work should therefore focus on more realistic hull shapes with non-simultaneous ice failure in bow and the resulting vessel dynamics. In near future, it is planned to do model tests with a similar vessel and mooring setup.

ACKNOWLEDGEMENT

This study was supported by the PETROMAKS programme of the Research Council of Norway through NTNU's PetroArctic project.

REFERENCES

Aksnes, V., Bonnemaire, B., 2009. Analysis of the behaviour of a moored ship in variable ice drift. In: Proceedings of the 20th International Conference on Port and Ocean Engineering under Arctic Conditions. Luleå, Sweden, In press.

Chopra, A. K., 2006. Dynamics of Structures, 3rd Edition. Prentice Hall.

Croasdale, K. R., 1980. Ice forces on fixed rigid structures. In: 1st IAHR State of the Art Report on Ice Forces on Structures. pp. 34–106.

Faltinsen, O. M., 1990. Sea Loads on Ships and Offshore Structures. Cambridge University Press.

Frankenstein, G. E., Garner, R., 1967. Equations for determining the brine volume of sea ice from -0.5 to -22.9°C. Journal of Glaciology 6 (48), 943–944.

Hetenyi, M., 1946. Beams on elastic foundations. The University of Michigan Press.

ISO/DIS 19906, 2009. Petroleum and natural gas industries - Arctic offshore structures. Geneva, Switzerland.

Jensen, A., Løset, S., Hellmann, J., Gudmestad, O. T., Ravndal, O., 2000a. Model tests of an arctic tanker concept for loading oil Part I: Maneuvering into loading position. In: Proceedings of the 15th International Symposium on Ice (IAHR). Vol. 1. Gdansk, Poland.

Jensen, A., Løset, S., Høyland, K. V., Hellmann, J., Vodahl, B. P., 2000b. Model tests of an arctic tanker concept for loading oil Part II: Barge in moored position. In: Proceedings of the 15th International Symposium on Ice (IAHR). Vol. 1. Gdansk, Poland.

Kotras, T. V., Baird, A. V., Naegle, J. N., 1983. Predicting ship performance in level ice. SNAME Transactions 91, 329–349.

Kärnä, T., Turunen, R., 1989. Dynamic response of narrow structures to ice crushing. Cold Regions Science and Technology 17, 173–187.

Lindqvist, G., 1989. A straightforward method for calculation of ice resistance of ships. In: Proceedings of the 10th International Conference on Port and Ocean Engineering under Arctic Conditions. Vol. 2. Luleå, Sweden, pp. 722–735.

Lundamo, T., Bonnemaire, B., Jensen, A., Gudmestad, O. T., 2008. Back-calculation of the ice load applying on a moored vessel. In: Proceedings of the 19th IAHR International Symposium on Ice. Vancouver, British Columbia, Canada.

Nevel, D. E., 1992. Ice forces on cones from floes. In: Proceedings of the IAHR Symposium on Ice. Banff, Alberta, Canada.

Qu, Y., Yue, Q., Bi, X., Kärnä, T., 2006. A random ice force model for narrow conical structures. Cold Regions Science and Technology 45, 148–157.

Shkhinek, K. N., Bolshev, A. S., Frolov, S. A., Malyutin, A. A., Chernetsov, B. A., 2004. Modeling of level ice action on floating anchored structure concepts for the Shtokman field. In: Proceedings of the 17th IAHR International Symposium on Ice. Vol. 2. St. Petersburg, Russia, pp. 84–95.

Timco, G. W., O'Brien, S., 1994. Flexural strength equation for sea ice. Cold Regions Science and Technology 22, 285–298.

Toyama, Y., Yashima, N., 1985. Dynamic response of moored conical structures to a moving ice sheet. In: Proceedings of the 8th International Conference on Port and Ocean Engineering under Arctic Conditions. Vol. 2. Narssarssuaq, Greenland, pp. 677–688.

Valanto, P., 1992. The icebreaking problem in two dimensions: experiments and theory. Journal of Ship Research 36 (4), 299–316.

Valanto, P., 2001. The resistance of ships in level ice. SNAME Transactions 109, 53–83.

Weeks, W., Assur, A., 1967. The mechanical properties of sea ice. Vol. 11-C3 of CRREL Monographs. U.S. Army Cold Reg. Res. and Eng. Lab, Hanover, NH.

Chapter 6

A simplified interaction model for moored ships in level ice

By Vegard Aksnes

Cold Regions Science and Technology, 2010; 63(1-2): 29-39.

Cold Regions Science and Technology 63 (2010) 29–39

Contents lists available at ScienceDirect

Cold Regions Science and Technology

journal homepage: www.elsevier.com/locate/coldregions

A simplified interaction model for moored ships in level ice

Vegard Aksnes *

Department of Civil and Transport Engineering, Norwegian University of Science and Technology (NTNU), 7491 Trondheim, Norway

ARTICLE INFO

Article history:
Received 18 March 2010
Accepted 5 May 2010

Keywords:
Moored ships
Ice loads
Dynamic response
Methodology

ABSTRACT

A one dimensional numerical model for the interaction between a moored ship and drifting level ice is presented. Elastic beam theory combined with friction theory was utilized to derive the ice force model. The ice force model took the relative motions and velocities between the ship and ice into account, such that the vessel response influenced the interaction force between the hull and the ice. The ship was modelled with a single degree of freedom, with hydrodynamic and mooring forces in addition to the ice forces. Hydrodynamic forces were derived from potential theory, while the mooring force was assumed to be a linear function of the displacement of the ship. The ice properties were sampled from probability distributions, and the equation of motion was integrated over time. Parameter sensitivity studies were performed for both the ice force model and the ice–ship interaction model. The mooring forces oscillated most at the lowest ice drift speeds and with the lowest natural period of the vessel, due to dynamic amplification and interaction effects between the ship's response and the drifting ice. The necessity of the model was assessed by comparing with a simpler model and the difference between the models increased with decreasing mass and decreasing ice drift speed.

© 2010 Elsevier B.V. All rights reserved.

1. Introduction

Moored structures are believed to be feasible for marine operations in ice covered waters, in particular for the drilling, storage, production and offloading of hydrocarbons. Model basin experiments are probably the best current tool for studying moored ships in drifting ice. However, costs associated with such tests are high, and thus, it is desirable to develop numerical tools for initial studies before model tests in ice basins. Interactions between a moored ship and drifting ice are complex, because the response of the ship may influence the ice load process. This process is generally nonlinear and thus challenging to model numerically.

Moored structures in open water are known to be vulnerable to certain wave periods. Resonant or nonlinear motions may occur, depending on the structure and the wave conditions. Such phenomena have only been briefly studied in the ice research literature. The ice drift speed plays a vital role in the dynamics of the ice load process for both broken (managed) ice, level ice and ridge ice, while the mooring stiffness determines some of the main dynamic properties of the vessel. It is clear that these two parameters should be simultaneously studied to investigate possible resonant or nonlinear motions of moored structures in any kind of ice scenario. The effect of ice drift speed on moored structures has been considered by Toyama and Yashima (1985), Løset et al. (1998), Comfort et al. (1999), Wright (1999), Aksnes and Bonnemaire (2009b), Bonnemaire et al. (2009), among others, while mooring stiffness effects have been discussed by Jensen et al. (2008), Aksnes and Bonnemaire (2009b), Bonnemaire et al. (2009). Most of these studies were based on data from full-scale experiences with the cylindrical floater *Kulluk* or model test data. Toyama and Yashima (1985) used both a numerical model and model test data, while Aksnes and Bonnemaire (2009b) used a precursor of the model developed herein. Bonnemaire et al. (2009) applied two different numerical models for ice ridge actions on a turret moored ship-shaped vessel and a SPAR platform. There is little agreement in the above references, as some report that there are effects of speed, and some not.

As a step towards a full numerical model of moored ships in drifting ice, it may be beneficial to investigate a simplified problem. In this paper, we have chosen to study the interaction between a two-dimensional ship and level ice with a constant drift direction. Level ice actions are also relevant for other ice scenarios than pure level ice; the consolidated layer of ice ridges is often modelled with level ice methodology, and the methodology may be applied for actions from broken or managed ice, at least when the floes are relatively large. A constant ice drift direction has been assumed to simplify the hull geometry. The ship has one degree of freedom and can move in the surge direction. The ice force is split into two major parts; one is dependent on the ship's penetration in the ice sheet, and the other is dependent on the relative velocity between the ship and the ice sheet. The ship's response will therefore influence the ice–ship interaction force. The current model does not account for the bow shape other than in terms of the stem angle and this makes it difficult to estimate accurate mooring force levels. Nevertheless, the model will be

* Tel.: +47 918 74 693.
E-mail addresses: vegard.aksnes@ntnu.no, vegard.aksnes@marintek.sintef.no.

0165-232X/$ – see front matter © 2010 Elsevier B.V. All rights reserved.
doi:10.1016/j.coldregions.2010.05.002

compared with model test data to verify the magnitudes of the forces. The main focus is on qualitative observations regarding ice drift speed or mooring stiffness dependence.

This paper first gives a description of the problem and the assumptions used. Thereafter, the mathematical model is developed, and the ice force model is analysed. Stochastic ice properties are then introduced and the numerical procedure is explained. Some examples of time series are given, and observations are analysed. Parameter sensitivity studies for the ice–ship interaction model are reported and conclusions are given in the end.

2. Problem definition and methodology

A moored ship is exposed to drifting level sea ice, as seen in Fig. 1. Only head on straight ice drift is considered, and it is assumed that surge motion dominates the response. A mechanical model with a single degree of freedom was used to calculate surge motions, and all other degrees of freedom were neglected. It was assumed that the interaction process could last as long as necessary. The hull geometry was assumed to be very simple, and it is shown in Fig. 1. Because the response model is one dimensional, the bow shape was not taken into account, except for the stem angle.

The ice–ship interaction process has to be described at least in the vertical plane in order to enable estimation of ice forces that act on the ship. Three different phases were used to describe the ice loading process, that is, the breaking of intact level ice, the rotation of broken ice pieces and the sliding of broken pieces along the hull. Simple mechanical principles were used to formulate the ice force mathematically. Furthermore, the ice thickness, flexural strength, ice breaking length and elastic modulus of ice were described by probability distributions. Simulations were performed by sampling ice properties from distributions and then integrating the equations of motion over time. The variations of ice thickness, the mass of the ship, the natural period of the ship and the ice drift speed were studied in a parametric analysis.

3. Mathematical model

3.1. Equation of motion

The equation of motion for a moored ship with one degree of freedom can be written

$$m\ddot{X} = F_{\mathrm{hd}} + F_{\mathrm{moor}} + F_{\mathrm{ice}}, \tag{1}$$

where m is the mass of the ship, X is surge displacement of the vessel, and F_{hd}, F_{moor} and F_{ice} are hydrodynamic, mooring and ice forces, respectively. The dot denotes differentiation with respect to time, and the initial conditions in this text are $X(0)=\dot{X}(0)=0$. The hydrodynamic force may be expressed as (Faltinsen, 1990)

$$F_{\mathrm{hd}} = -A_{11}\ddot{X} - B_{11}\dot{X}, \tag{2}$$

if we assume linear viscous damping, and that added mass A_{11} and the damping coefficient B_{11} are frequency independent and constant. The mooring force is assumed to be a linear function of position

$$F_{\mathrm{moor}} = -kX, \tag{3}$$

where the constant k is referred to as the mooring stiffness. Forces from catenary mooring systems are generally nonlinear, but the linearity assumption is valid if the vessel experiences small oscillations around a mean position (Faltinsen, 1990). Hydrodynamic damping can then be expressed as a percentage of critical damping

$$\zeta_{\mathrm{hd}} = \frac{B_{11}}{2(m + A_{11})\omega_{\mathrm{n}}}, \tag{4}$$

where ω_{n} is the (undamped) natural frequency:

$$\omega_{\mathrm{n}} = \sqrt{\frac{k}{(m + A_{11})}}. \tag{5}$$

Eq. (1) can now be written as

$$\ddot{X} + 2\zeta_{\mathrm{hd}}\omega_{\mathrm{n}}\dot{X} + \omega_{\mathrm{n}}^2 X = \frac{1}{m + A_{11}}F_{\mathrm{ice}}, \tag{6}$$

using Eqs. (2)–(5).

3.2. Modelling of ice forces

Moored ships may be displaced from their intended position, and the ice force F_{ice} should be a function of the ship's penetration into the ice sheet and the relative velocity between the ship and the ice sheet. One may write $F_{\mathrm{ice}}=F_{\mathrm{ice}}(\kappa(t),\ \dot{\kappa}(t))$, where $\kappa(t)$ and $\dot{\kappa}(t)$ are penetration, i.e. the position of the bow in the ice sheet, and relative velocity, respectively. The variable $\kappa(t)$ can be defined as

$$\kappa(t) = \int_0^t v_i(\tau)\mathrm{d}\tau - X(t), \tag{7}$$

where v_i is the ice drift velocity. If v_i is constant, then

$$\kappa(t) = v_i t - X(t) \tag{8}$$

and $\dot{\kappa}(t)=v_i-\dot{X}(t)$. In the following it is assumed that the ice force can be split additively into one function that depends on the penetration and another that depends on the relative velocity; that is,

$$F_{\mathrm{ice}}(\kappa(t),\ \dot{\kappa}(t)) = F_{\mathrm{ice}}^{\mathrm{pen}}(\kappa(t)) + F_{\mathrm{ice}}^{\mathrm{vel}}(\dot{\kappa}(t)). \tag{9}$$

The penetration dependent term $F_{\mathrm{ice}}^{\mathrm{pen}}(\kappa(t))$ is associated with breaking of ambient level ice, the rotation of broken pieces and sliding of broken pieces along the hull. The damping of ship motions caused by ice is included in the relative velocity dependent term, $F_{\mathrm{ice}}^{\mathrm{vel}}(\dot{\kappa}(t))$. By formulating the ice force as a function of penetration and relative

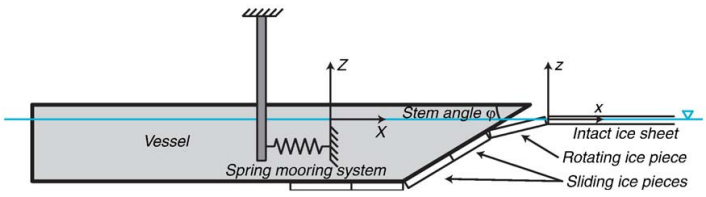

Fig. 1. The geometry used in the modelling.

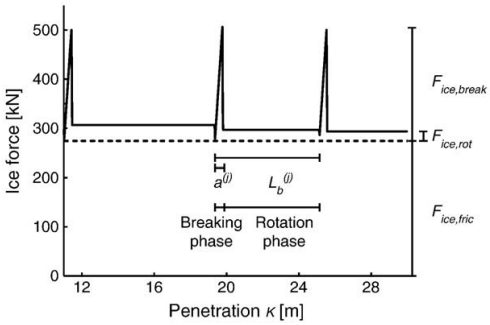

Fig. 2. Idealized penetration dependent part of the ice force. Contributions from breaking force, rotation force and friction force are indicated.

velocity, nonlinearities are introduced in Eq. (1) and numerical integration is required to solve this equation.

The penetration dependent part of the ice force $F_{\text{ice}}^{\text{pen}}$ is modelled as a cyclic function in the penetration domain (Fig. 2). In each cycle, the ice sheet is bent until flexural failure. The broken ice piece is then rotated and is finally parallel to the hull. After some time, the vessel meets the intact ice edge again and a new cycle starts. The three interaction phases, breaking, rotation and sliding, are illustrated in Fig. 3. Due to the ice–ship interaction process assumed, $F_{\text{ice}}^{\text{pen}}$ is split into breaking F_{break}, rotation F_{rot} and sliding F_{fric} terms, in the following way:

$$F_{\text{ice}}^{\text{pen}}(\kappa(t)) = F_{\text{break}}(\kappa(t)) + F_{\text{rot}}(\kappa(t)) + F_{\text{fric}}(\kappa(t)), \tag{10}$$

as illustrated in Fig. 2. This decomposition is assumed to be valid for the current geometry. Other geometries, such as cylindrical floaters (Kulluk), may experience rubble accumulation. A rubble accumulation in the vicinity of intact ice sheet in the breaking phase will possibly influence the forces needed to break and rotate the ice. For such geometries one should be careful about assuming decoupled phases of the ice–ship interaction process.

Our approach is a combination of different earlier approaches. Croasdale (1980), Nevel (1992) and others have modelled the ice force caused by bending by using an elastic material model for the ice sheet. The forces caused by rotation and friction are modelled similarly to what was done by Lindqvist (1989), while a similar decomposition of ice forces was used by Kotras et al. (1983), Frederking and Timco (1985), Valanto (1992, 2001). Furthermore, Kärnä and Turunen (1989) also used relative displacement and velocity when modelling level ice actions on a fixed vertical

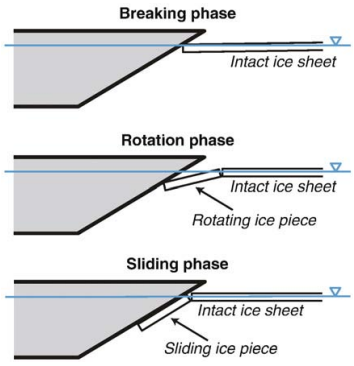

Fig. 3. Illustration of the breaking phase, the rotation phase and the sliding phase.

structure. Shkhinek et al. (2004) introduced a numerical procedure for estimating level ice actions on moored structures. Their approach was to integrate the equations of motion for the moored structure and the ice sheet simultaneously. Ice actions, especially those caused by breaking, might be more accurately estimated by Shkhinek et al. (2004), but at the cost of computational time, as more equations have to be numerically integrated.

Expressions for F_{break}, F_{rot}, F_{fric} and $F_{\text{ice}}^{\text{vel}}$ are derived in the next subsections.

3.2.1. Breaking force

In this section a relation between the deflection of the ice sheet and the horizontal force is derived. Thereafter, a failure criterion based on deflection is defined. Deflection of the ice sheet is related to the vessel penetration in the ice by a geometric argument, and thus the breaking force can be given as a function of penetration.

It is assumed that the ice sheet in the breaking phase can be described as a semi-infinite elastic beam on an elastic foundation. Dynamic effects for the beam and the foundation are neglected due to the low indentation speed. The differential equation describing the vertical deflection $u(x)$ at a distance x from the free edge of a semi-infinite elastic beam on an elastic foundation subjected to a concentrated vertical load P on the free edge, with a horizontal force N is (e.g., Hetenyi, 1946)

$$EI\frac{\mathrm{d}^4u}{\mathrm{d}x^4} + N\frac{\mathrm{d}^2u}{\mathrm{d}x^2} + \rho_{\text{w}}gBu = 0, \quad x > 0, \tag{11}$$

with boundary conditions

$$\lim_{x\to\infty} u(x) = 0, \quad \lim_{x\to\infty}\frac{\mathrm{d}u}{\mathrm{d}x} = 0, \quad \frac{\mathrm{d}^2u(0)}{\mathrm{d}x^2} = 0, \quad -EI\frac{\mathrm{d}^3u(0)}{\mathrm{d}x^3} = -P. \tag{12}$$

In Eq. (11), E is the modulus of elasticity, I is the second moment of area of the beam, ρ_{w} is the water density, g is the gravitational acceleration, and B is the width of the ice beam, which again is assumed to be as wide as the vessel. The solution to this boundary value problem is

$$u(x) = e^{-\beta x}(C_1 cos\alpha x + C_2 sin\alpha x), \tag{13}$$

where

$$C_1 = \frac{2P}{EI}\frac{\alpha\beta}{2\alpha^3\beta^2 + \alpha\beta^4 + \alpha^5}, \tag{14}$$

$$C_2 = \frac{P}{EI}\frac{\beta^2-\alpha^2}{2\alpha^3\beta^2 + \alpha\beta^4 + \alpha^5} \tag{15}$$

and

$$\alpha = \sqrt{\lambda^2 + \frac{N}{4EI}}, \quad \beta = \sqrt{\lambda^2 - \frac{N}{4EI}} \quad \text{and} \quad \lambda = \sqrt[4]{\frac{\rho_{\text{w}}gB}{4EI}}. \tag{16}$$

The deflection of the beam edge

$$u(0) = \frac{2P}{EI}\frac{\alpha\beta}{2\alpha^3\beta^2 + \alpha\beta^4 + \alpha^5} \tag{17}$$

can now be related to the distance penetrated by the vessel into the ice sheet $\kappa(t) = v_i t - X(t)$. By denoting the stem angle of the vessel by φ, the edge deflection can be expressed as $u(0) = (v_i t - X(t))\tan\varphi$. Mechanical arguments (ISO/FDIS 19906, 2010) give a relation between the horizontal force N and the vertical force P,

$$N = P\xi, \tag{18}$$

where

$$\xi = \frac{\sin\varphi + \mu\cos\varphi}{\cos\varphi - \mu\sin\varphi} \tag{19}$$

and μ is the kinetic friction coefficient between the ice and hull. Given a penetration κ, we can solve Eq. (17) for the horizontal force N. The contact force up to failure has been derived, and a failure criterion must be determined. The bending moment at point x is

$$M(x) = -EI\frac{d^2u}{dx^2}. \tag{20}$$

The flexural strength σ_f is for a beam of width B and thickness h_i related to the ultimate bending moment M_0 by

$$\sigma_f = \frac{6M_0}{Bh_i^2}, \tag{21}$$

where h_i is the ice thickness. The ice beam fails when the maximal bending moment equals the ultimate bending moment. Strictly speaking, Eq. (21) should include a term with the horizontal force N as well. However, with the low stem angle and the ice cross-sectional area used herein, the contribution from this term is small and the term is therefore neglected in the following.

The jth period of the force function associated with breaking can be expressed as

$$F_{\text{break}}^{(j)}(t,X(t)) = \begin{cases} N(t,X(t)), & \kappa\in\left[\sum_{i=0}^{j-1}L_b^{(i)}, \sum_{i=0}^{j-1}L_b^{(i)} + a^{(j)}\right] \\ 0, & \text{otherwise} \end{cases} \tag{22}$$

where $\{L_b^{(i)}\}$ is a sequence of breaking lengths and $a^{(j)}$ is the penetration into the ice sheet at failure. The total ice force associated with bending the ice sheet up to flexural failure is $F_{\text{break}}(t,X(t)) = \sum_{j=1}^{n} F_{\text{break}}^{(j)}(t,X(t))$, and the total length of the ice sheet is $L_{\text{ice}} = \sum_{i=0}^{n} L_b^{(i)}$.

3.2.2. Rotation force

An energy approach is used to calculate the rotation force. The difference in potential energy for a floating floe and a floe parallel to the bow, with its upper end in the water plane, is

$$E_p^{(j)} = \frac{1}{2}(\rho_w - \rho_i)g\left(L_b^{(j)}\right)^2 Bh_i^{(j)}\sin(\varphi), \tag{23}$$

where $h_i^{(j)}$ is the thickness of ice floe number j. We assume that the rotation phase lasts from $\kappa = \sum_{i=0}^{j-1} L_b^{(i)} + a^{(j)}$ to $\kappa = \sum_{i=0}^{j} L_b^{(i)}$, such that the average vertical force needed to submerge floe j is

$$v_{\text{rot}}^{(j)} = \frac{E_p^{(j)}}{L_b^{(j)} - a^{(j)}}. \tag{24}$$

The horizontal force on the vessel associated with rotation of floe j is according to Eq. (18)

$$F_{\text{rot}}^{(j)}(t,X(t)) = \begin{cases} v_{\text{rot}}^{(j)}\xi, & \kappa\in[\sum_{i=0}^{j-1}L_b^i + a^{(j)}, \sum_{i=0}^{j}L_b^i) \\ 0, & \text{otherwise}, \end{cases} \tag{25}$$

such that the total rotation force is $F_{\text{rot}}(t,X(t)) = \sum_{j=1}^{n} F_{\text{rot}}^{(j)}(t,X(t))$.

3.2.3. Sliding force

Due to our simplified geometry, we assume that parts of the bottom of the vessel are covered with broken ice floes, while the sides are not. From hydrostatics we obtain

$$F_{\text{fric}} = \mu(\rho_w - \rho_i)gLBh_i, \tag{26}$$

where L is the length of the ice covered part of the bottom of the vessel. Moored vessels operating in ice will most likely have a bow shape that will push ice sideways and limit the amount of ice sliding under the vessel. This means that only a part of the bottom of the vessel will be covered with ice. In the following we will assume that L is constant, regardless of the size of the vessel. This also enables us to study effects of variations in the mass of the vessel.

In simulations, the ice thickness h_i is a random variable. The sliding force is calculated using the average ice thickness of the broken ice floes under the vessel at a certain penetration in the ice sheet. Thus, the sliding force is also a function of the penetration and will vary slowly during the ice–ship interaction.

3.2.4. Velocity dependent ice force

Damping from ice is modelled as a function of the relative velocity between the drifting ice and the moored ship $\dot{\kappa}(t) = v_i - \dot{X}(t)$. It is assumed that the damping force is linearly proportional to $\dot{\kappa}$, such that

$$F_{\text{ice}}^{\text{vel}}(\dot{\kappa}(t)) = B_{\text{ice}}\left(v_i - \dot{X}(t)\right), \tag{27}$$

where B_{ice} is a damping coefficient. Eq. (1) may be written

$$(M + A_{11})\ddot{X} + (B_{\text{hd}} + B_{\text{ice}})\dot{X} + kX = F_{\text{ice}}^{\text{pen}}(\kappa) + B_{\text{ice}}v_i \tag{28}$$

or in the form

$$\ddot{X} + \left(2\zeta_{\text{hd}}\omega_n + \frac{B_{\text{ice}}}{M + A_{11}}\right)\dot{X} + \omega_n^2 X = \frac{1}{m + A_{11}}F_{\text{ice}}^{\text{pen}}(\kappa) + \frac{B_{\text{ice}}}{m + A_{11}}v_i. \tag{29}$$

From Eq. (28) it can be seen that the formulation introduced in Eq. (27) gives an ice damping term, similar to the hydrodynamic damping, and one term directly proportional to the ice drift speed. If B_{ice} is chosen to be constant, then the term depending on ice drift speed will be the same for all mooring and vessel configurations, but the ice damping term will be of a different nature than the hydrodynamic damping. If we let

$$\zeta_{\text{ice}} = \frac{B_{\text{ice}}}{2(m + A_{11})\omega_n}, \tag{30}$$

then the ice damping term will behave in the same way as the hydrodynamic damping. On the other hand, the term depending on the ice drift speed will depend on the square root of the vessels mass and square root of the mooring stiffness. In this paper, the parameter B_{ice} was determined by Eq. (30) to get a consistent ice damping term. Consequences of this choice will be discussed in Section 4.2.

4. Analysis of the ice force model

In this section we will study the ice force model itself, without the coupling to the ship response model.

Table 1
Base value and range for parameters used in the sensitivity study for $F_{\text{ice}}^{\text{pen}}$. The ice thickness is denoted h_i, friction coefficient μ, ice density ρ_i, flexural strength σ_f, modulus of elasticity E and ice breaking length L_b.

Parameter	Base value	Range	Unit
h_i	1	[0.2, 2]	[m]
μ	0.1	[0.05, 0.2]	[–]
ρ_i	917	[800, 930]	[kg/m^3]
σ_f	450	[100,700]	[kPa]
E	5	[1,8]	[GPa]
L_b	$5h_i$	$[3h_i, 7h_i]$	[m]

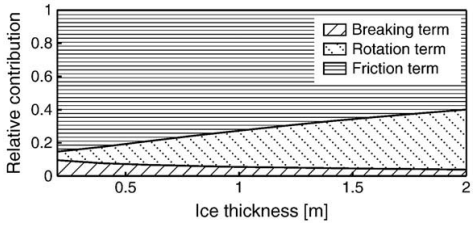

Fig. 4. Relative contribution of the mean of the different terms of the penetration dependent part of the ice force as a function of the ice thickness.

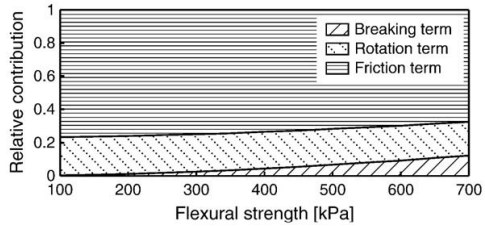

Fig. 6. Relative contribution of the mean of the different terms of the penetration dependent part of the ice force as a function of the flexural strength.

4.1. The penetration dependent part of the ice force

A parameter sensitivity analysis for the penetration dependent part of the ice force $F_{\text{ice}}^{\text{pen}}$ (Eq. (10)) was performed with deterministic ice properties. Values for the ice thickness, flexural strength, modulus of elasticity, friction coefficient and ice density were varied one at time while keeping the others fixed. The base value and range for each of the parameters are given in Table 1. The analysis is split into two parts; relative contribution of the various terms of $F_{\text{ice}}^{\text{pen}}$, and how the mean and the standard deviation of $F_{\text{ice}}^{\text{pen}}$ varies with various parameters.

The relative contribution of the mean of each of the terms of $F_{\text{ice}}^{\text{pen}}$ are plotted in Figs. 4–7. By relative contribution, we mean the ratios $\bar{F}_{\text{break}}/\bar{F}_{\text{ice}}^{\text{pen}}$, $\bar{F}_{\text{rot}}/\bar{F}_{\text{ice}}^{\text{pen}}$ and $\bar{F}_{\text{fric}}/\bar{F}_{\text{ice}}^{\text{pen}}$. The breaking term generally contributed to 5–10% of the penetration dependent part of the ice force, the rotation term 20–30%, and the friction term 60–80%. Moreover, variations of the ice thickness, flexural strength, elastic modulus, friction coefficient and ice density gave the following effects on the relative contributions:

- Both the rotation term and the friction term depend linearly on the ice thickness. In addition, the rotation term also depend on the breaking length, which was given as a multiple of the ice thickness, and thus the relative contribution of the rotation term increased with the ice thickness, while relative contribution of the friction term decreased (Fig. 4).
- The friction coefficient μ had effects on the relative contribution of the friction term and the rotation term, but not on the breaking term (Fig. 5). The friction term depends linearly on μ, while the rotation term depends on the factor $\xi = (\sin\varphi + \mu\cos\varphi)/(\cos\varphi - \mu\sin\varphi)$. The friction coefficient μ had therefore larger effects on the friction term than the rotation term.
- The ice density did not affect the relative contributions of the terms, though it affected $F_{\text{ice}}^{\text{pen}}$.
- The breaking term is the only term which depends on flexural strength and modulus of elasticity. Variations in flexural strength and modulus of elasticity changed the mean of the breaking term and of $F_{\text{ice}}^{\text{pen}}$, while the magnitudes of the rotation and friction terms remained the same (Figs. 6 and 7).
- The breaking length L_b determines the duration of the breaking term and the rotation term. Further, the magnitude of the rotation term is influenced by the breaking length, as the size of the piece to be rotated depends on L_b (Fig. 8).

To summarize, variations of the ice thickness and the friction coefficient induced the most significant changes in the relative contribution of the different phases.

The effects of the ice thickness, flexural strength, elastic modulus, friction coefficient and ice density on the mean and the standard deviation of $F_{\text{ice}}^{\text{pen}}$ are plotted in Figs. 9–13. The results can be summarized as follows:

- The ice thickness, friction coefficient and ice density had a large influence on the mean force. The friction force constitute the main part of $F_{\text{ice}}^{\text{pen}}$, and it depends linearly on the ice thickness, friction coefficient, the difference between the ice and water densities and the length of the part of the hull which is exposed to friction forces. The mean force was not influenced by the flexural strength and modulus of elasticity because they only affect the breaking phase. As seen above, the mean breaking force only accounts for 5–10% of the mean of the total ice force $F_{\text{ice}}^{\text{pen}}$.
- The standard deviation is a measure for the oscillatory nature of $F_{\text{ice}}^{\text{pen}}$. The breaking phase is the phase that gives the largest contributions to the oscillations of the total ice force. Because the breaking phase is affected by ice thickness, flexural strength and modulus of elasticity, the standard deviation should vary more with these parameters than with the friction coefficient and ice density. Figs. 9–13 support this reasoning.

4.2. The velocity dependent part of the ice force

Recall Eq. (27) and that the velocity dependent part of the ice force $F_{\text{ice}}^{\text{vel}}$ could be separated into two terms

$$F_{\text{ice}}^{\text{vel}}(\dot{\kappa}(t)) = -B_{\text{ice}}\dot{X}(t) + B_{\text{ice}}v_{\text{i}}, \tag{31}$$

where B_{ice} was a damping coefficient. In Eq. (31), the first term is proportional to the vessel's speed, while the second term is proportional to the ice drift speed.

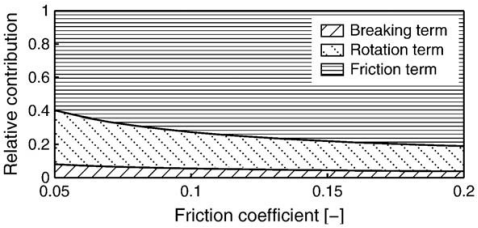

Fig. 5. Relative contribution of the mean of the different terms of the penetration dependent part of the ice force as a function of the friction coefficient.

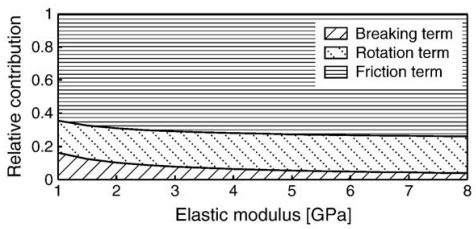

Fig. 7. Relative contribution of the mean of the different terms of the penetration dependent part of the ice force as a function of the elastic modulus.

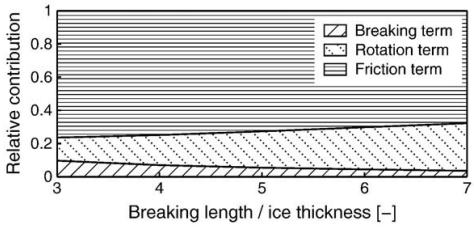

Fig. 8. Relative contribution of the mean of the different terms of the penetration dependent part of the ice force as a function of the breaking length.

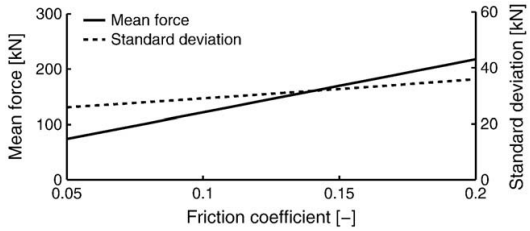

Fig. 10. Mean and standard deviation of $F_{\mathrm{ice}}^{\mathrm{pen}}$ as a function of friction coefficient.

With our assumption on B_{ice} (see Eq. (30)), the first term behaves exactly as the hydrodynamic damping term (Eq. (2)). In practice, this means that more linear viscous damping is introduced in the system, relative to the critical damping.

According to Eq. (30), the second term behaves as $\sqrt{(m+A_{11})k}v_{\mathrm{i}}$, and for a given vessel and mooring setup it is linear with respect to the ice drift speed. Full-scale and model test data from free-going vessels show a linear dependence on v_i (Jones, 1989). Moreover, Lindqvist (1989) used a linear speed dependence in his model for level ice resistance for free-going vessels. For fixed sloping structures there does not seem to be full agreement about speed effects, as Shkhinek and Uvarova (2001) and Matskevitch (2002) claim that there is a speed effect, while Brown (2008) was not able to find such a dependence from full-scale data from the *Confederation Bridge*. For moored vessels, different results have been reported. Comfort et al. (1999) found a clear increase of mean mooring force with speed for the *Kulluk*, turret moored drillships and tankers in level ice, based on model test data. On the other hand, Wright (1999) did not find a speed dependence in the full-scale measurements of the *Kulluk*. Recently, Aksnes (2010) performed model tests in level ice, and found that both the mean mooring force and the mean of the ice forces in the bow increased with ice drift speed. Due to these observations a linear model was introduced in this paper.

In addition to speed dependence, the second term also introduces dependence on mass and mooring stiffness. The term increases with the square root of the mass and the mooring stiffness, which is clearly an effect of our choice of B_{ice}. If and possibly how this term vary with mass and mooring stiffness is still an open question.

Due to the above observations, it is clear that the model for $F_{\mathrm{ice}}^{\mathrm{vel}}$, must be regarded as an initial attempt to describe ice forces related to relative velocity between a moored ship and drifting ice. More research is needed to establish physically sound models for these type of forces.

5. Stochastic ice properties and numerical implementation of the model

5.1. Ice properties

Ice properties experience seasonal changes, as well as spatial variations in each ice floe. Seasonal changes are important for the long-term behaviour of the ship, while spatial changes are more relevant for short-term response, such as the response to the actions from a large ice floe. Spatial ice properties were sampled from probability distributions. Truncated normal distributions were assumed for the flexural strength σ_{f}, modulus of elasticity E, ice thickness h_i and the ration between breaking length and ice thickness L_b/h_i. This means that they are normally distributed random variables, but are only allowed to assume values within a specified range (Fig. 14). Details regarding the particular distributions are given in Table 2.

The ice properties used in this study are realistic, but not specific to a particular season or geographic location. In the simulations, σ_{f}, h_i and E were sampled once per breaking length, and thus the resolution of the ice properties in penetration domain were in the range of 3 to 7 times the mean ice thickness (Fig. 15). It would be natural to use the breaking length corresponding to the point where the bending moment reaches it maximum. Several researchers (Keinonen, 1983; Tatinclaux, 1986; Izumiyama et al., 1994; Lau et al., 1999; ISO/FDIS 19906, 2010) has studied the breaking length or ice piece size for ships and various sloping structures and concluded that the breaking length predicted by elastic theory is longer than what is experienced in nature. Our assumption about ice breaking length is in reasonable correspondence with the research literature.

5.2. Numerical implementation

Simulations were carried out by first generating an ice sheet of a specified length, and then to sample ice thickness, ice breaking length, modulus of elasticity and flexural strength from the distributions mentioned above. The spatial resolution was determined by the breaking length as a set of new ice properties were sampled for each breaking length (Fig.15). Using this ice sheet, the penetration dependent part of the ice force was found and the equation of motion was then integrated over time with an explicit multi-step Adams–Bashforth integration scheme (Kreyszig, 1999). An explicit scheme was necessary because a control formulation had to be added to ensure that a completed breaking phase could not be entered again in the case the vessel moved away from the ice sheet. The three-step Adams–Bashforth method was chosen due to its accuracy, with an

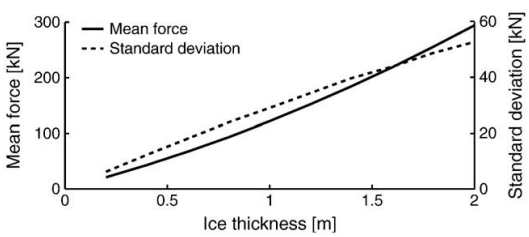

Fig. 9. Mean and standard deviation of $F_{\mathrm{ice}}^{\mathrm{pen}}$ as a function of ice thickness.

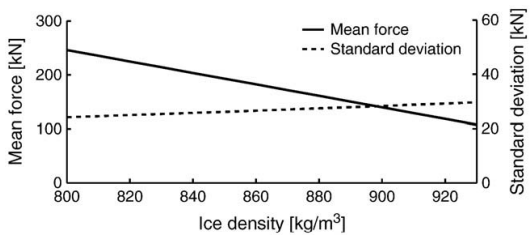

Fig. 11. Mean and standard deviation of $F_{\mathrm{ice}}^{\mathrm{pen}}$ as a function of ice density.

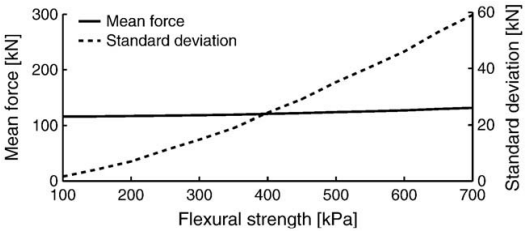

Fig. 12. Mean and standard deviation of $F_{\mathrm{ice}}^{\mathrm{pen}}$ as a function of flexural strength.

error of $O(\Delta t^4)$, where Δt is the time step (Kreyszig, 1999), and due to its simplicity with respect to implementation.

Recall Eq. (6)

$$\ddot{X} + 2\zeta_{\mathrm{hd}}\omega_{\mathrm{n}}\dot{X} + \omega_{\mathrm{n}}^2 X = \frac{1}{m + A_{11}} F_{\mathrm{ice}}\left(\kappa,\ \dot{\kappa}\right). \tag{32}$$

It is convenient to formulate this second order ordinary differential equation (ODE) to a system of first order equations, and thus

$$\dot{X} = Y \tag{33}$$

$$\dot{Y} = \frac{1}{m + A_{11}} F_{\mathrm{ice}}\left(\kappa,\ \dot{\kappa}\right) - 2\zeta_{\mathrm{hd}}\omega_{\mathrm{n}} Y - \omega_{\mathrm{n}}^2 X. \tag{34}$$

Let

$$\mathbf{X} = \begin{bmatrix} X \\ Y \end{bmatrix} \tag{35}$$

and

$$\mathbf{f}(\mathbf{X}, \mathbf{t}) = \begin{bmatrix} Y \\ \frac{1}{m + A_{11}} F_{\mathrm{ice}}\left(\kappa,\ \dot{\kappa}\right) - 2\zeta_{\mathrm{hd}}\omega_{\mathrm{n}} Y - \omega_{\mathrm{n}}^2 X \end{bmatrix}, \tag{36}$$

then the system of ODEs can be written

$$\dot{\mathbf{X}} = \mathbf{f}(\mathbf{X}, t). \tag{37}$$

The 3-step Adams–Bashforth integration scheme for this system of equations read

$$\mathbf{X}_{n+3} = \mathbf{X}_{n+2} + \Delta t\left[\frac{23}{12}\mathbf{f}(\mathbf{X}_{n+2}, t_{n+2}) - \frac{4}{3}\mathbf{f}(\mathbf{X}_{n+1}, t_{n+1}) + \frac{5}{12}\mathbf{f}(\mathbf{X}_n, t_n)\right]. \tag{38}$$

6. Analysis of the ice-moored ship interaction model

This section starts with examples of time series of mooring and ice forces from simulations. The time series are included to show

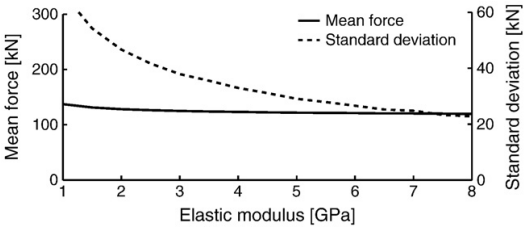

Fig. 13. Mean and standard deviation of $F_{\mathrm{ice}}^{\mathrm{pen}}$ as a function of modulus of elasticity.

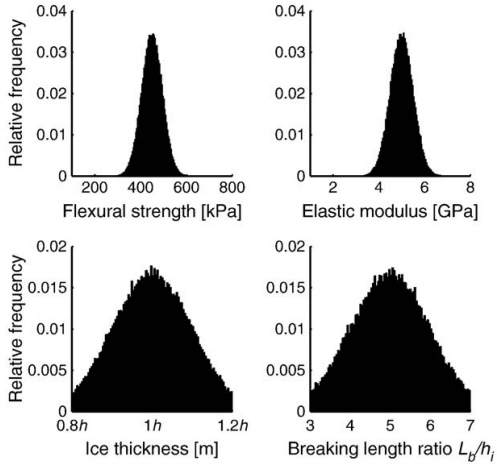

Fig. 14. Histograms of simulated flexural strength, elastic modulus, ice thickness and ratio between breaking length and ice thickness.

characteristic features of the mooring force and the ice force. Then follows a sensitivity study of mooring and ice forces focusing on effects from the ice drift speed, the natural period and the ship's mass. Lastly, the ice force model is compared with a simpler one and differences between them are identified.

6.1. Examples of time series from simulations

In this section time series of mooring and ice forces from selected simulations are studied. Fig. 16 shows plots from six different simulations, three with a soft mooring system giving a surge natural period of 200 s and three with stiff mooring system giving a surge natural period of 40 s. The mass of the vessel was 125,000 tonnes in all simulations. Three different ice drift speeds, 0.05, 0.25 and 0.5 m/s, were used for each of the two mooring stiffnesses. Ice properties were as given in Table 2, with a mean ice thickness of 1 m.

First of all, one should note that the mean mooring force is in the range from 0.8 to 1.3 MN (Fig. 16), depending on the stiffness of the mooring system and the ice drift speed. Due to simplifications of the hull geometry it is difficult to do direct comparisons with model test results, but a check of the plausibility can still be made. Aksnes (2010) performed model tests of moored ship in level ice and measured average mooring forces between 0.5 and 1 MN. Taking into account that the ice thickness and the ship's beam and mass were lower in the model tests than in the simulations, one may conclude that the load level of the numerical model is reasonable.

Let us briefly describe some observations with respect to variations in ice drift speed and mooring stiffness based on observations from Fig. 16. There is a stronger speed effect on the mean mooring and ice forces for the stiff system than for the soft system as they increase substantially more with speed for the stiff

Table 2
Statistical properties for flexural strength σ_{f}, modulus of elasticity E, ice thickness h_i and breaking length L_b used in the simulations. The value h is the mean ice thickness as specified before each simulation.

Parameter	Mean	Standard deviation	Range	Unit
σ_{f}	450	45	[100,800]	[kPa]
E	5	0.5	[1,8]	[GPa]
h_i	h	$0.1h$	$[0.8h, 1.2h]$	[m]
L_b	$5h$	h	$[3h, 7h]$	[m]

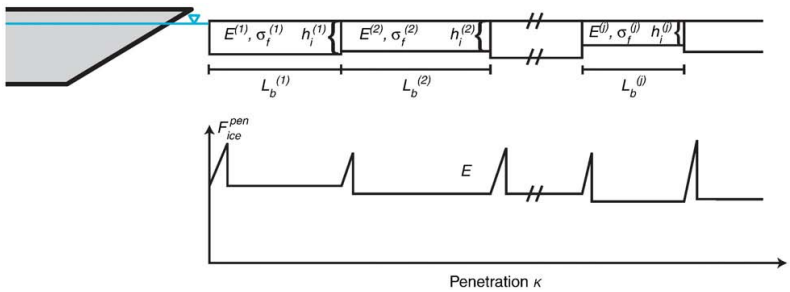

Fig. 15. A sketch of the spatial resolution of the ice properties and the penetration dependent term of the ice force.

system. This is a direct result of the chosen model for $F_{\text{ice}}^{\text{vel}}$, since this term depends on the square root of the mooring stiffness. There is also a speed effect on the stiff system in terms of surge oscillations because larger oscillations are experienced at low ice drift speed than at medium and high speeds. At the lowest ice drift speed, the time period between each pair of breaking phases is two to three times the vessel's natural period and thus the surge oscillations get amplified. A similar trend can not be visually observed for the soft system. The latter speed effect is caused by $F_{\text{ice}}^{\text{pen}}$.

The ice force varies at two scales. The breaking phase is of short duration and appears as impulse peaks compared to the slowly varying part caused by variations in the friction force, which depends on the (stochastic) ice thickness. For the stiff system, these two processes can be identified in the surge response of the structure, at least for medium and high ice drift speeds. For these speeds, the system experiences oscillations at both low and high frequencies. The high frequency oscillations are caused by the breaking of intact ice, while the low frequency oscillations are caused by variations in the friction force. For the soft system, the two processes are not easy to distinguish. This is mainly because the system has lower natural frequency and acts as a low pass filter such that high frequency loads, such as the impulse loads caused by the breaking of ice, are not transferred to the response in the same way as for a stiff system.

Fig. 17 shows the mooring and ice forces from another simulation. The mass of the vessel was 25,000 tonnes, and the natural period was 200 s. The mean ice thickness was 1 m, and the drift speed was 0.05 m/s. The other ice properties are listed in Table 2. This simulation illustrates a particular phenomenon called feedback effect. Feedback is caused by the surge response of the ship. As the breaking, rotation and friction forces are parameterized by the penetration of the ship into the ice sheet, the resulting ice–hull interaction force will depend on the surge motion of the ship. In principle, a feedback effect can

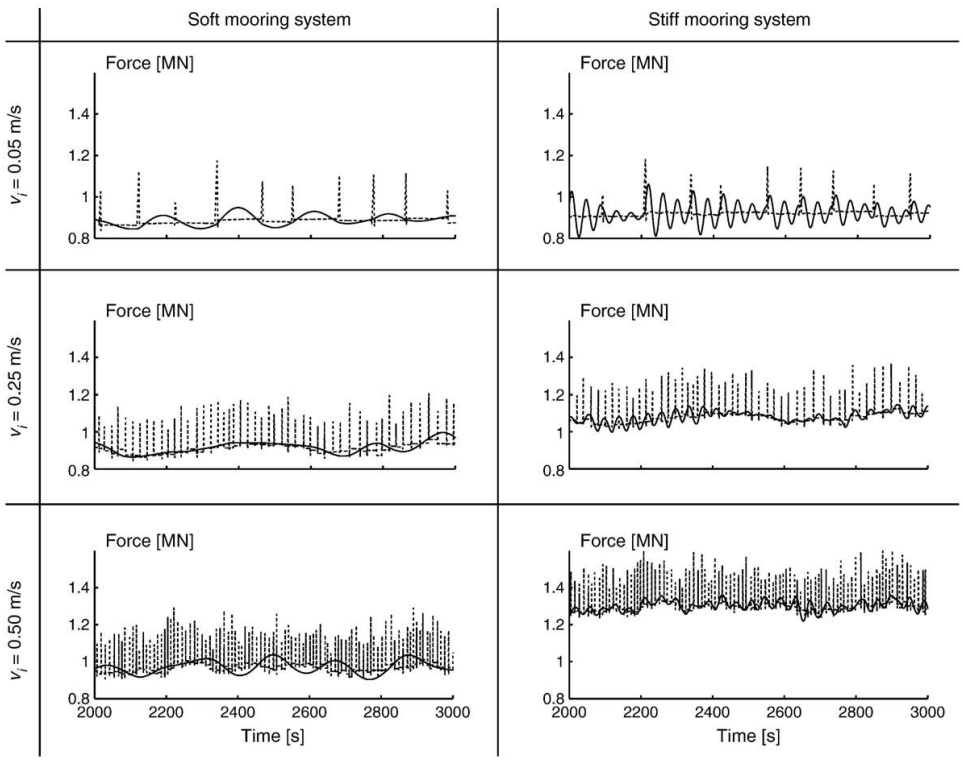

Fig. 16. Time series of mooring (solid line) and ice forces (dashed line) from simulations. Ice thickness was 1 m and the ship's mass was 25,000 tonnes in all simulations.

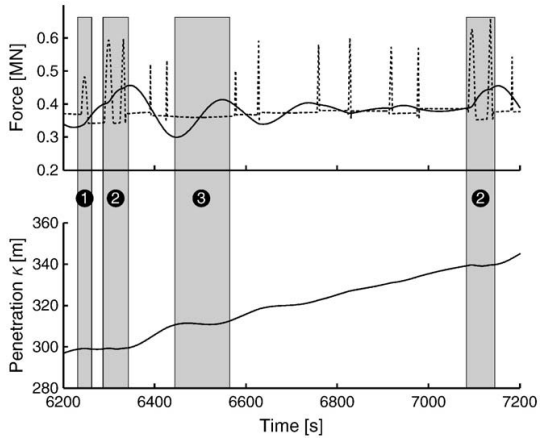

Fig. 17. Plots from simulations with a ship with a mass of 25,000 tonnes, a natural period of 200 s, an ice thickness of 1 m and an ice drift speed of 0.05 m/s. Time series of mooring (solid line) and ice forces (dashed line) in the upper plot. Time series of the penetration of the vessel in the ice sheet in the lower plot. Feedback effects in the breaking phase are indicated by ❶ and ❷, and in the rotation phase by ❸.

occur both in the breaking phase and in the rotation phase. Both phases can be lengthened or shortened in time compared to the duration of these phases for a fixed structure, due to the surge motions of the vessel. Feedback in the breaking and rotation phases are marked by ❶ and ❸ in Fig. 17, respectively. Moreover, if the vessel moves in the same direction and faster than the ice sheet, the breaking phase can be left, the bow may lose contact with the intact ice sheet, and the breaking phase has to be started again when the vessel surges back; see ❷ in Fig. 17. This situation will usually give large mooring forces, since the breaking phase will last for a longer time period than for regular breaking phases. A similar situation may occur for the rotation phase, and the ice force will then drop to the level of the sliding force. This case is not pictured in Fig. 17.

6.2. Parameter sensitivity analysis

A parametric analysis with stochastic ice properties was performed to investigate effects on the standard deviation of mooring and ice forces of some of the main model parameters. Three different values were used for the ship's mass and natural period. The mooring stiffness varied with the ship's mass and natural period according to Eq. (4). Twenty simulations, each corresponding to a time period of three hours, were performed for each set of parameters and for each ice drift speed. An overview of the simulation parameters can be found in Table 3, and the ice properties are found in Table 2.

Table 3
Parameters used in the sensitivity study.

Parameter	Values
Mass M [kt]	25, 125, 250
Beam B [m]	40
Friction length L [m]	18
Draught T [m]	15
Natural period T_n [s]	40, 120, 200
Stem angle φ [deg]	25
Hull–ice friction μ [–]	0.1
Ice thickness h_i [m]	0.5, 1.0, 1.5
Ice drift speed v_i [m/s]	0.05–0.5
Ice damping ratio ζ_{ice} [–]	0.02
Hydrodynamic damping ratio ζ_{hd} [–]	0.04

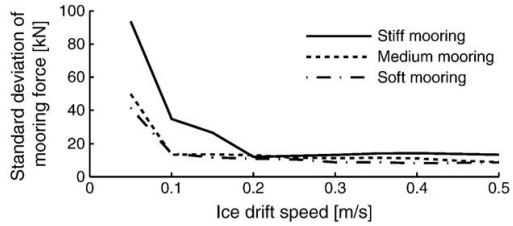

Fig. 18. Ice drift speed effects on the standard deviation of the mooring force for stiff, intermediate and soft mooring systems from simulations using a ship with a mass of 25,000 tonnes and a mean ice thickness of 1 m.

6.2.1. Mooring force

The mooring force is directly proportional to surge motions in the assumed model. Surge motions are mainly governed by the ship's natural period, the ice drift speed and the mass. The analysis of effects of these parameters showed the following:

- A clear speed dependency for the standard deviation of the mooring force for the small ship with all mooring systems (Fig. 18) was seen. For medium and large ships, this dependency was only present with the lowest natural period.
- The mooring force standard deviation decreased with increasing natural period for small ships (Fig. 19).
- The ship's mass was not seen to affect the standard deviation of the mooring force, except at the lowest ice drift speed, where it decreased with increasing mass.
- The mean mooring force behaved like $\sqrt{mk}v_i$ due to the assumed model for F_{ice}^{vel}.

Effects of the natural period and the ice drift speed can be explained in terms of dynamic amplification. The vessel's motions will be amplified when the excitation force has an energy peak close to the vessel's natural period. A relatively common quantity (ISO/FDIS 19906, 2010) is the ice breaking period for a fixed structure $T_i = L_b/v_i$ and one would expect to have dynamic amplification when T_i is close to the vessel's natural period T_n. However, if one performs a spatial spectral analysis of an ice force function, as used in this text, but with a deterministic breaking length, then the analysis will give energy peaks at n/L_b, where $n = 1, 2, 3, \ldots$ This implies that there will be dynamic amplification at a variety of ice drift speeds, that is, when $v_i = L_b/nT_n$. The upper bound is thus $v_i = L_b/T_n$. In the current simulations, natural periods of 40, 120 and 200 s were used, and the lowest ice drift speed was 0.05 m/s. Upper bounds for dynamic amplification for these natural periods are 0.125, 0.04 and 0.025 m/s. With the random breaking length used here, on would therefore expect that the stiffest system would experience dynamic amplification at speeds below 0.15 m/s and that the medium and the soft systems would be weakly dynamically amplified at $v_i = 0.05$ m/s. This corresponds well with observations from our simulations (Fig. 18).

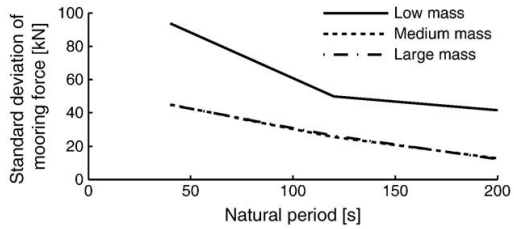

Fig. 19. Effects of the natural period on the standard deviation of the mooring force for a ship with a mass of 25,000 tonnes, 125,000 tonnes and 250,000 tonnes. The ice drift speed was 0.05 m/s and the mean ice thickness was 1 m.

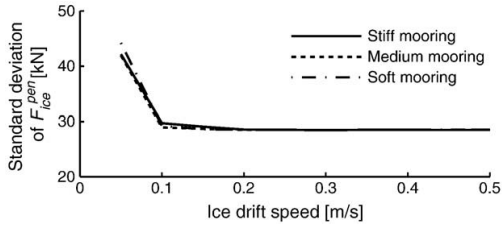

Fig. 20. Ice drift speed effects on the standard deviation of F_{ice}^{pen} in time domain for stiff, intermediate and soft mooring systems from simulations using a ship with a mass of 25,000 tonnes and a mean ice thickness of 1 m.

Fig. 19 shows effects of the natural period for different masses and that there is a difference between the masses. Without the penetration dependent ice force formulation, this difference would not have been present. This effect is caused by the feedback phenomenon described in Section 5. As seen from Fig. 19, the feedback effect is limited by mass, as it decreases with increasing mass.

For a designer it is important to know how to minimize vessel motions. From the above analysis, long natural periods and large mass seem to be preferable in terms of surge oscillations. However, a long natural period implies a soft mooring system and allows larger offsets, which again may cause large deformations in risers and umbilicals.

The largest oscillations occurred at low ice drift speeds. The ice drift speed is of course outside of the designer's control and very low ice drift speeds do occur in reality, for instance at shifts in the ice drift direction.

6.2.2. Ice–hull interaction force

The resulting time series for F_{ice}^{pen} from interaction with the ship will possibly exhibit different statistical properties than the penetration series. The ship response varies with ice drift speed, mooring stiffness and mass and thus the time series for F_{ice}^{pen} (the ice–hull interaction force) will depend on these parameters as well. The main effects on the time series for F_{ice}^{pen} were:

- There was generally no effect from the ice drift speed on the standard deviation of F_{ice}^{pen}. However, for the smallest ship there was a large increase when the drift speed decreased towards very low speeds (Fig. 20), caused by the feedback effects analysed earlier.
- The feedback effects can also explain the mass effect at the lowest ice drift speed (Fig. 21).
- No effects from the natural period were seen.

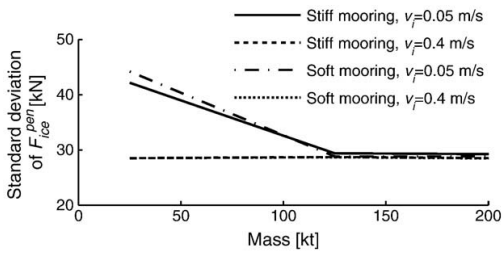

Fig. 21. Effects of the ship's mass on the standard deviation of F_{ice}^{pen} in time domain for the stiff mooring system and ice drift speeds of 0.05 m/s and 0.4 m/s, and for the soft mooring system and ice drift speeds of 0.05 m/s and 0.4 m/s from simulations with a mean ice thickness of 1 m.

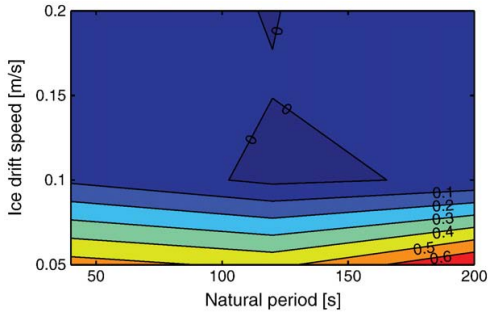

Fig. 22. Relative difference between *mooring force* standard deviation from simulations with penetration and time descriptions of the breaking, rotation and friction terms of the ice force. A ship with a mass of 25,000 tonnes and a mean ice thickness of 1 m was used in the simulations.

6.3. Comparison with a simpler ice force model

Simulations with the parameters in Table 3 were also performed with breaking, rotation and friction forces, parameterized by time, instead of the penetration of the vessel into the ice. This means that the ship's response was not accounted for in the ice–hull interaction force.

There was practically no difference between penetration and time description in the mean values for the mooring and ice forces. However, large effects on standard deviation of the mooring force were seen for the smallest ship at low ice drift speeds (Fig. 22). The effect was similar for all natural periods and decreased with increasing drift speed. For larger ships there was little or no difference between penetration and time descriptions. The difference between the formulations were caused by the feedback effect. The time parameterized formulation was non-conservative, as the standard deviation of the mooring force was underestimated by up to 60% compared to the penetration formulation.

Penetration description could be equally or more important for response in other degrees of freedom. Aksnes and Bonnemaire (2009a) analysed a turret moored icebreaker in varying ice drift and found that the vessel response affected the ice failure modes and thus the ice–ship interaction force. A penetration description would be necessary when modelling such events.

The analysis above showed that for the present vessel there were many cases where the penetration description was redundant and the ice forces could have been described simply in time domain. It is important to identify such cases, since the model is linear when ice forces are described in time domain and frequency domain methods may be applied. An ice force spectrum could possibly be estimated and the transfer function for the moored ship could be used to estimate a mooring force spectrum. Such frequency domain methods are in general faster to perform than time domain analyses.

7. Conclusions

A simplified numerical model for estimating the response of moored ships in level ice with constant drift direction was established. The model accounts for the ship response in the ice force formulation by defining the ice force as a function of the ship's penetration into the ice sheet and relative velocity. Only the surge response of the vessel was modelled because the model is one dimensional. Due to this simplification, a simplified hull geometry could be used.

Validation of the model was not straight forward mainly due to the one dimensionality of the model. Nevertheless, the methods used in the model are well known; it is the application to moored ships and the combination of methods that are new. Comparisons with model

tests showed that the numerical model predicts reasonable load levels. The formulation for the penetration dependent part of the ice force was investigated to understand the significance of the parameters. The ice thickness, friction coefficient and ice density had a large influence on the mean force, while the flexural strength, modulus of elasticity and ice thickness gave large variations in the standard deviation. This parameter sensitivity study could be applied in planning of model basin tests, by focusing on scaling and measuring the parameters most important for the problem at hand. For instance, it would be important to control the ice density and the ice–hull friction when accurate estimates of average mooring forces are wanted. The linear formulation of the velocity dependent ice force can be considered as a first attempt, and model test data are needed to investigate this formulation further.

A parameter sensitivity study was performed to investigate the importance of various parameters such as ice drift speed, ice thickness, ship size and natural period. The main findings were the following:

- The standard deviation of the mooring force was mainly governed by vessel's natural period and mass, and the ice drift speed.
- Mooring force oscillations were largest for low speeds and the lowest natural period. The oscillations were explained by dynamic amplification, because the energy of the ice force was located near the natural period of the vessel.
- The surge motion of the ship affected the ice–hull interaction force at the lowest speed. This was called a feedback effect and caused increase in the mooring force. The effect was limited by mass, as it decreased rapidly with increasing mass.
- Our choice of velocity dependent ice force model introduced speed dependence for the mean mooring force, with the bi-effect that the mean mooring force also depended on mooring stiffness and vessel mass. Further research is needed in order to establish physically sound methodology for the velocity dependent ice forces.

When performing a parameter sensitivity study it is important to keep in mind the parameters we have the ability to control in the design phase and those that are controlled by nature. All ice properties, such as thickness, density, drift speed and mechanical properties, are given by nature at each specific site and cannot be controlled during the design phase. However, it is important to understand the significance of the ice parameters to be able to perform favourable design considerations with respect to ship size, hull shape and mooring characteristics. These parameters form the core of the design phase when it comes to the ship response in ice.

The necessity of the penetration dependent ice force formulation was investigated. It was seen that the penetration description is necessary at the lowest ice drift speeds, for which the feedback effect was present. The standard deviation of the mooring force was underestimated by up to 60% when the ship's response was neglected in the ice force formulation. It is suggested that a penetration description of ice forces will be useful when modelling response in other degrees of freedom as well, where the motions of the vessel may cause even stronger nonlinearities.

Further research should focus on extending the model to account for more realistic hull shapes and then to variable ice drift. As the ice force formulations in this study were idealized and simplified, it could be beneficial to apply model test data in further research to improve the methodology for both the penetration and the velocity dependent ice forces.

Acknowledgements

The author would like to thank Basile Bonnemaire and Sveinung Løset for their scientific support. The study was funded by the PETROMAKS programme of the Research Council of Norway through NTNU's PetroArctic project.

References

Aksnes, V., 2010. Model Tests of the Interaction Between a Moored Vessel and Level Ice. Proceedings of the 20th IAHR International Symposium on Ice. Lahti, Finland.
Aksnes, V., Bonnemaire, B., 2009a. Analysis of the Behaviour of a Moored Ship in Variable Ice Drift. Proceedings of the 20th International Conference on Port and Ocean Engineering under Arctic Conditions. Luleå, Sweden, POAC09-25.
Aksnes, V., Bonnemaire, B., 2009b. A Simplified Approach for Modelling Stochastic Response of Moored Vessels in Level Ice. Proceedings of the 20th International Conference on Port and Ocean Engineering under Arctic Conditions. Luleå, Sweden, POAC09-134.
Bonnemaire, B., Shkhinek, K., Lundamo, T., Liferov, P., Le Guennec, S., 2009. Dynamic Effects in the Response of Moored Structures to Ice Ridge Interaction. Proceedings of the 20th International Conference on Port and Ocean Engineering under Arctic Conditions. Luleå, Sweden, pOAC09-135.
Brown, T.G., 2008. Ice Failure on Conical Structures — Effect of Speed. Proceedings of the 19th IAHR International Symposium on Ice. Vol. 2. Vancouver, British Columbia, Canada, pp. 887–896.
Comfort, G., Singh, S., Spencer, D., 1999. Evaluation of Ice Model Test Data for Moored Structures. PERD/CHC Report 26-195.
Croasdale, K.R., 1980. Ice forces on fixed rigid structures. 1st IAHR State of the Art Report on Ice Forces on Structures, pp. 34–106.
Faltinsen, O.M., 1990. Sea Loads on Ships and Offshore Structures. Cambridge University Press.
Frederking, R.M.W., Timco, G.W., 1985. Quantitative analysis of ice sheet failure against an inclined plane. Journal of Energy Resources Technology 107, 381–387.
Hetenyi, M., 1946. Beams on Elastic Foundations. The University of Michigan Press.
ISO/FDIS 19906, 2010. Petroleum and Natural Gas Industries — Arctic Offshore Structures, ISO TC 67/SC 7. Final Draft International Standard, International Standardization Organization. Geneva, Switzerland.
Izumiyama, K., Irani, M.B., Timco, G.W., 1994. Influence of a Rubble Field in Front of a Conical Structure. Proc. 4th Intl. Offshore and Polar Engineering Conf. Vol. 2. Osaka, pp. 553–558.
Jensen, A., Bonnemaire, B., Løset, S., Breivik, K.G., Evers, K.U., Ravndal, O., Aksnes, V., Lundamo, T., Lønøy, C., 2008. First Ice Model Testing of the Arctic Tandem Offloading Terminal. Proceedings of the 19th IAHR International Symposium on Ice. Vancouver, British Columbia, Canada.
Jones, S.J., 1989. A Review of Ship Performance in Level Ice. Proceedings of the 8th International Conference on Offshore Mechanics and Arctic Engineering. Vol. 4. The Hague, Netherlands, pp. 325–342.
Kärnä, T., Turunen, R., 1989. Dynamic response of narrow structures to ice crushing. Cold Regions Science and Technology 17, 173–187.
Keinonen, A., 1983. Major Scaling Problems with Ice Model Testing of Ships. Proc. 20th American Towing Tank Conf. Vol. 2. Davidson Laboratory, Stevens Institute of Technology, Hoboken, N.J, pp. 595–612.
Kotras, T.V., Baird, A.V., Naegle, J.N., 1983. Predicting ship performance in level ice. SNAME Transactions 91, 329–349.
Kreyszig, E., 1999. Advanced Engineering Mathematics, 8th Edition. John Wiley & Sons Inc., New York.
Lau, M., Molgaard, J., Williams, F.M., Swamidas, A.S.J., 1999. An Analysis of Ice Breaking Pattern and Ice Piece Size Around Sloping Structures. Proceedings of 18th International Conference on Offshore Mechanics and Arctic Engineering. St. John's, Newfoundland, Canada.
Lindqvist, G., 1989. A Straightforward Method for Calculation of Ice Resistance of Ships. Proceedings of the 10th International Conference on Port and Ocean Engineering under Arctic Conditions. Vol. 2. Luleå, Sweden, pp. 722–735.
Løset, S., Kanestrøm, Ø., Pytte, T., 1998. Model tests of a submerged turret loading concept in level ice, broken ice and pressure ridges. Cold Regions Science and Technology 27, 57–73.
Matskevitch, D., 2002. Velocity Effects on Conical Structure Ice Loads. Proceedings of 18th International Conference on Offshore Mechanics and Arctic Engineering. Oslo, Norway.
Nevel, D.E., 1992. Ice Forces on Cones from Floes. Proceedings of the IAHR Symposium on Ice. Banff, Alberta, Canada.
Shkhinek, K., Uvarova, E., 2001. Dynamics of the Ice Sheet Interaction with the Sloping Structure. Proceedings of the 16th International Conference on Port and Ocean Engineering under Arctic Conditions. Ottawa, Ontario, Canada.
Shkhinek, K.N., Bolshev, A.S., Frolov, S.A., Malyutin, A.A., Chernetsov, B.A., 2004. Modeling of Level Ice Action on Floating Anchored Structure Concepts for the Shtokman Field. Proceedings of the 17th IAHR International Symposium on Ice. Vol. 2. St. Petersburg, Russia, pp. 84–95.
Tatinclaux, J.C., 1986. Ice Floe Distribution in the Wake of a Simple Wedge. Proc. 5th Intl. Conf. on Offshore Mechanics and Arctic Engineering. Vol. 4. Tokyo, pp. 622–629.
Toyama, Y., Yashima, N., 1985. Dynamic Response of Moored Conical Structures to a Moving Ice Sheet. Proceedings of the 8th International Conference on Port and Ocean Engineering under Arctic Conditions. Vol. 2. Narssarssuaq, Greenland, pp. 677–688.
Valanto, P., 1992. The icebreaking problem in two dimensions: experiments and theory. Journal of Ship Research 36 (4), 299–316.
Valanto, P., 2001. The resistance of ships in level ice. SNAME Transactions 109, 53–83.
Wright, B., 1999. Evaluation of Full Scale Data for Moored Vessel Stationkeeping in Pack Ice. PERD/CHC Report 26-200.

Chapter 7

Model test investigation of the interaction between a moored vessel and level ice

By Vegard Aksnes

Proceedings of the 20th IAHR International Symposium on Ice, Lahti, Finland, 2010.

20th IAHR International Symposium on Ice
Lahti, Finland, June 14 to 18, 2010

Model tests of the interaction between a moored vessel and level ice

Vegard Aksnes
Norwegian University of Science and Technology
Department of Civil and Transport Engineering, 7491 Trondheim, Norway
vegard.aksnes@ntnu.no

Model tests of a moored ship with a simplified geometry have been performed in level ice. The model was only able to move in surge, and was moored with a linear spring setup. Two different natural periods were achieved by using springs with different stiffness characteristics. Two different ice drift speeds were used. Different dynamic properties of the model as well as the drifting ice could therefore be studied. The model was also tested in a fixed configuration to enable a comparison between fixed and moored setups.

The dynamic response of the model was investigated and effects from variations in the mooring stiffness and ice drift speed were identified and analysed. It was seen that the largest mean mooring force and the largest surge oscillations occurred for the lowest mooring stiffness at the lowest speed, probably caused by stick-slip friction along the sides of the model. The mooring force for the stiff springs and the fixed configuration both increased with ice drift speed. The configuration with stiff springs experienced lowest forces. Ice forces on the waterline of the bow increased with ice drift speed and were larger for the soft configuration than for the stiff one.

1. Introduction

Moored ships are believed to be feasible for operations in ice infested waters. Potential operations of application can be exploration drilling, production, storage and offloading. Various ice features and ice conditions will be challenging for different concepts. A variable ice drift direction is believed to be a challenge for moored ships, because they have to vane against the drift direction to minimize the mooring forces. However, there are no general methods for estimation of the vessel response or the mooring forces in such situations. The simplified problem of straight drifting level ice was investigated in an ice model basin to better understand the interaction between level ice and moored structures.

Some questions that motivated us were:

- Does dynamic properties of the mooring force (equivalently, the response) change with the ice drift speed and the mooring stiffness?
- How is the response of the ship in level ice influenced by the mooring stiffness?
- What is the relation between dynamic properties of the ice force and the ship response?

It is difficult to draw conclusions about effects of ice drift speed and mooring stiffness in level ice from existing literature. For conical moored structures, Comfort et al. (1999) and Dalane et al. (2008) reported that the mean and the peak mooring forces increased with the ice drift speed, while Toyama and Yashima (1985) claimed that the surge response was larger for low ice drift speeds. Comfort et al. (1999) and Løset et al. (1998) could not find any trends when looking at speed effects on turret moored ships. A simple numerical method by Aksnes and Bonnemaire (2009) predicted larger surge motions at low speeds for a moored ship. The effects of mooring stiffness were also studied by Aksnes and Bonnemaire (2009) and it was found that the amplitude of the oscillations increased with increasing natural period.

This paper starts by explaining the test setup and the test matrix. The test data is then analysed and discussed. Some conclusions are given in the end.

2. Experimental setup

The model tests were performed in April 2009 at the Large Ice Model Basin at HSVA, which is 72 m long, 10 m wide and 2.5 m deep. The so-called trim tank occupies the first 12 m of the tank and is used for model preparations. The remaining 60 m are used for model ice production and testing.

Froude scaling was used because of the importance of gravitational and inertial forces, with scaling ratio $\lambda = 25$. Lengths are scaled by λ, forces are scaled by λ^3 and speeds are scaled by $\lambda^{1/2}$. This means that for instance model scale (ms) and full scale (fs) speeds scale as $v_{fs} = \lambda^{1/2} v_{ms}$. All values in this paper are scaled to represent full scale data unless other is mentioned.

2.1. Vessel and mooring system

A simple hull was towed through the basin in stationary level ice, simulating drifting ice driven by current. The length of the waterline of the hull was 106 m, the beam was 33 m and the draught was 9 m. The main dimensions are summarized in Table 1. The hull was connected to a driving carriage through a spring configuration, modelling a simplified mooring system (Figs. 1 and 2). Two rails were mounted together with rollers such that the model could move in the surge direction, restrained by springs. The model was fixed with respect to the other modes of motion (sway, heave, roll, pitch and yaw), such that the motions in these modes were minimized. A frame with six uniaxial load cells was mounted between the upper rail and a column which was fixed to the driving carriage. This assembly of load cells measured what is referred to as mooring or global forces.

Table 1. Properties of the vessel and the mooring system.

Model characteristics	Model scale	Full scale
Length of waterline L_{WL}	4.24 m	106 m
Beam B	1.32 m	33 m
Draught T	0.35 m	8.8 m
Stem angle φ	25°	25°
Kinetic ice-hull friction μ	0.04	0.04
Volume displacement ∇	1.8 m^3	28125 m^3
Soft mooring stiffness k^{soft}	0.4 kN/m	250 kN/m
Stiff mooring stiffness k^{stiff}	1.8 kN/m	1125 kN/m
Soft mooring surge natural period T_n^{soft}	13.4 s	67 s
Stiff mooring surge natural period T_n^{stiff}	6.4 s	32 s
Fixed mooring natural period T_n^{fixed}	0.36 s	1.8 s

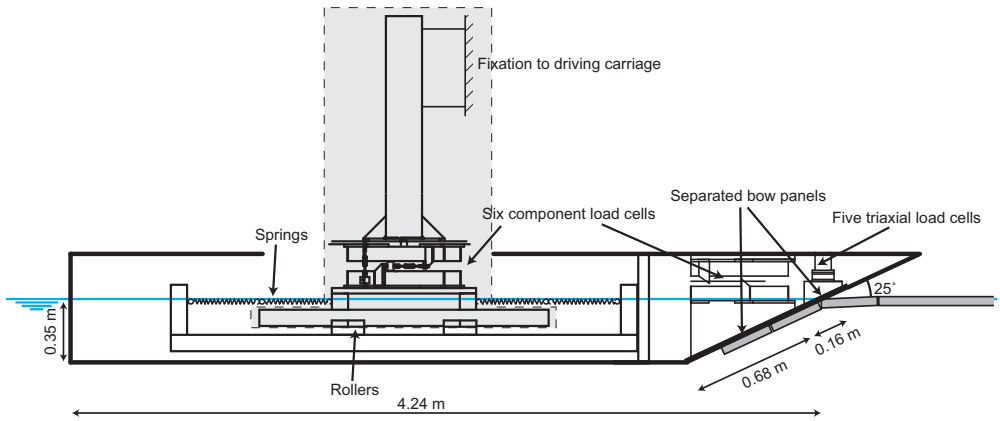

Figure 1. Cross-sectional view of the model with the mounting frame and the instrumentation. The dimensions are in model scale. The grey shaded area was fixed to the driving carriage.

Two different types of springs were used, giving a total stiffness of 250 kN/m and 1125 kN/m, respectively. The stiffness was linear through the whole displacement range of the model. The

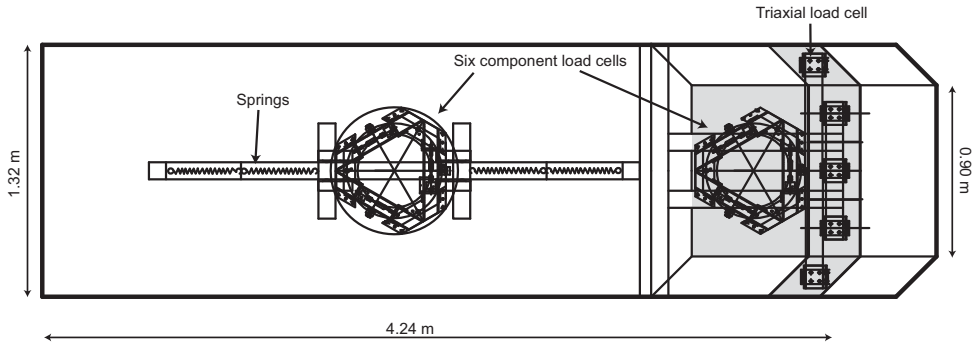

Figure 2. Top view of the model with the mounting frame and the instrumentation. The dimensions are in model scale. The load panels are shaded in grey.

mass was approximately 28000 tons, thus the two stiffnesses gave natural periods of 67 and 32 s. It was possible to fix the rails, such that the model was hindered to surge. In reality, the system was not perfectly stiff and had a surge natural period of 1.8 s with the fixed configuration. The amplitudes of the oscillations were very limited with the fixed configuration.

The bow of the model was segmented into five waterline panels and one submerged panel (Fig. 3). Each of the five waterline panels was mounted on a triaxial load cell (ME-Meßsysteme K3D120). The objective of these panels was to measure the ice actions near the design waterline. The three central panels were aligned and the two outer ones were oriented 45° relative to the central panels in the horizontal plane (Fig. 2). Each of the waterline panels had dimensions of 7.5 by 7.5 m. The main objective of the submerged panel was to measure frictional ice forces. The submerged panel was mounted to an arrangement of six uniaxial load cells, similarly to the one that was used for the mooring forces. The width of the submerged panel was 22.5 m, while its height was 17 m. The lubricated kinetic friction between the top surface of the ice and the hull was estimated to be 0.04 in a controlled environment.

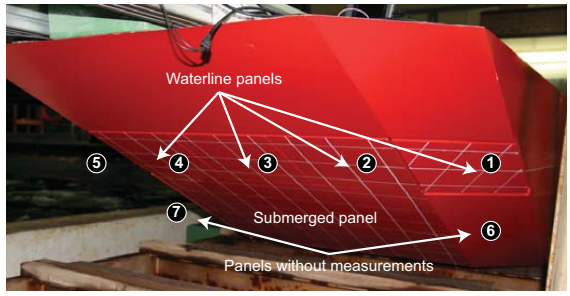

Figure 3. The segmentation of the bow into five waterline panels and one submerged panel.

2.2. Ice properties

Three sheets of level ice were grown naturally from a 0.7% sodium chloride solution. The ice was of a fine-grained columnar type and the preparation technique was described thoroughly

by Evers and Jochmann (1993). After the desired thickness was reached, the ice was heated to achieve the target flexural strength. Measurements of flexural strength σ_f were performed before and after each test by means of cantilever beam tests as recommended by Schwarz et al. (1981). Cantilever beam tests were carried out at four different locations in the tank and then averaged. The values for flexural strength presented in Table 2 are interpolated values based on measurements before and after the tests. The spatial variation of the flexural strength was low, however it typically increased towards the end of the basin.

The modulus of elasticity, E, was estimated by measuring the deflection of a cantilever beam when a certain vertical force was applied to the free end. These measurements were performed on ice sheets number 2 and 3. The results are given in Table 2. In the literature (Schwarz, 1977; Ashton, 1986) it is reported that the ratio between modulus of elasticity and flexural strength E/σ_f should be larger than 2000 to simulate natural ice. From Table 2 we can see that this criterion was fulfilled for the tests where measurements of the modulus of elasticity exist, but that the values were in the lower part of the acceptable range.

Ice thickness profiles were made in the wake after each test had been executed. The ice thicknesses reported in Table 2 are average values from each ice sheet. The ice density was measured for the last ice sheet only. An average value of 929 kg/m^3 was obtained. According to Evers and Jochmann (1993), this was in the upper range of values at HSVA and they reported that a typical value is 870 kg/m^3.

Table 2. The mean ice properties for all the ice sheets. The flexural strength is denoted σ_f, the ice thickness h_i, the modulus of elasticity E, and the ice density ρ_i.

	Model scale				Full scale			
Ice sheet	h_i [mm]	σ_f [kPa]	E [MPa]	ρ_i [kg/m^3]	h_i [m]	σ_f [kPa]	E [GPa]	ρ_i [kg/m^3]
Target	30	25	NA	NA	0.75	625	NA	NA
2000	32	35	NA	NA	0.80	875	NA	NA
3000	29	27	≈ 70	NA	0.73	675	≈ 1.8	NA
4000	28	25	≈ 50	929	0.70	625	≈ 1.3	929

2.3. Test matrix

Three test runs were performed in level ice; one test run with the soft mooring configuration, one with the fixed configuration and one with the stiff configuration. A brief description of a test run is as follows. The speed was constant at 0.05 m/s for about 500 m. The first 100 m gave transient results because the model was not completely embedded in ice, and they were not used in the analysis. After about 500 m, the speed of the driving carriage changed abruptly to 0.25 m/s. A section of 800 m followed, from which the first 100 m were transient due to the change of speed and not included in the analysis. After 800 m, the vessel stopped abruptly. Only the stable parts of the test runs are used in the following analysis, that is, 400 m with ice drift speed 0.05 m/s and 700 m with ice drift speed 0.25 m/s. Thus, both the size of the ice sheets and the ice drift speed were modelled with values representative for many Arctic or ice-infested waters (Løset et al., 1999). The performed test runs are summarized in Table 3.

Table 3. The test matrix for all the ice tests. T_n^{fs} denotes the surge natural period, v_i^{fs} the ice drift speed, and L^{fs} the length of the ice sheet used in the test run. The values are in full scale.

Run #	Description	v_i^{fs} [m/s]	T_n^{fs} [s]	L^{fs} [m]
2100	Towing in level ice	0.05	67 (soft)	575
2200	Towing in level ice	0.25	67 (soft)	775
3100	Towing in level ice	0.05	1.8 (fixed)	500
3200	Towing in level ice	0.25	1.8 (fixed)	825
4100	Towing in level ice	0.05	32 (stiff)	525
4200	Towing in level ice	0.25	32 (stiff)	750

3. Mooring forces

Excerpts from time series of the mooring force from all the test runs are shown in Figs. 4, 5 and 6. The combination of soft mooring configuration and low speed gave large surge motions in large parts of the test run (Fig. 4a). These motions were sawtooth-shaped and their periods were much longer than the natural period of the model. Such oscillations were not seen in the other test runs, although the test setup remained the same. Thus, the oscillations were a result of the ice ship interaction.

Spectral analysis of the mooring force was performed. The energy for the soft configuration and low speed was concentrated at two distinct periods, approximately two and four times the natural period. The same observation was also made by inspecting the time series directly. The oscillations with a period of $4T_n^{soft}$ had larger amplitude than those with a period of $2T_n^{soft}$. These oscillations disappeared when the drift speed was increased to 0.25 m/s. For this speed the response was characterized by irregular low frequency motions.

No energy was concentrated around the surge natural frequency or its multiples in test runs with the stiff mooring system. With a drift speed of 0.05 m/s, there was some energy between 10 and 20 s, which was not present for soft mooring and low speed. At the highest speed, the spectra for soft and stiff mooring systems were similar. The fixed configuration vibrated at its natural period (1.8 s) with varying amplitude at both speeds. At low speed there was also energy concentrated around 1.0 and 12.5 s.

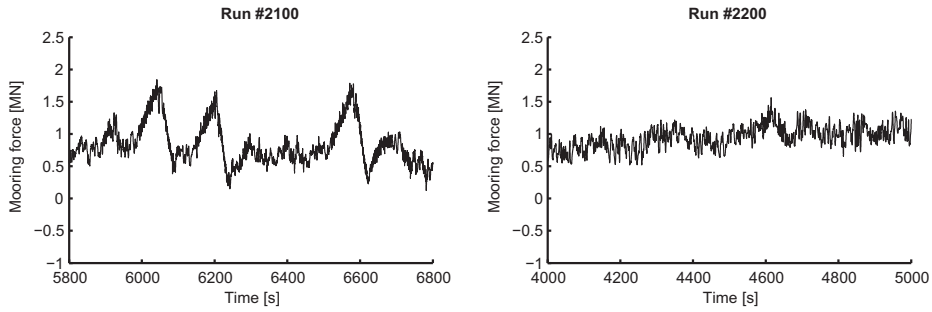

Figure 4. Excerpts of time series of the mooring force from the test runs with the soft mooring configuration. The ice drift speed is 0.05 m/s in a) and 0.25 m/s in b).

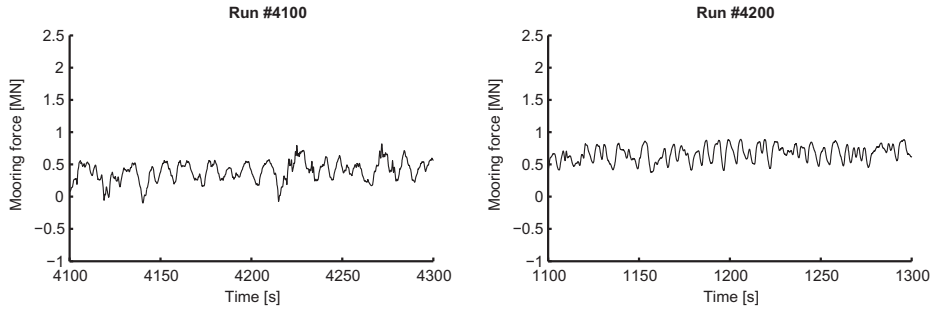

Figure 5. Excerpts of time series of the mooring force from the test runs with the stiff mooring configuration. The ice drift speed is 0.05 m/s in a) and 0.25 m/s in b).

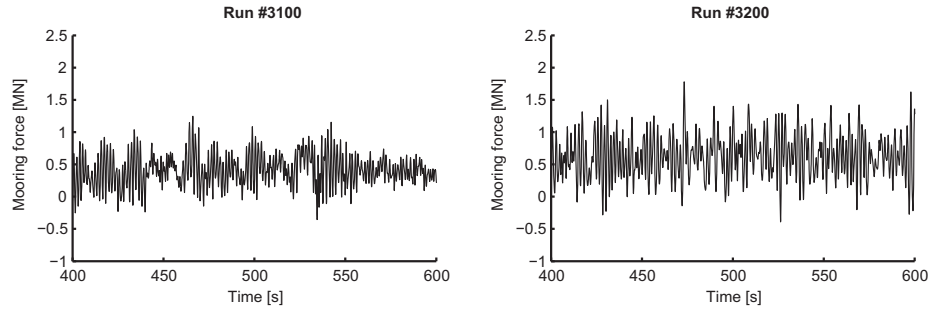

Figure 6. Excerpts of time series of the mooring force from the test runs with the fixed mooring configuration. The ice drift speed is 0.05 m/s in (a) and 0.25 m/s in (b).

The mean, the standard deviation and the coefficient of variation (the ratio between the standard deviation and the mean) of the mooring force were plotted for each spring configuration in Fig. 7. The stiff and fixed configurations followed the same trends; the mean force increased with ice drift speed, while the standard deviation was more or less constant. This means that the coefficient of variation decreased with the ice drift speed for both configurations. Both the mean and the standard deviation were larger for the fixed than for the stiff spring configuration. The mean mooring force for the fixed configuration was 20 and 10 % higher than for the stiff configuration for ice drift speeds of 0.05 m/s and 0.25 m/s, respectively. The standard deviation was approximately two times larger for the fixed than for the stiff configuration. The coefficient of variation was 50 % larger for the fixed than for the stiff configuration. The ice was slightly thinner and weaker in the test series with the stiff configuration, compared to the fixed configuration. These small variations in ice properties may have caused some of the differences between the configurations.

The soft spring configuration behaved differently. The mean mooring force decreased with increasing ice drift speed and was about twice as large as for the other configurations for the low speed. The differences were smaller for the highest speed. The standard deviation also decreased with increasing ice drift speed. For the lowest speed, the standard deviation was 3 times larger than for the highest speed. Because the standard deviation decreased much more than the mean, the coefficient of variation also decreased with increasing ice drift speed.

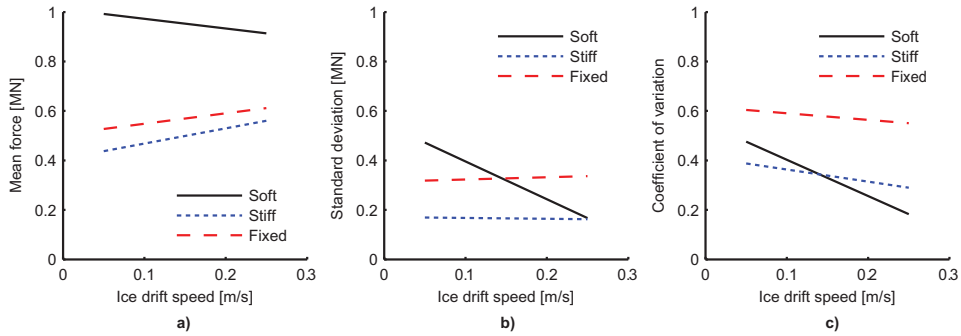

Figure 7. a) The mean, b) the standard deviation and c) the coefficient of variation for the **mooring** force plotted against the ice drift speed for all the model configurations.

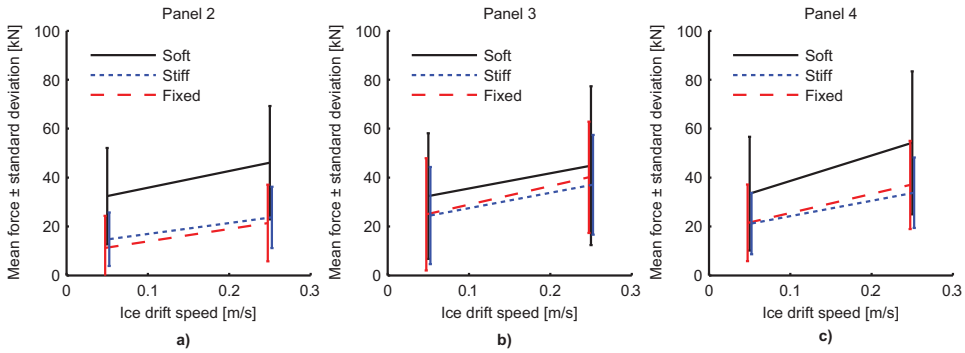

Figure 8. The mean and the standard deviation for the **ice** force measured on panels 2, 3 and 4.

4. Ice forces

4.1. Measured ice forces

The forces on the five panels in the waterline and the submerged panel were measured with triaxial load cells. The mean and the standard deviation of forces in x-direction on panels 2, 3 and 4 and the submerged panel for each of the test runs were plotted in Figs. 8 and 9. Panels 1 and 5 suffered from unwanted effects from internal water waves in the bow and were therefore excluded from the analysis.

We first consider the forces on panels 2, 3 and 4. The mean force generally increased with increasing ice drift speed. The mean force was largest with the soft configuration. The difference between mooring configurations was more noticeable for panels 2 and 4 than for panel 3. The stiff and fixed configurations had mean forces of similar size. The standard deviation increased with v_i for all panels, and was largest on panel 3. It was largest for the soft configuration and smallest for the stiff configuration. It was slightly larger for the fixed than for the stiff configuration.

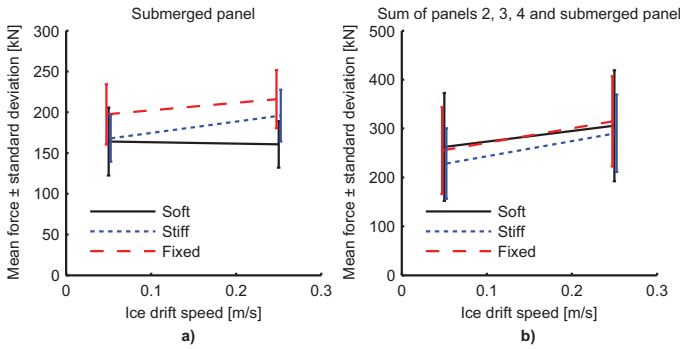

Figure 9. The mean and the standard deviation for **ice** forces on a) the submerged panel and b) the sum of panels 2, 3 and 4 and the submerged panel.

On the submerged panel, the mean force increased with v_i for fixed and stiff configurations and was constant for the soft configuration. The standard deviation also increased for the fixed and stiff configurations, while it decreased for the soft configuration.

The mean and the standard deviation of the sum of forces measured on panels 2, 3 and 4 and the submerged panel were plotted in Fig. 9. The total mean force and the standard deviation increased with the ice drift speed for all the mooring configurations.

4.2. Estimated ice friction forces

Only the forces exerted on the bow were measured directly. From video observations it was clear that very small amounts of ice interacted with panels 6 and 7, on which ice actions were not monitored. Any forces on these panels were therefore excluded from the analysis. Ice forces also acted on the sides and the bottom of the model. The bottom of the model was usually fully covered with ice and the ice forces were caused by friction. A rough estimate of the mean friction force on the bottom can be given as

$$F_{fric} = \mu(\rho_w - \rho_i)gL_{bottom}B\overline{h}_i, \qquad \textbf{[1]}$$

where ρ_w is the water density, ρ_i the ice density, g the gravitational acceleration, L_{bottom} the length of the bottom plate, B the width of the model, and $\overline{h}_i$ the mean ice thickness. The results in Fig. 10 were obtained by using Eq. (1) with $\mu = 0.04$, $\rho_w = 1006$ kg/m^3, $\rho_i = 930$ kg/m3, $g = 9.81$ m/s^2, $L_{bottom} = 87$ m, $B = 33$ m and mean ice thickness as given in Table 2. With this formulation this force was constant with respect to the ice drift speed and proportional to the mean ice thickness for the relevant ice sheet.

The model was slightly ($\approx 1^\circ$) out of course in most of the test runs. This caused frictional forces on the sides of the model. Using the measured global force in y-direction, one can estimate the frictional force by multiplying it by the frictional coefficient $\mu = 0.04$, Fig. 10. This friction force reached its maximum with the soft springs and its minimum with the stiff ones. With the soft and the stiff springs it increased with ice drift speed, while it decreased with the fixed springs.

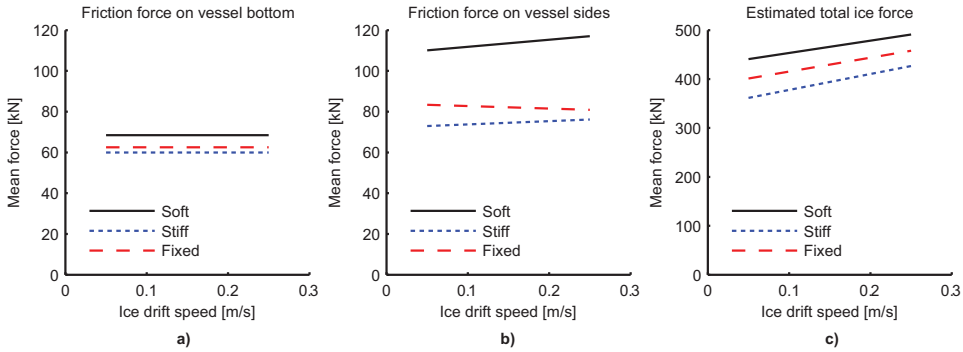

Figure 10. The estimated mean of ice forces on a) the bottom and b) the sides of the vessel, and c) the estimated total mean of all ice forces acting on the vessel.

4.3. Total ice force estimate

The sum of the measured and the estimated mean ice forces is given in Fig. 10. All spring configurations showed the same speed dependence; the mean force increased with the drift speed. The soft spring configuration experienced larger forces than the fixed configuration, which again experienced larger forces than the stiff configuration.

5. Discussion

Large oscillations occurred at the lowest ice drift speed with the soft mooring system. The model was slightly out of course and frictional forces built up on the sides of the model. These frictional forces, caused by lateral pressure, caused a locking effect, in the sense that the model was locked in the ice sheet and not released until the mooring force was large enough to overcome the friction force. An attempt was made to estimate the mean value of these friction forces, by using the only friction coefficient we knew, namely the kinetic friction coefficient between the hull and the upper surface of the ice. The estimate may be too low, because the friction coefficient should be higher due to the rough surface of a broken ice edge. Further, at low speed and with the soft mooring system, the ice-hull interaction happens slowly, and it is possible that static friction, rather than kinetic friction, was experienced.

Lishman et al. (2009) investigated ice-ice friction along broken ice edges at HSVA. Their results showed that this friction coefficient was rate-dependent and decreased with increasing speed. Even though one of the surfaces (the hull) was very smooth in our case, it is likely that there was a rate-dependence also in our case and it may be a reason for why the large stick-slip like oscillations occurred only at the lowest ice drift speed. For a given ice drift speed, a soft system needs more time to build up spring forces to overcome the friction force than a stiff system. During this time, the vessel may jam more and more, the lateral pressure will build up and therefore the friction force will increase as well. This could be one of the reasons for the large oscillations seen with soft springs.

It is interesting to see that there was no dominant motion at the natural frequency for soft and

stiff spring systems. However, the largest oscillations with soft springs at the lowest speed had periods of two and four times the natural period. The fixed system did not experience the stick slip friction forces on the sides of the vessel and hence vibrated at its natural frequency.

One may compare mooring forces with the sum of the measured and the estimated ice forces. Let us consider a linear and time-invariant system, that is, a system where the response u is related to the external load f by the impulse response function h, such that

$$u(t) = \int_{-\infty}^{\infty} h(s) f(t-s)\, ds. \qquad \textbf{[2]}$$

If we assume that the load is a stationary stochastic process, then the expectation value $E[f]$ is a constant. It can then be shown that the mean value for the response is (Naess, 2007)

$$E[u(t)] = H(0)E[f(t)], \qquad \textbf{[3]}$$

where H is the transfer function for the system, i.e. the Fourier transform of the impulse response function. For a linear mass-spring-damper system, $H(0) = 1/k$, where k is the spring stiffness. If our system is assumed to be of this type, then the mean value of the mooring force should be equal to the mean value of the ice forces. Figure 11 shows that there was a difference between the mean ice force and the mean mooring force. The difference was similar for the stiff and fixed systems and there are at least three possible reasons for the discrepancy:

- The ice density was quite high (and only measured for one ice sheet) and small errors in this value will give large variations in the friction force on the bottom, because this depends on the difference between the ice and water densities.
- The friction coefficient was estimated in a separate test under idealized conditions. It is likely that this coefficient was different in the actual interaction process than in the idealized friction test.
- One layer of ice was used in the calculation, but ice accumulated under the vessel in several of the tests and a correct estimate of the ice thickness is difficult to give.

With these sources of error in mind, we observe that the mooring and ice forces for the stiff and fixed configurations were of comparable magnitude. This indicates that the system behaved approximately linearly for these configurations and ice drift speeds. For the soft configuration the forces were far from similar and we may assume that the system behaved nonlinearly for this spring stiffness.

Shkhinek and Uvarova (2001) and Matskevitch (2002) have argued that ice forces on fixed sloping structures increases with the interaction speed, while Brown (2008) claims that this dependence is very weak and often negliable, based on measurements from the Confederation Bridge. In the tests considered herein, a clear speed dependence of the ice action was seen for both the mean forces and the standard deviations on the waterline panels. Furthermore, it was seen that mean ice force, as well as the ice force standard deviation, was largest for the soft mooring configuration. Aksnes and Bonnemaire (2009) noticed a similar dependency for low ice drift speeds with a numerical model. In their model, no explicit speed dependence was included, the speed dependency was a result of the interaction between the ship and ice.

Figure 8 showed that panels 2, 3 and 4 experienced ice forces of similar magnitude when the mooring system was soft. Such a mooring system resulted in a very slow interaction between

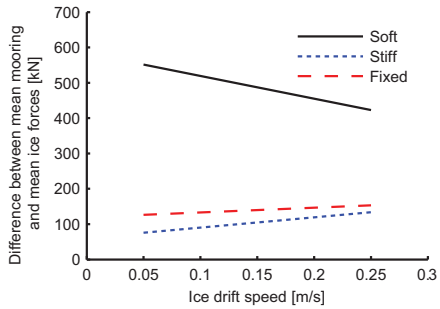

Figure 11. The difference between the measured spring forces and the estimated and measured ice forces for all the test runs.

ice and hull, and a relatively even contact surface was built up. From Fig. 8, it can be seen that this was not the case for the stiff or the fixed configuration. For these configurations, boundary effects were more pronounced and lower forces where experienced on panels 2 and 4, than on panel 3.

6. Conclusive remarks

The most important findings in this study were the following:

- The mean mooring force increased with the ice drift speed for the stiff and fixed systems, but decreased for the soft system.
- The model experienced largest oscillations at the lowest speed with the soft mooring system.
- These oscillations were caused by stick-slip friction along the sides of the model.
- No resonant motions were seen for the soft and stiff mooring systems.
- A simple analytic single degree of freedom model indicated that the system may have behaved linearly for the stiff and the fixed configuration, but not for the soft one.
- The local ice forces on the bow waterline increased with the ice drift speed and were highest for the soft mooring configuration.

Acknowledgements

The work described in this report/publication was supported by the European Community's Sixth Framework Programme through the grant to the budget of the Integrated Infrastructure Initiative HYDRALAB III, Contract no. 022441(RII3). The author would like to thank the Hamburg Ship Model Basin (HSVA), especially the ice tank crew, for the hospitality, technical and scientific support and the professional execution of the test programme in the Research Infrastructure ARCTECLAB.

Funding of equipment by Statoil ASA was highly appreciated. The work was supported by the PetroArctic project, part of the Petromaks project of the Research Council of Norway. The author would like to thank Basile Bonnemaire and Sveinung Løset for their scientific support.

References

Aksnes, V., Bonnemaire, B., 2009. A simplified approach for modelling stochastic response of moored vessels in level ice. In: Proceedings of the 20th International Conference on Port and Ocean Engineering under Arctic Conditions. Luleå, Sweden, POAC09-134.

Ashton, G. D. (Ed.), 1986. River and Lake Ice Engineering. Water Resources Publications. Book Crafters Inc., Chelsea, Michigan.

Brown, T. G., 2008. Ice failure on conical structures - Effect of speed. In: Proceedings of the 19th IAHR International Symposium on Ice. Vol. 2. Vancouver, British Columbia, Canada, pp. 887–896.

Comfort, G., Singh, S., Spencer, D., 1999. Evaluation of Ice Model Test Data for Moored Structures. PERD/CHC report 26-195.

Dalane, O., Gudmestad, O. T., Løset, S., Amdahl, J., Fjell, K. H., Hildèn, T. E., 2008. Ice tank testing of a surface buoy for Arctic conditions. In: Proceedings of the 27th International Conference on Offshore Mechanics and Arctic Engineering. Estoril, Portugal.

Evers, K. U., Jochmann, P., 1993. An advanced technique to improve the mechanical properties of model ice developed at the HSVA ice tank. In: Proceedings of the 12th International Conference on Port and Ocean Engineering under Arctic Conditions. Hamburg, Germany, pp. 877–888.

Lishman, B., Sammonds, P., Feltham, D., Wilchinsky, A., 2009. The rate- and state-dependence of sea ice friction. In: Proceedings of the 20th International Conference on Port and Ocean Engineering under Arctic Conditions. Luleå, Sweden, POAC09-66.

Løset, S., Kanestrøm, Ø., Pytte, T., 1998. Model tests of a submerged turret loading concept in level ice, broken ice and pressure ridges. Cold Regions Science and Technology 27, 57–73.

Løset, S., Shkhinek, K., Gudmestad, O. T., Strass, P., Michalenko, E., Frederking, R., Kärnä, T., 1999. Comparison of the physical environment of some Arctic seas. Cold Regions Science and Technology 29, 201–214.

Matskevitch, D., 2002. Velocity effects on conical structure ice loads. In: Proceedings of 18th International Conference on Offshore Mechanics and Arctic Engineering. Oslo, Norway.

Naess, A., 2007. An Introduction to Random Vibrations, Norwegian University of Science and Technology, Trondheim, Norway.

Schwarz, J., 1977. New developments in modelling ice problems. In: Proceedings of the 4th International Conference on Port and Ocean Engineering under Arctic Conditions. St. Johns, Newfoundland, Canada, pp. 45–61.

Schwarz, J., Frederking, R., Gavrillo, V., Petrov, I. G., Hirayama, K.-I., Mellor, M., Tryde, P., Vaudrey, K. D., 1981. Standarized testing methods for measuring mechanical properties of ice. Cold Regions Science and Technology 4, 245–253.

Shkhinek, K., Uvarova, E., 2001. Dynamics of the ice sheet interaction with the sloping structure. In: Proceedings of the 16th International Conference on Port and Ocean Engineering under Arctic Conditions. Ottawa, Ontario, Canada.

Toyama, Y., Yashima, N., 1985. Dynamic response of moored conical structures to a moving ice sheet. In: Proceedings of the 8th International Conference on Port and Ocean Engineering under Arctic Conditions. Vol. 2. Narssarssuaq, Greenland, pp. 677–688.

Chapter 8

A panel method for modelling level ice actions on moored ships. Part 1: Local ice force formulation

By Vegard Aksnes

Cold Regions Science and Technology, 2011; 65(2): 128-136.

Is not included due to copyright

Chapter 9

A panel method for modelling level ice actions on moored ships. Part 2: Simulations

By Vegard Aksnes

Cold Regions Science and Technology, 2011; 65(2): 137-144.

Is not included due to copyright

Chapter 10

Conclusions and recommendations for further work

10.1 Conclusions

10.1.1 Model tests of the Arctic Tandem Offloading Terminal

Two papers discussed the behaviour of the Arctic Tandem Offloading Terminal in ice.

Model tests of two vessels moored in tandem in level ice and first-year ice ridges:

- The tandem mooring loads were higher in ridges than in level ice.
- The system of two vessels showed sufficient yaw stability under slowly varying changes of the ice drift direction.
- The reamers on the offloading icebreaker were less effective in ridges, than in level ice, due to pronounced pitch motion in ridges.

Model tests of a turret moored offloading icebreaker in level ice with variable drift direction:

- The mooring forces and the vessel response depended significantly on the relative ice drift direction. Mooring forces usually increased with the relative ice drift direction.
- The ice failure modes were determined by the local hull geometry and the vessel response.
- The turret position, the helmsman actions and the waterline geometry were decisive for the horizontal stability of the vessel.
- The magnitude of the mooring forces was comparable in severe ice drift scenarios and in first-year ice ridges.

10.1.2 Model tests of a moored simplified hull

Two papers presented results from the model tests of a moored simplified hull.

General results from the model tests:

- The average mooring force increased with the ice drift speed for stiff and fixed systems, but decreased for the soft system.
- The local ice forces increased with the ice drift speed.
- The largest surge oscillations were experienced at the lowest ice drift speed and with the softest mooring. These oscillations were caused by stick-slip friction on the sides of the vessel.

Local ice force formulations based on model test data and observations:

- The ice actions were split into ice actions near the waterline and on the wet part of the hull.
- Mechanical arguments and observations from the model tests were applied to determine the shape of the synthetic local ice forces.
- Randomness was included by deriving statistical properties from the model test data.
- The synthetic signals compared very well with model test measurements in terms of statistical properties and power density spectra.

10.1.3 Numerical modelling of moored ships in level ice

Numerical modelling of moored ships in level ice was discussed in three papers. All of them presented models with a single-degree-of-freedom and level ice with constant drift direction. Ice forces were parameterized by the penetration of the moored vessel into the ice sheet. Two different approaches were applied for modelling of the ice forces.

Ice forces based on elastic beam theory applied to a simple hull:

- The level ice was modelled as an elastic beam on an elastic (Winkler) foundation.
- Randomness in the ice force was included by sampling from probability distributions for temperature and salinity and then using well-known empirical formulas to calculate ice mechanical properties.
- Studies of effects of the surge natural period and the ice drift speed showed that the largest surge oscillations occurred at the lowest speeds.

- Feedback effects from the vessel response to the resulting ice actions were possible due to the penetration parameterization of the ice forces. The effects occurred mostly for low speeds and usually induced large mooring forces.

Semi-empirical ice force model applied to a real hull:

- The local ice force model derived from model tests was implemented for a real hull.
- The simulated mooring forces showed satisfactory agreement with the mooring forces measured during the model tests of the Arctic Tandem Offloading Terminal.
- Feedback effects from the vessel response were present mostly for low ice drift speeds.
- Weak dynamic amplification was experienced for ice drift speeds around 0.1-0.15 m/s.

The two methods for calculating ice forces were similar, but the latter one was adjusted with model test data and applied to a real hull. They both gave similar results in terms of effects of the ice drift speed and the surge natural period. The penetration parameterization of ice forces enabled feedback effects from the vessel response to the resulting ice actions for both models. Feedback effects are important for assessing the dynamic response of a moored ship in level ice.

10.2 Recommendations for further work

During the work with this thesis, several topics for further work have been identified. These include the following:

10.2.1 Experimental modelling of moored ships in ice

- Damping forces are crucial for modelling of dynamic response of moored structures, in particular for the extreme values. The author suggests to study ice induced damping forces both theoretically and experimentally.
- Local ice force methodology based on measurements was developed. The data set was relatively small and a comprehensive model test campaign with panels with different geometric properties would be beneficial for further progress in this direction.

10.2.2 Numerical modelling of moored ships in ice

- The average forces caused by ice are to a large extent caused by friction forces between ice and the hull. It would be interesting to develop methodology

for estimation of the subsurface contact area between ice and the hull, either based on model test observations or based on calculated motions of broken ice pieces. It is crucial to model this contact area correctly in order to obtain reliable estimates for friction forces.

- The numerical model developed in Chapters 8 and 9 can be extended to level ice with variable drift direction and vessel response in other modes of motion. This means that ice-hull interactions at other parts of the waterline have to be taken into account. Variations in the interaction geometry will possibly induce transitions between flexural and crushing failure of the ice and should be studied. One should also study breaking patterns, for instance by finite element modelling, to investigate effects of the panel size and the hull geometry.
- The author suggests to parameterize ice forces caused by ice ridges or ice rubble fields by the vessels penetration into the ice.